Neural Networks and Early Fast Doppler for Prediction in Meteor-Burst Communications Systems

David Douglas Fraser

December 1994

Submitted in partial fulfilment of the requirements for the degree of Doctor of Philosophy in the Department of Electronic Engineering, University of Natal, South Africa.

Abstract

In meteor-burst communications systems, the channel is bursty with a continuously fluctuating signal-to-noise ratio. Adaptive data rate systems attempt to use the channel more optimally by varying the bit rate. Current adaptive rate systems use a method of closed-loop decision-feedback to control the transmitted data rate.

It is proposed that an open-loop adaptive data rate system without a decision feedback path may be possible using implicit channel information carried in the first few milliseconds of the link establishment probe signal. The system would have primary application in low-cost half-duplex telemetry systems. It is shown that the key elements in such a system would be channel predictors. The development of these predictors is the focus of this research. Two novel methods of predicting channel parameters are developed.

The first utilises early fast Doppler information that precedes many long duration, large signal-to-noise-ratio overdense trails. The presence of early fast Doppler at the trail commencement is used as a toggle to operate at a higher data rate. Factors influencing the use of early fast Doppler for this purpose are also presented.

The second method uses artificial neural networks. Data measured during trail formation is processed and presented to the neural networks for prediction of trail parameters. Several successful neural networks are presented which predict trail type, underdense or overdense, and peak trail amplitude from the first 50ms of the trail's lifetime. This method allows better estimation of the developing trail. This fact can be used to implement a multi-rate open-loop adaptive data rate system.

Preface

The research work described in this thesis was performed in the Department of Electronic Engineering at the University of Natal, Durban, under the supervision of Professor Anthony D. Broadhurst.

These studies represent original work by the author and have not been submitted in any form to another university. Where use has been made of the work of others, it has been duly acknowledged in the text.

Acknowledgments

I gratefully acknowledge those who assisted me and those with whom I had the pleasure of working during this thesis project. In particular I would like to thank:

Professor Anthony Broadhurst for his friendship, supervision and assistance with the completion of this document.

Dr Stuart Melville for his warm friendship, keen wit and exceptional support, especially with the use of *TrailStar* and the data preprocessing software.

Dr Robert Mawrey for his discussions as an engineer, his advice as a friend and his support as a brother-in-law.

Dr Hilton Goldstein for his software assistance early on in this project.

Peter Handley for his efficient and professional running of the Meteor-Scatter Research Programme for much of the period of this work.

Rod Radford for whom running the measurement system and performing countless other tasks was never too much trouble.

I would also like to thank Salbu (Pty) Ltd and the Natal University Research Foundation for their financial and infrastructural support. In particular, I would like to thank Mr Dave Larsen of Salbu (Pty) Ltd for generously supporting, encouraging and nurturing the Meteor-Scatter Research Project since its inception.

And of course, special thanks go to my wife Leigh-Anne who patiently tolerated me and inspired me through the period of thesis preparation.

Table of Contents

List of Figures

Chapter 1

Introduction, problem statement and thesis claims

1.1 Meteor-burst communications systems

A connection between meteors and radio reflections was first postulated by *Nagaoka* [1929]. His initial premise that these meteors would be impediments to radio communication was questioned by *Pickard* [1931] and *Skellet* [1932]. *Skellet* identified meteor ionisation columns as phenomena that could enable enhanced radio reflection to occur at very high frequencies (typically from 40 to 90 MHz). The lower limit is defined by the maximum usable frequency of the ionosphere and the upper limit by a decrease in reflected signal amplitude with increasing incident frequency.

The use of naturally occurring ionization trails left by meteors ablating in the earth's upper atmosphere to communicate reliably and cheaply over long distances is now an established communication technique. Every day billions of meteors, in orbit around the sun, collide with the earth's atmosphere. The meteors, typically comparable in size to grains of sand, burn up at heights ranging between 80 and 120 kilometres above the earth's surface forming trails of ionization tens of kilometres long with an initial diameter of approximately one metre. These trails may be used to reflect radio waves between two points on the earth's surface. The curvature of the earth's surface limits the separation between two points to a maximum of approximately 2000 kilometres. Very high frequency radio waves, rather than high frequency radio waves, are typically used for communication purposes

to avoid interference caused by ionospheric reflections. The duration of the reflected signal is limited by diffusion of the ionized trail, but is sufficiently long to support burst-mode data communication.

Table 1-1 below, based on a table presented by *Schanker* [1990] , allows for a perspective of meteor-burst communications in comparison with other systems.

Table 1-1 Comparison of meteor-burst communications and other communications systems

Type of System	Telephone	HF Radio	Satellite	VHF Radio	Microwave	Meteor-Burst
Initial Cost	Low to user	Moderate	High	Low/ moderate	Very high	Moderate
Operating Cost	Usage dependent	Low to moderate	High	Low	Very high	Low to moderate
Frequency Range	300 - 3000 Hz	3 - 30 MHz	Above 3 GHz	30 - 300 MHz	Above 1.2 GHz	30 - 50 MHz
Throughput capacity	0-28.8 kbps currently	300 bps 2400 - 4800 bps possible	Very high	Currently 9600 - 19200 bps	High	Currently 50 - 4000 bps
Communication Range	worldwide	Typically 6000 km	worldwide	50 - 200 km	40 - 60 km between relays	2000 km
Antenna Size	N/A	Dependent on frequency and directivity	typically 1-10 m	Small, tower mounted	Moderate, tower mounted	Small/medium
Training requirements	Minimal	Can be very extensive	Can be very extensive	Minimal to moderate	User training minimal, system operator training extensive	Minimal
Overall reliability	High	Poor to moderate	Generally high	Moderate	Generally high	Very high
Other Features	User has no control over network operation	Requires continual frequency alteration	Vulnerable to satellite failure	Restricted to LOS without repeaters	Approaching obsolescence	Not real time, transmission delays

A review of meteor-burst communications technology is found in [*Melville & Fraser*, 1992, 1993]. Developments in meteor-burst technology in Southern Africa are presented in [*Handley & Fraser*, 1992, 1993].

1.2 Problem statement

Meteor-burst communication systems rely on protocols with decision-feedback to relay information regarding the signal-to-noise ratio of the channel to the sending station. The primary purpose is to determine whether a trail is present or not and whether the transmitted signal is above the required detection threshold.

In addition, the feedback channel can be used to provide a near real-time measure of the channel so that the data rate being sent can be optimally matched to the maximum signal-to-noise ratio supported by the trail. Adaptive data rates are typically used in the higher data rate meteor-burst communication systems operating at full-duplex.

Investigations by the author into current methods of adaptive data rate techniques has revealed the following shortcomings:

- There appears to be very little information on any other technique other than closed-loop decision-feedback systems for adaptive data rate selection.
- The vast majority of current adaptive data rate systems require full-duplex capabilities for optimal use of their protocols.
- There are no workable solutions or methodologies for prediction of meteor-burst communications trail characteristics from the limited information available in the first few milliseconds of the trail's existence. Predictors of trail type, probable trail duration and trail peak amplitude are essential for an adaptive data rate system without a continuous decision-feedback loop (i.e. open-loop control).

1.3 Thesis claims and summary

This thesis attempts to answer some of the difficulties presented in the problem statement. The emphasis of the work is on the development of relevant and reliable methods of predicting future trail characteristics from information gathered during the first few milliseconds of its existence. Two novel techniques were developed; the first uses the presence or absence of the early fast Doppler phenomenon as a simple predictor of trail type. The second method uses artificial neural networks to estimate trail duration, peak amplitude and trail type, from metrics extracted from the first few milliseconds of trail life. Both techniques were successful.

Each technique has trade-offs in simplicity and performance. The first method is simpler to implement but allows only bi-rate adaptation of the data rate. The second method is considerably more complex but provides better estimation of trail development and therefore finer control of the adaptive data rate. Even though it was not the author's intention to develop new protocols, possible inclusion of these methods in a basic protocol are presented. The use of these predictors, however, goes beyond their application to adaptive data rates and may include applications in trucking and defense systems where trail type and amplitude are important parameters.

This thesis documents the steps taken to derive these techniques. Chapter 2 gives a brief review of current meteor-burst communication protocols and adaptive data rate systems. This serves as the basis for a proposed half-duplex open-loop adaptive data rate system to improve throughput of the meteor-burst communications channel by matching data rate to trail signal-to-noise ratio. The need for meteor-burst communications parametric predictors is shown.

The proposed predictors make use of the amplitude and phase data of the meteor-burst communications link. The system which was used to capture the data from a test link is described in Chapter 3.

Chapter 4 introduces the early fast Doppler phenomenon. Early fast Doppler is then analysed from both an heuristic and statistical viewpoint for use as a trail type predictor. As a result of the investigations, early fast Doppler information is proposed as a method of trail type prediction for bi-rate adaptive data rate protocols without the need for a decision-feedback loop.

For systems requiring more than bi-rate signaling, a more sophisticated approach using artificial neural networks is presented in Chapters 5 and 6. Methods of data preparation and preprocessing are given which are essential for correct neural network operation. Several neural network models are developed and proposed as predictors of trail type and peak trail amplitude in open-loop adaptive data rate schemes without decision-feedback. Parts of Chapter 5 may be omitted by readers with a knowledge of artificial neural networks.

Finally, in Chapter 7 conclusions are drawn based on the findings. Recommendations for future work and possible extensions of the techniques within meteor-burst communications are presented.

Chapter 2

Meteor-burst communication protocols

2.1 Introduction

This chapter reviews typical meteor-burst communication protocols and adaptive rate schemes. These closed-loop systems are compared to a proposed open-loop system which does not rely on the decision-feedback mechanisms of the former, but on channel prediction techniques developed in later chapters.

2.2 Closed-loop meteor-burst communication protocols

There are three types of data transfer protocols that are typical in meteor-burst communication systems: remote-to-master messaging, master-to-remote messaging and master-to-all remotes broadcasting. Intrinsic to all these schemes is the automatic repeat request protocol (ARQ). A simple diagrammatic representation is given in Figure 2-1.

There are many different protocols which have either been adapted for meteor-burst communication use such as the AX.25 protocol and the HX.25 protocol [*Schanker*, 1990] based on the CCITT X.25 [*Black*, 1983] or specially developed such as the draft MIL-STD-188-135C [*NCSOTS*, 1989]. Details of the half-duplex (HDX) and full-duplex (FDX) MIL-STD protocol are shown in Figures 2-2 and 2-3 [*Schilling*, 1993].

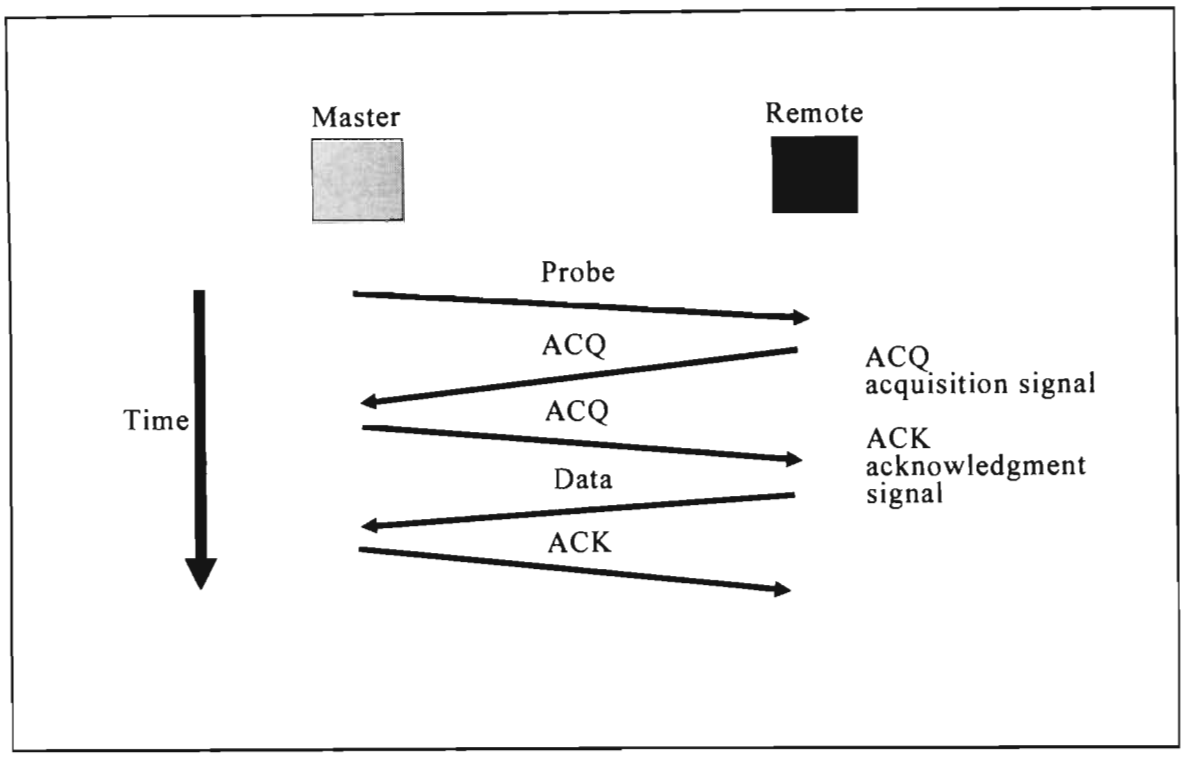

Figure 2-1 Simplified meteor-burst communication ARQ protocol

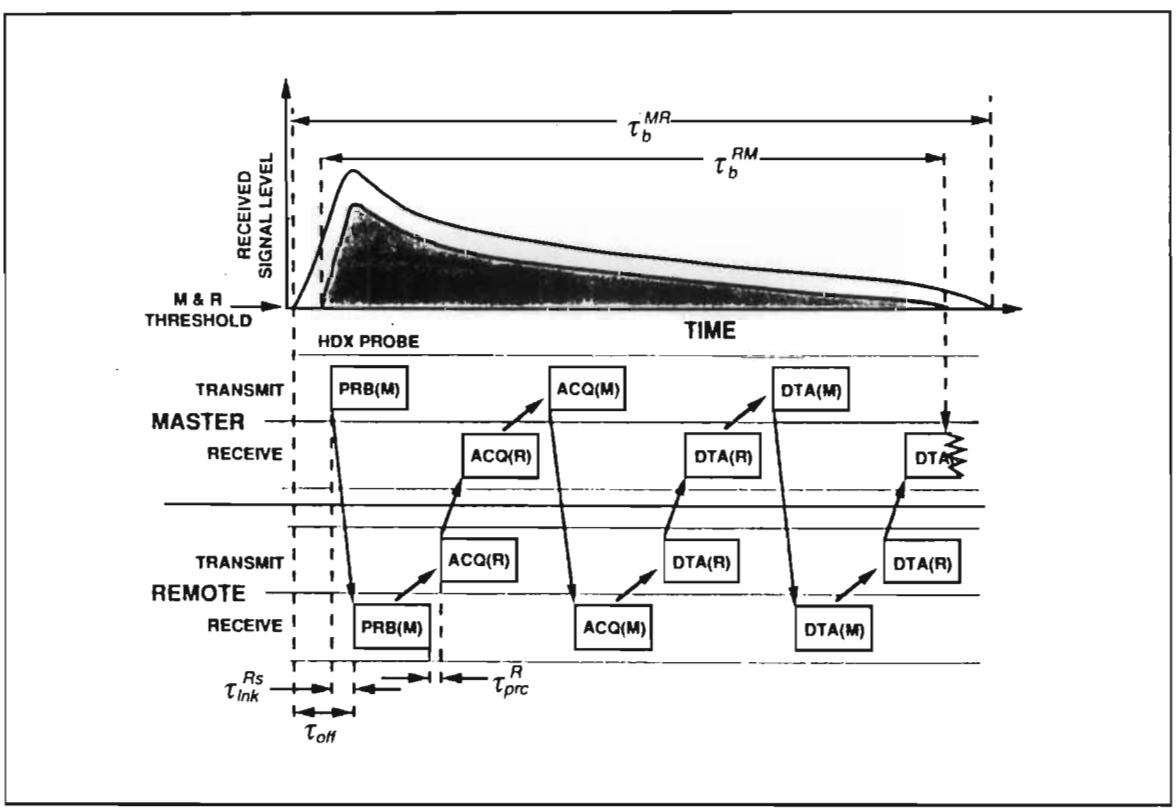

Figure 2-2 Half-duplex MIL-STD protocol, *Schilling* [1993]

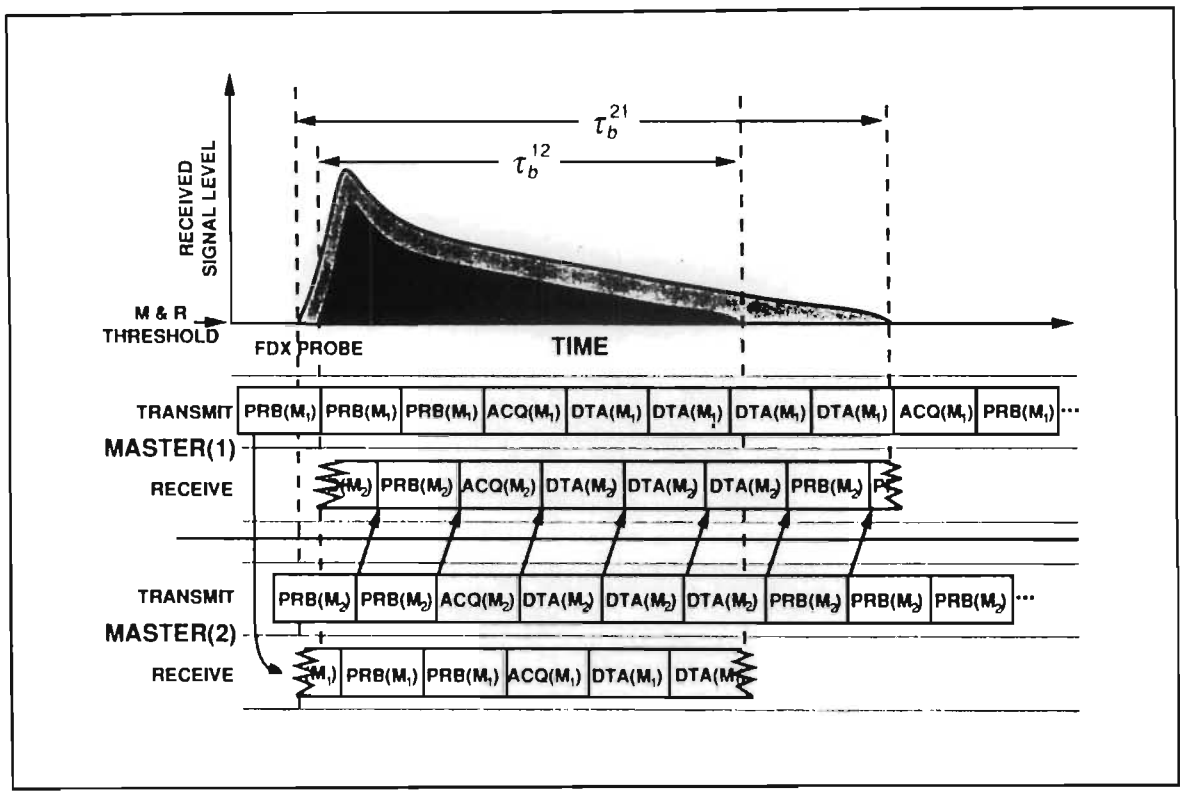

Figure 2-3 Full-duplex MIL-STD protocol, *Schilling* [1993]

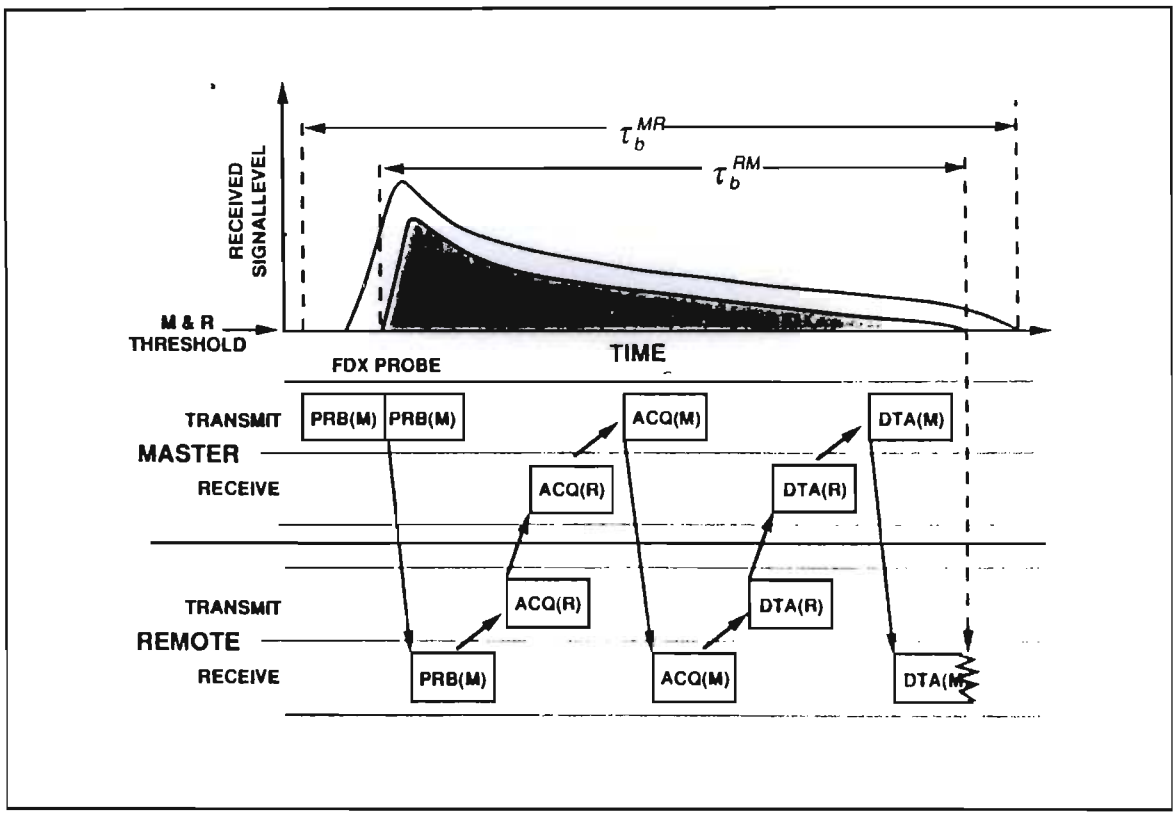

Figure 2-4 Full-duplex-probe MIL-STD protocol, *Schilling* [1993]

Both HDX and FDX protocols define a three-stage process which involves channel probing, link acquisition and data exchange. The master station transmits a short repetitive probing signal to one or more master stations or remote stations. The probe (PRB) of 128 bit duration identifies the transmitting master station by a unique code and provides a signal correlation pattern to assist acquisition. If a usable trail is present between the transmitting and receiving station, the receiving station returns an acquire probe (ACQ) to the originating station. The ACQ signal identifies the station responding and control data. Once this has been correctly received at the originating station, an ACQ probe is sent to the respondent. Once both ACQ probes have been sent and correctly received, data transmission may begin. The data blocks (DTA) consist of a control frame and up to four message frames, each message frame consisting of 14 seven-bit characters and a two-byte checksum. The control frame indicates the last correct message received and points to the message currently being transmitted. This allows decision-feedback to take place in both directions.

In the HDX system there is considerable wastage of useful trail time owing to the idle-time while waiting for responses. The FDX system makes better use of the available channel time but with a cost and complexity penalty. A hybrid combination of these schemes is useful in master-to-remote messaging and is called full-duplex probe (FDX-probe). With FDX-probe, the remote station is capable of transmitting and receiving on two frequencies though not simultaneously. The advantage of this method over HDX is that the probe signals can be transmitted contiguously, eliminating the interprobe delay. This results in more channel time becoming available. The FDX-probe protocol is shown in Figure 2-4.

Common to all these systems is closed-loop control to ensure acquisition, data flow control and acknowledgment. In low-cost telemetry applications, the higher cost of an FDX system force the use of HDX (or FDX-probe) operation despite their inherent inefficiencies.

2.3 Adaptive data rate protocols

Adaptive data rate schemes attempt to perform closer to the Shannon limit of the meteor-burst communication channel, by varying the bit rate to provide an effective continuous signal-to-noise ratio for the channel. This would maximise the number of bits transmitted at a desired error rate by varying the bit duration so that the energy per bit remained constant. This is illustrated in Figure 2-5 [*Schilling*, 1993].

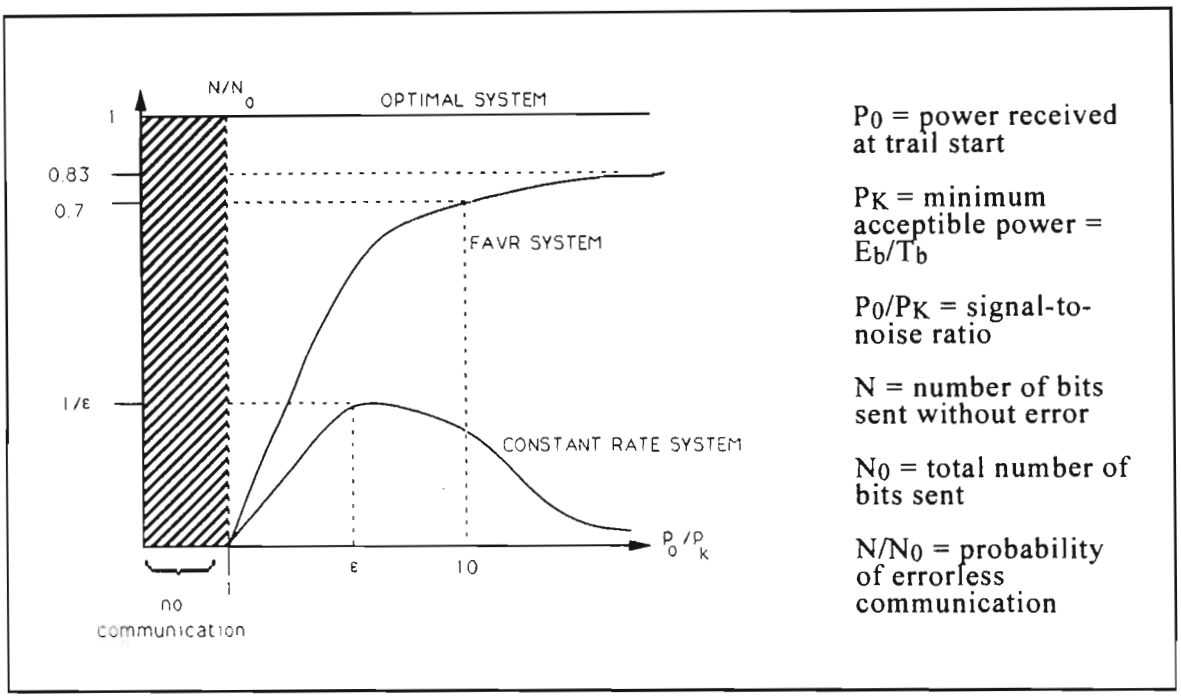

Figure 2-5 Comparison of feedback adaptive variable rate (FAVR) and constant rate systems, *Schilling* [1993].

Several adaptive data rate schemes have been proposed and implemented. *Cavers* [1972] discussed variable rate systems for HF and troposcatter channels. The channel was modeled using a time-varying bit rate approach by *Weitzen* [1983, *Weitzen* et al. 1983, *Weitzen* et al. 1984]. *Weitzen* showed theoretically and by simulation, that a closed-loop variable rate meteor-burst system could achieve superior performance to a fixed rate system. *Abel* [1986] derived two performance bounds, viz. the maximum number of bits that can be sent over a single burst under constant and continuously varying bit rates. However, his work failed to account for the channel statistics with varying trail types. A similar analysis was per-

formed by *Larsen* et al. [1990a, 1990b] which included simulations of adaptive rates using real data from a test link. The feedback adaptive variable rate system (FAVR) [*Schilling*, 1993] highlights the need for accurate and timely determination of the signal-to-noise ratio and communication of the bit rate information between sites. *Meteor Communications Corporation* has implemented a feedback adaptive data rate system based on the signal-to-noise ratio at the receiving station [*Smith & Donich*, 1989]. The system provides a piecewise approximation to the signal envelope as shown below in Figure 2-6. For effective rate adaptation, all the systems and methods described required decision-feedback between stations under closed-loop conditions.

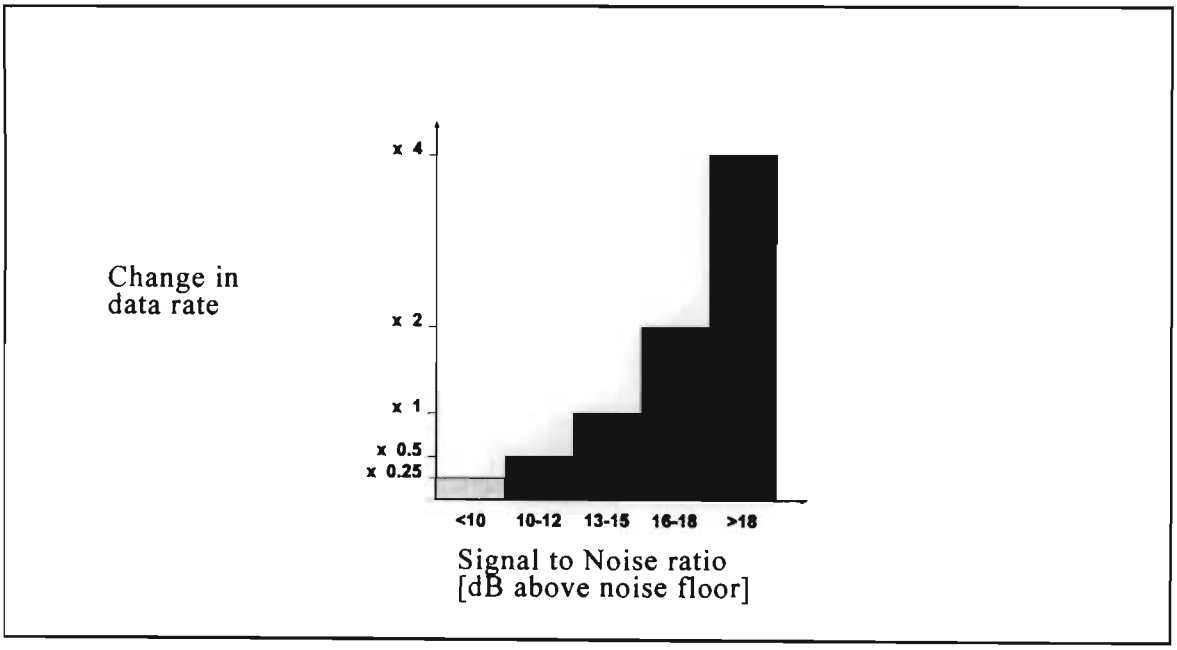

Figure 2-6 *Meteor Communications Corporation's* implementation of a signal-to-noise ratio-based variable data rate system, after *Smith & Donich*[1989]

2.4 Open-loop meteor-burst communication protocols

For both optimal usage of trail duration and effective feedback adaptive data rate systems, a full-duplex system is desirable. There can be near-instantaneous feedback of link signal-to-noise ratio which reduces the granularity of the piecewise approximation of the trail amplitude envelope. However cost constraints for mul-

tiple remote deployment particularly in telemetry applications preclude full-duplex in favour of half-duplex operation. In an HDX application, there are no near-instantaneous feedback mechanisms to facilitate closed-loop adaptive rate signaling. The only mechanism that may be used is the acknowledgment frame following the data frames. However, compared to FDX, the piecewise signal-to-noise ratio approximation would be considerably more coarse.

As a basis for the development of meteor-burst channel predictors, it is proposed that an adapted form of the go-back N ARQ protocol is used in an half-duplex open-loop predictive manner. Open-loop means that no explicit decision-feedback path for data rate adaptation exists between sender and receiver. Figure 2-7 shows the timeline of the proposed open-loop half-duplex predictive protocol:

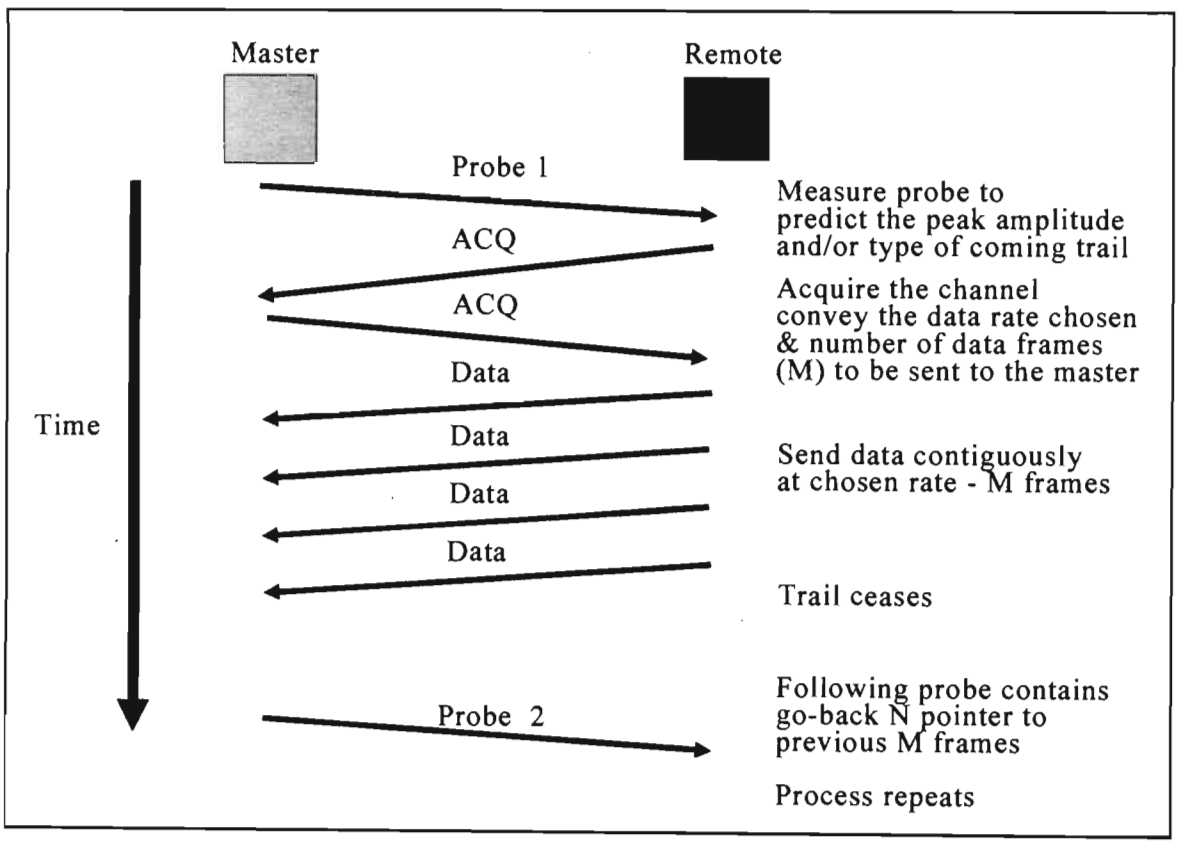

Figure 2-7 Half-duplex open-loop predictive go-back N ARQ protocol

In Figure 2-7 the Probe 1 signal is used to provide an estimate of the characteristics of the remainder of the trail based on the assumption of reasonable link reciprocity. The trail predictor measures the first few milliseconds of the probe. The probe amplitude envelope and/or carrier frequency offset are then processed to give peak trail amplitude and/or trail type predictions. The predictions may be linked to data rate by a lookup table in the remote station.

The ACQ signal from remote to master bears predicted optimal data rate information in addition to the usual synchronisation data. A stream of M data frames are then sent at the data rate appropriate to the predicted trail signal-to-noise ratio without the exchange of handshaking frames, thus saving channel time.

The choice of the number of frames (M) per block may also be estimated at trail commencement. For example the block size would be larger and the data rate higher for a large signal-to-noise ratio overdense trail than a short, low signal-to-noise ratio underdense trail. The receive terminal (master in this case) would update a pointer to the number of correct packets received (M-N). This pointer would then form part of the following probe to the originating remote which would go-back N data frames and recommence the same process.

This scheme, while by no means optimal, provides an improvement over fixed-rate systems by trail-to-trail data rate adaptation in a half-duplex go-back N ARQ protocol without explicit feedback. Furthermore by using no acknowledgment (ACK) frames, channel time is saved. This protocol is ideal for telemetry applications and short messages in which the signal-to-noise ratio fluctuation is small. No further investigation and validation of this protocol was made since the major effort was towards the development of meteor-burst communication predictors.

Chapter 3

Data measurement system

3.1 Introduction

The development of meteor trail predictors such as peak amplitude, trail type and trail duration, requires the amplitude and phase of signal reflections from real trails. A measurement system has been operational in South Africa for several years for the purpose of obtaining a large database of trail signal envelopes. The initial equipment for this test link was developed by *Mawrey* [1988]. It recorded the amplitude of meteor reflections on a continuous basis. Subsequently, it was replaced by equipment developed by the author as part of an MSc programme [*Fraser*, 1990, 1991a]. The data capturing system developed by the author included both amplitude and phase measurement on a continuous basis. This system was used to obtain the data for development of the channel predictors. This chapter briefly describes the measurement system.

3.2 Measurement system details

The measurement system consists of a forward-scatter mid-path illumination link operating between Pretoria (25.6° S 28.0° E) and Durban (29.5° S 31.0° E), South Africa (Figure 3-1). A second temporary link was operational for a few months between Pretoria and Cape Town (Arniston). This link was a long-path forward-scatter link and was configured for both mid-path and end-path illumination. The data presented in this document was obtained from the shorter Pretoria-Durban link.

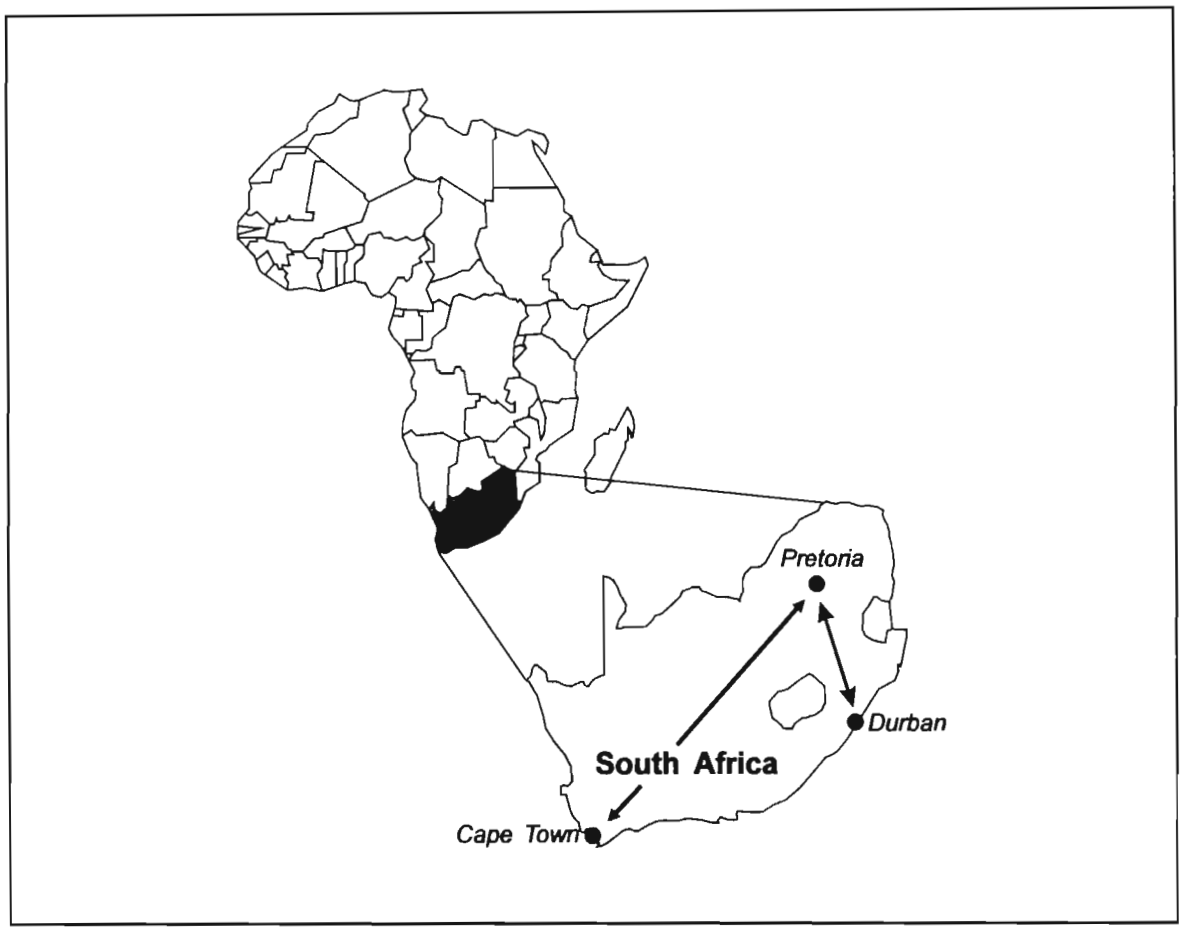

Figure 3-1 Data measurement links between Pretoria and Durban (550km) and Pretoria and Cape Town (1100km), South Africa

The global specifications of the Meteor Monitoring Unit measurement system were defined as follows [*Fraser,* 1990, 1991a]:

- Measurement of signal amplitude & frequency are required
- Measurement of background noise is required
- 5 ms sampling intervals of measured data
- Continuous 24 hour per day data capture
- Interface to IBM PC for data capture & processing
- Equipment must be self-calibrating and self-testing

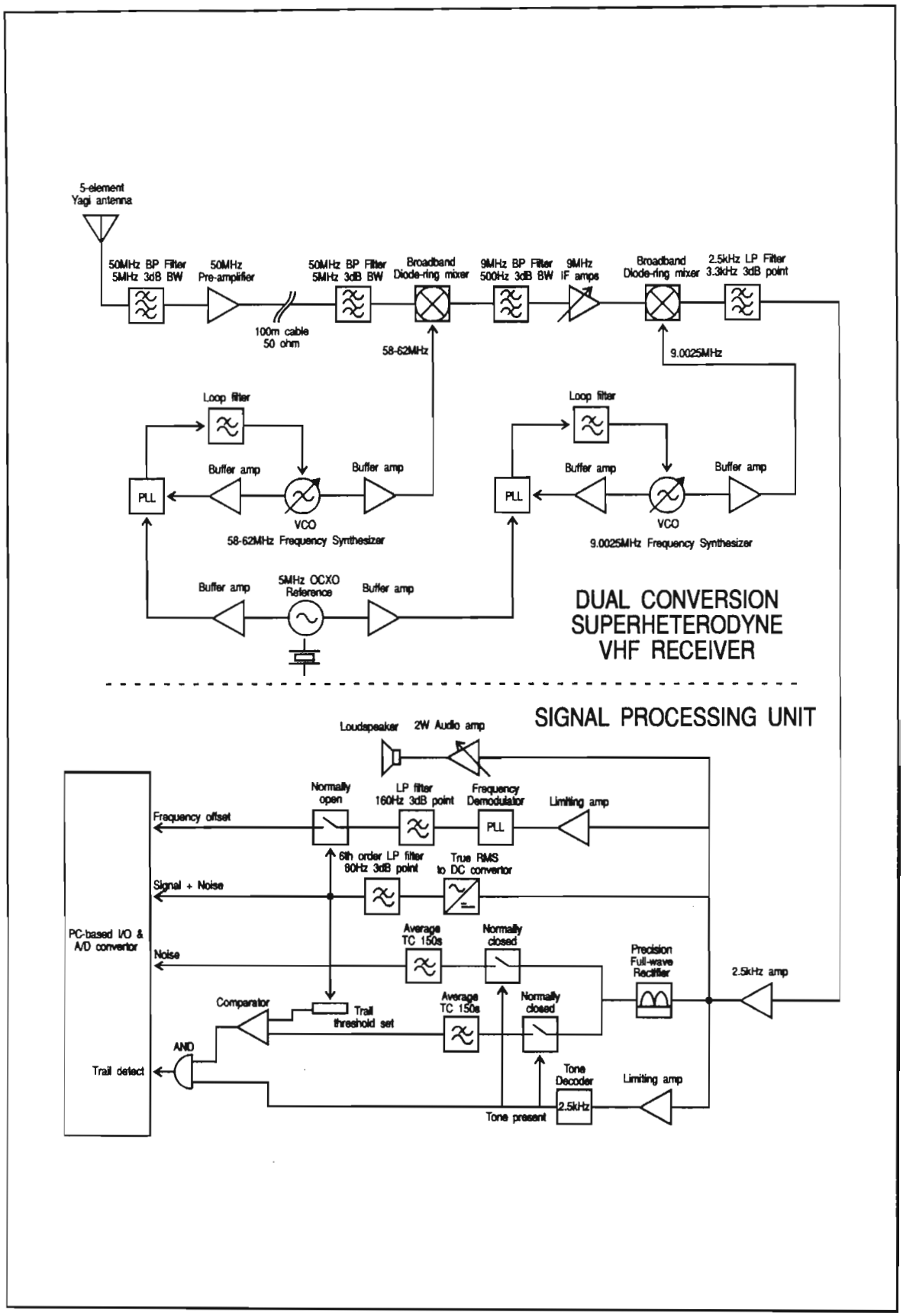

Figure 3-2 Diagram of Meteor Monitoring Unit, *Fraser* [1991a]

A fixed frequency continuous wave (CW) carrier is transmitted from Pretoria and received at Durban. Two transmit frequencies are available, 50.050 and 50.055 MHz. Custom designed VHF receiver and baseband circuitry was constructed by the author to meet the requirements of a Meteor Monitoring Unit. A block diagram for the Meteor Monitoring Unit system is shown in Figure 3-2. The design can be broken into two sections viz. the VHF receiver and the signal processing unit.

The CW signal transmitted from Pretoria is received by a five-element Yagi antenna of conventional design mounted 3 metres above the ground. The preamplifier mounted at the antenna includes a pre-selection filter to reduce interference from FM broadcast stations in the vicinity and thereby reduce possible intermodulation products. The VHF receiver is a dual-conversion synthesized superheterodyne design with good gain and frequency stability. Frequency synthesizers locked to an oven-controlled crystal oscillator (OCXO) in the receiver, provide a high-side oscillator signal of 58-62 MHz as the first local oscillator and a 9.0025 kHz fixed frequency signal as the second. The baseband signal is a 2.5 kHz tone, the result of "detuning" the receiver off the CW carrier by 2.5 kHz. No limitations were placed on the length of signal receivable.

The signal processing unit extracts the signal-plus-noise amplitude, noise amplitude and frequency shift information from the baseband tone. The measurement techniques employed for the signal-plus-noise channel, noise channel and trail detect monitoring are similar to those developed by *Mawrey* [1988]. The signal-plus-noise amplitude of the 2.5 kHz tone was converted to the equivalent DC level by an RMS-to-DC convertor with a 60 dB dynamic range. For the noise channel, the long-term averaged wideband input noise power was represented by a corresponding DC level. To exclude trail amplitudes from the noise average, the gated noise path was opened during the presence of a trail. This was achieved using a narrow-band tone decoder that triggered in the presence of a 2.5 kHz tone, opening the gates shown in Figure 3-2. Using this method, the errors caused by trail breakthrough are less than 2% [*Mawrey*, 1988].

As an indication of a valid trail, the level of the signal-plus-noise channel is compared to the average noise level and if above a predetermined signal-to-noise ratio (usually 10-13 dB), the trail detect output is triggered. Once the trail has diffused, the trail detect output returns to its low state.

Measurement of frequency shift in the received carrier used a variation of the continuous wave technique described by *March* [1966], *Sander* et al. [1966] and *Stone* et al. [1975]. The carrier is stabilized at the transmitter by a 5 MHz oven-controlled crystal oscillator (OCXO) whose specifications claim a long-term drift in frequency of 0.015 Hz per day and 0.01 Hz per degree celsius temperature change. Short-term drifts in frequency were considerably less than these figures. A reference OCXO with similar performance was used in the Meteor Monitoring Unit receiver. *March* [1966] showed that the change in frequency of the received carrier reflected by a meteor trail is around 1-2 Hz for the body of the trail. For the system to resolve this change with an error of around 10%, the short-term stability of the reference oscillators would have to be better than 0.1 Hz. In the measurement system, the OCXO's had short-term drifts which were at worst a factor of 100 smaller than the minimum stability required. Temperature changes were minimised by operating both transmitter and receiver in an air-conditioned environment.

In the variation of *March's* technique that was used, the phase of the received signal is interpreted from the time rate of change of phase, i.e. frequency shifts. The received signal is frequency modulated by the rate of change of phase of the meteor trail reflection coefficient. A phase-locked loop acts as an FM demodulator to produce a DC output proportional to the frequency offset from the centre frequency. The control voltage of the PLL's VCO represents the frequency offset from the 2.5 kHz centre frequency by ±100 Hz.

Rather than using *March's* method of quadrature components to determine whether the rate of change of phase was increasing or decreasing, the sign of the

frequency offset indicates this by a positive or negative prefix respectively. Thus a sliding tone from 2.6 kHz to 2.5 kHz produces a negative value and hence a decrease in the rate of change of phase (i.e. frequency).

Similarly, a fixed tone represents no variation in the rate of change of phase. Provided absolute phase knowledge is not required, measurement of received frequency offset is simpler than direct phase measurements since these require the maintenance of phase-locked references at both transmitter and receiver.

Finally in the Meteor Monitoring Unit, the signal-plus-noise, noise and frequency offset channels are sampled at a rate of 200 Hz (5 ms intervals) by a PC-based 12 bit analog-to-digital convertor for processing, display and storage. The sampling interval provided sufficient resolution of meteor-burst characteristics without the collection of vast amounts of redundant data.

Software was developed by *Rodman* [1991] in conjunction with the author to buffer, store and display amplitude, frequency and noise data and statistics. The software also controlled Meteor Monitoring Unit functions such as system calibration and operating frequency selection. Table 3-1 gives the measured system parameters.

Elimination of bad data owing to noise or interference was achieved by two methods, viz. gating the signal (Figure 3-2) and by post-processing received data. Automatic post-processing placed unusual data into one of two categories, "unknown" or "bad data" depending on the severity of the interference. These categories were removed from the data set.

Table 3-1 Measured Meteor Monitoring Unit performance, *Fraser* [1991a]

	Measured Parameter
Transmit power	350 W
System centre frequency	50 MHz tunable by ±4.5 MHz
System bandwidth (3 dB)	550 Hz
Spurious-free dynamic range	70 dB
Gain stability (50 °C Range)	±1.25 dB
Measured gain linearity	0.01 dB change per 1 dB increment from -140 to -80 dBm at constant temperature
Measured gain stability	0.2 dB change per 24 hours at constant temperature
System frequency stability over 50 °C range	0.75 Hz
System noise figure	5.9 dB
System noise floor	-146.3 dBm
Sensitivity (10 dB S/N)	0.14 μV
3rd order intercept	+20 dBm
Input VSWR	1.02:1
Input filter rejection of broadcast signals	70 dB

3.3 Measured data

The measurement system was used to sample the received amplitude and frequency offset signals of over 100000 trails. Software developed by *Melville* [1991a, 1991b] post-processed the sampled signals to provide a graphical view of the envelopes. It also helped to derive the statistics of the early fast Doppler and body Doppler regions of the trail envelope as well as the maximum frequency-offset from 2.5 kHz. Figure 3-3 represents the received amplitude of a CW signal reflected by a trail. For this figure only, the receiver was tuned exactly on frequency to produce a zero hertz baseband. The baseband signal was stored using a Hewlett Packard low-frequency analyser. Therefore changes from the 0V axis are caused by the amplitude and frequency modulation effects of trail reflection coefficient. The sharp transition from the early fast Doppler period at trail commencement to the body Doppler period in the rest of the trail can be clearly seen 100 ms after the signal rises above the noise.

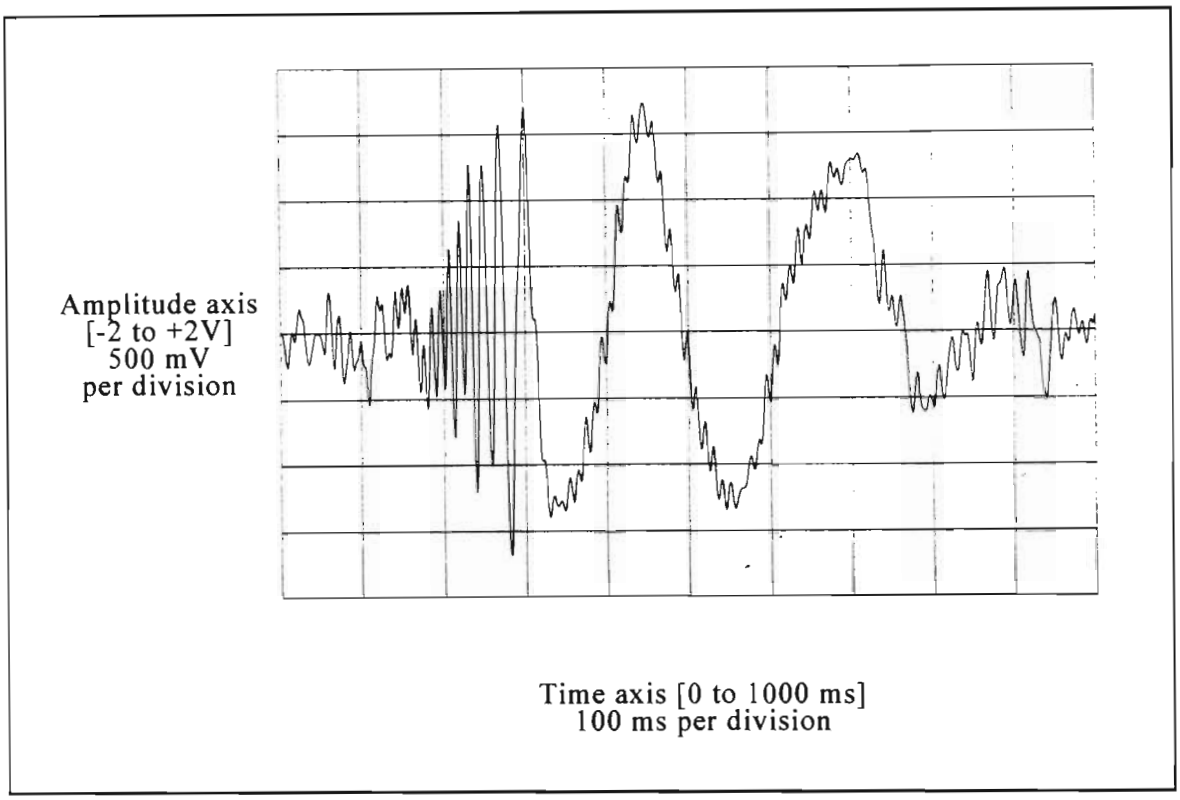

Figure 3-3 Received signal from the reflection of a CW carrier by a meteor trail. The signal is mixed to 0 Hz baseband to reveal the amplitude and phase characteristics of the MBC channel, *Fraser* [1991a].

Figures 3-4 and 3-5 show typical overdense and underdense trail amplitude and frequency-offset envelopes with time. Both exhibit a near-zero frequency-offset for the majority of their lifetime. This is characteristic of body Doppler. In order to show trail amplitude and phase characteristics in these diagrams, the received signal was referenced to the 2.5 kHz baseband signal.

Figure 3-6 shows a long overdense trail with pronounced early fast Doppler at the trail commencement and thereafter very little frequency offset during the period of body Doppler.

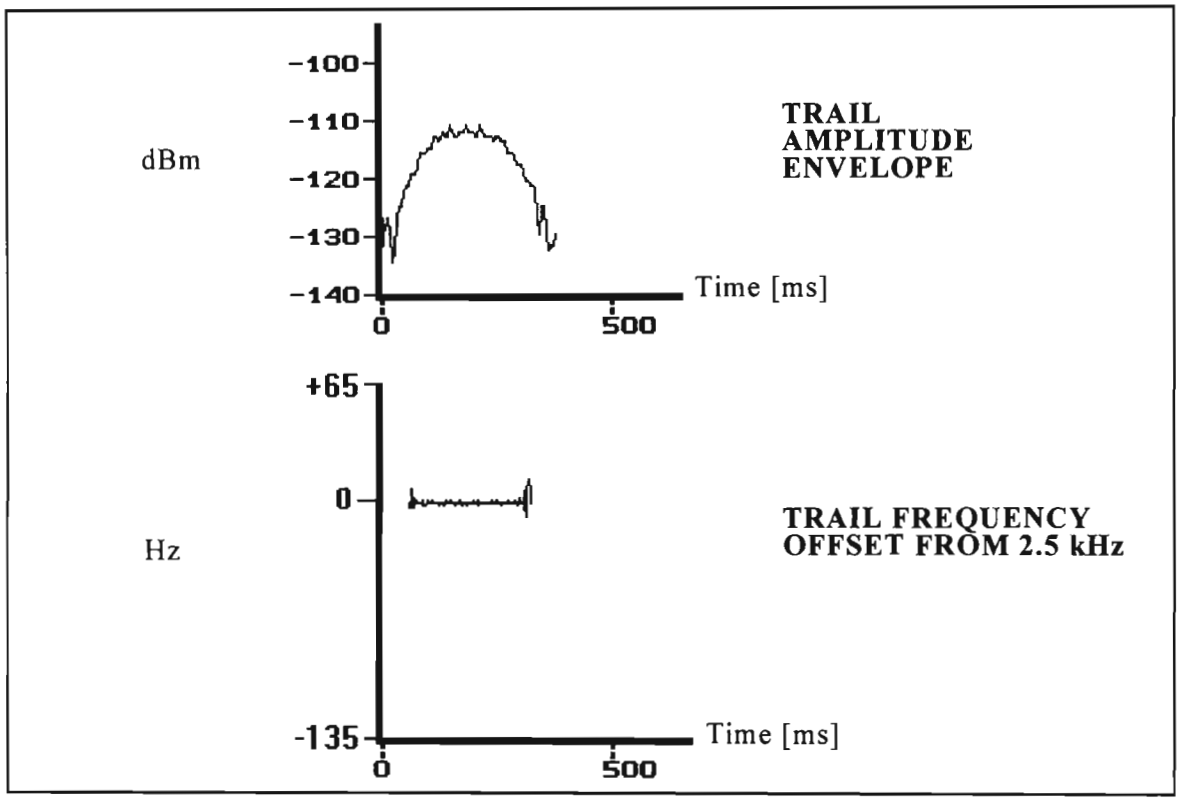

Figure 3-4 Typical overdense trail, *Fraser* [1991a].

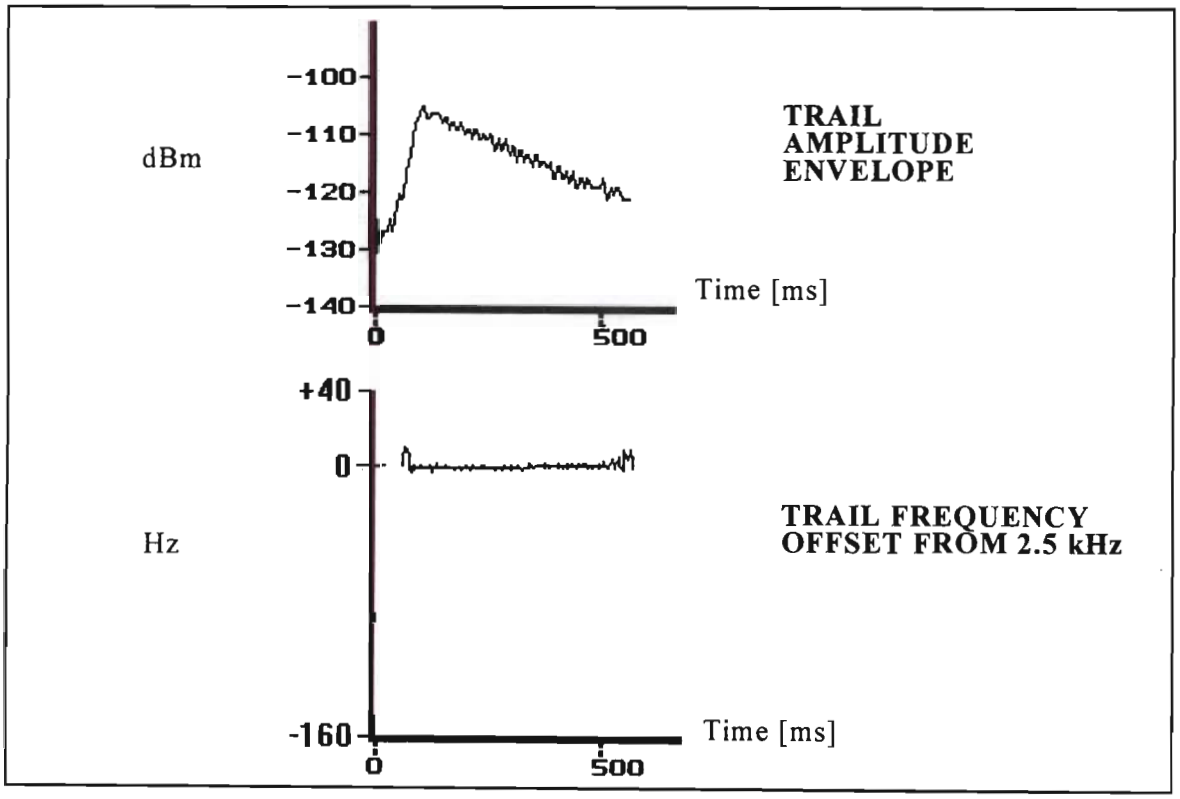

Figure 3-5 Typical underdense trail, *Fraser* [1991a].

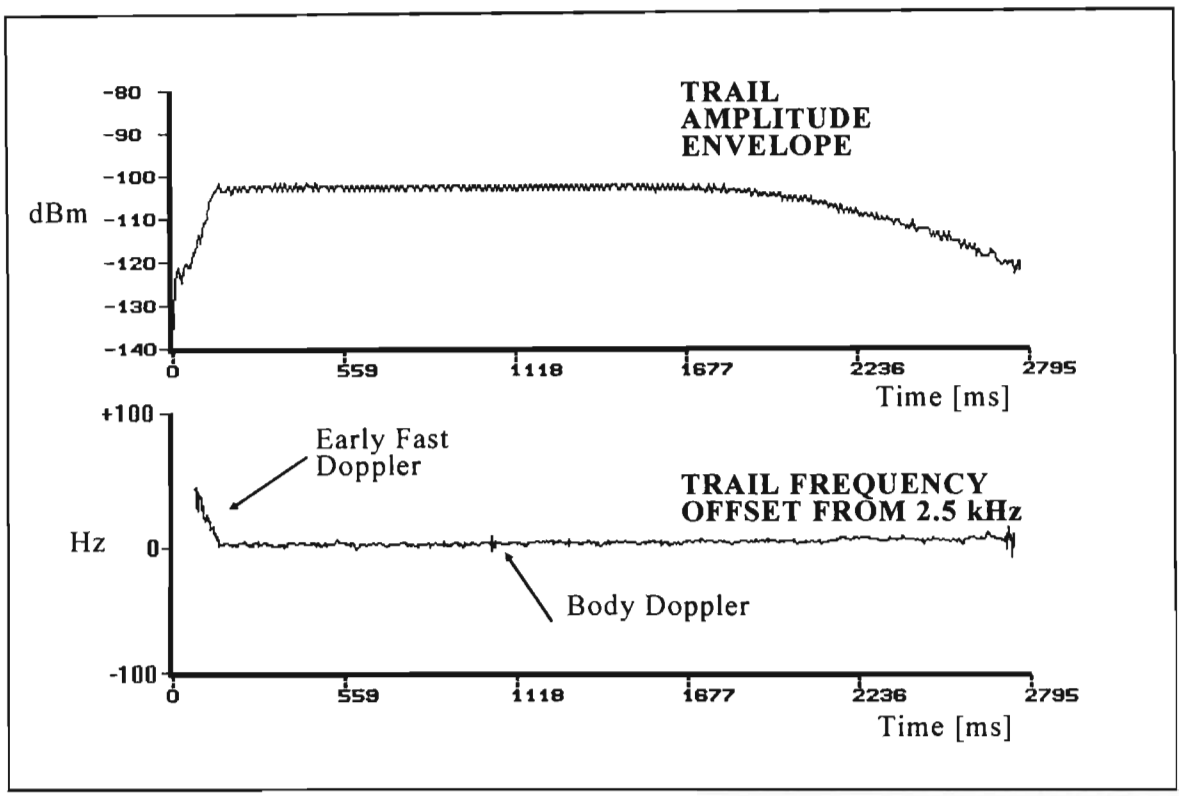

Figure 3-6 Typical overdense trail, *Fraser* [1991a].

3.4 Conclusion

The Meteor Monitoring Unit constructed performed according to specification and provided the data necessary for investigation of predictors in meteor-burst communication. In comparison to its predecessor, the Meteor Monitoring Unit provided five major improvements:

- measurement of frequency offset and signal amplitude
- detection of many more trails of smaller amplitude due to a narrower system bandwidth
- compact, easily maintainable equipment
- improved PC control of Meteor Monitoring Unit functions such as archiving and data processing
- a greatly enhanced PC-based user interface.

Chapter 4

Early fast Doppler for meteor-burst channel prediction

4.1 Introduction to phase effects

The phase characteristics of the meteor-burst communications (MBC) channel have been investigated by several researchers such as *Stone & March* [1975], *Lovell & Clegg* [1948], *McKinley* [1961], *Kaiser* [1953a, 1953b], *Greenhow & Neufeld* [1956], *Manning, Villard & Peterson* [1952], and more recently *Grossi & Javed* [1978] and *Weitzen* et al. [1983]. Historically, trail phase aberrations were mostly used as a method of studying meteor phenomena. This led to most early work concentrating on back-scatter radar measurements. Later research emphasised the use of meteor trails as a communications medium with the focus on phase as a limiting factor in high speed meteor-burst data communications. The work performed by the author served to confirm and extend the results previously obtained, and provide a basis for the prediction of meteor phase mechanisms, [*Fraser*, 1989a, 1989b, 1991a].

Any communications channel may be characterised in terms of amplitude and phase. For an ideal channel, the received and transmitted signals differ only in amplitude and phase. If, as is the case with the meteor-burst channel, the phase of the received signal changes with time, a frequency shift in the signal occurs. The instantaneous frequency $\omega(t)$ of the received signal is given by Equation (4-1) :

$$\omega(t) = 2\,\pi f(t) = \omega_c + \frac{d\varphi(t)}{dt} \qquad [\text{rad.s}^{-1}] \tag{4-1}$$

where

ω_c is the carrier frequency of the signal [rad/s]
$f(t)$ is the carrier frequency of the signal [Hz]
$\varphi(t)$ is the time varying phase of the signal [rad]

The phase distortion of the signal may be found by taking the time integral of the received radian frequency (Equation (4-2)). This condition holds so long as the phase stability of the reference oscillator at the transmitter and receiver is far greater than that of the time varying channel.

$$\varphi(t) = \int(\omega_c \pm \omega(t))\,dt = \omega_c\,t \pm \int\omega(t)\,dt \qquad [\text{rad}] \tag{4-2}$$

The phase changes in meteor-burst communication are primarily a combination of early fast Doppler and body Doppler effects [*Stone & March*, 1975].

4.2 Phase mechanisms

4.2.1 Early fast Doppler

Early fast Doppler occurs at the commencement of meteor trail formation as the meteor transits the principal Fresnel zone. With respect to a fixed carrier signal, early fast Doppler produces a rapidly changing received frequency of a few tens of hertz. This transient effect may last up to 200 ms but is often more short-lived [*Stone & March*, 1975]. A typical phase-versus-time plot is shown in Figure 4-1.

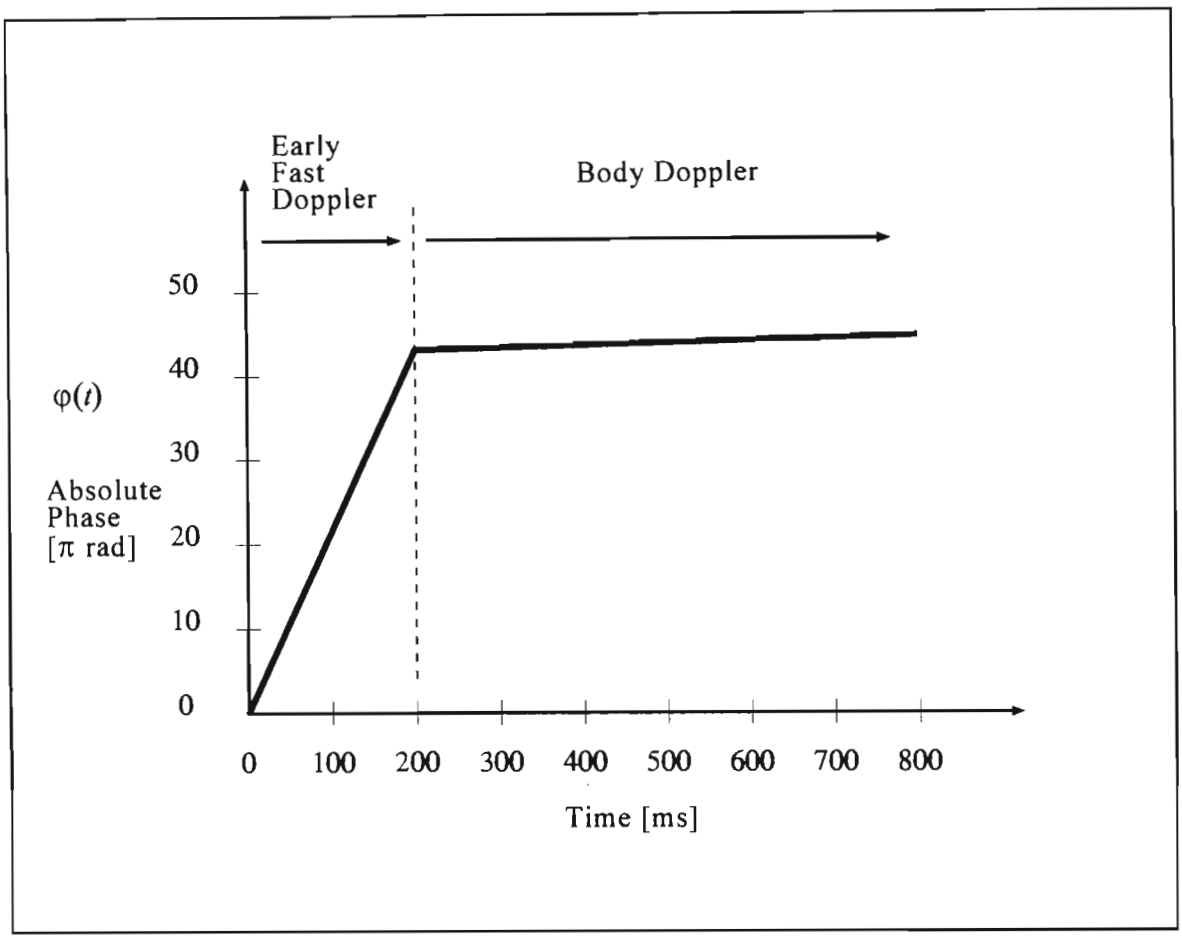

Figure 4-1 Measured phase profile showing early fast Doppler during the first 200 ms, after *Stone & March*, [1975]

The rapid change in phase attributable to early fast Doppler is clearly seen in the first 200 ms. Thereafter, the change in phase is small by comparison. Early fast Doppler is caused by the combination of three main effects: diffraction, head echo, and resonance. These combined produce the largest continuous rate of change of phase in the lifetime of the trail.

Diffraction effects were first noted by researchers such as *Lovell & Clegg* [1948] who showed that the equations applicable to the diffraction of radio waves from a single reflection point at the head of a trail are analogous to those obtained from optical theory for the diffraction of light at a straight edge. Their results, confirmed by a backscatter radar experiment, show that the amplitude and phase of a radiowave scattered from a meteor trail prior to the formation of the principal Fresnel

zone are governed by the solution of the Fresnel integral for geometrical diffraction. *McKinley* [1961] showed that the effects of diffraction found in backscatter radar measurements would also be present in forward-scatter links, but that the effects would be considerably attenuated. Thus if early fast Doppler is seen on a forward-scatter link, the trail will be of a high amplitude. The transformation between back- and forward-scatter is described by *McKinley* [1961]. The power received from an underdense trail over a forward-scatter link (Figure 4-2) is given by *Sugar*, [1964] and adapted to include the effects of diffraction (which produce amplitude and phase fluctuations early in trail lifetime), [*McKinley*, 1961]:

$$P_R = \frac{P_T G_T G_R \lambda^3 q^3 r_e^2 S_p^2}{16 \pi^2 R_1 R_2 (R_1 + R_2)(1 - \sin^2\varphi \cos^2\beta)} \exp\left(\frac{t}{\tau} + t_i + r_i\right) \cdot \left[\frac{C^2 + S^2}{2}\right] \qquad (4\text{-}3)$$

where

$\tau = \frac{\lambda^2 sec^2\varphi}{32 \pi^2 d}$ is the time constant of the reflected signal power

$t_i = \frac{-32 \pi^2 d\, t_0}{\lambda^2 sec^2\varphi}$ is the increase in trail radius by diffusion

$r_i = \frac{-8 \pi^2 r_0^2}{\lambda^2 sec^2\varphi}$ is the loss caused by electron re-radiation when the radius of the trail at formation is comparable to the λ

P_T and P_R are the transmit and receive power [W]
G_T, G_R is the transmit and receive antenna gain respectively
λ is the radio wavelength [m]
q is the electron line density [e^-/m]
r_e is the radius of an electron [$\approx 2.8\times10^{-15}$m]
S_p^2 is the antenna polarization factor described
R_1 & R_2 the distances of the transmitter and the receiver to the trail [m]
φ is the half angle between R_1 and R_2 [rad]
β is the angle between the trail axis and the plane containing the transmitter, receiver and trail [rad]
d is the radial diffusion constant of the meteor trail [m^2/s]
r_0 is the initial trail radius [m]

C is the cosine Fresnel integral $= \int_{x_1}^{x} \cos \frac{\pi x^2}{2} dx$

S is the sine Fresnel integral $= \int_{x_1}^{x} \sin \frac{\pi x^2}{2} dx$

where $x = \sqrt{\frac{2s}{R_0 \lambda}}$

s is the distance traveled by the meteor head in time t

R_0 is the perpendicular line from the transmitter to the trail

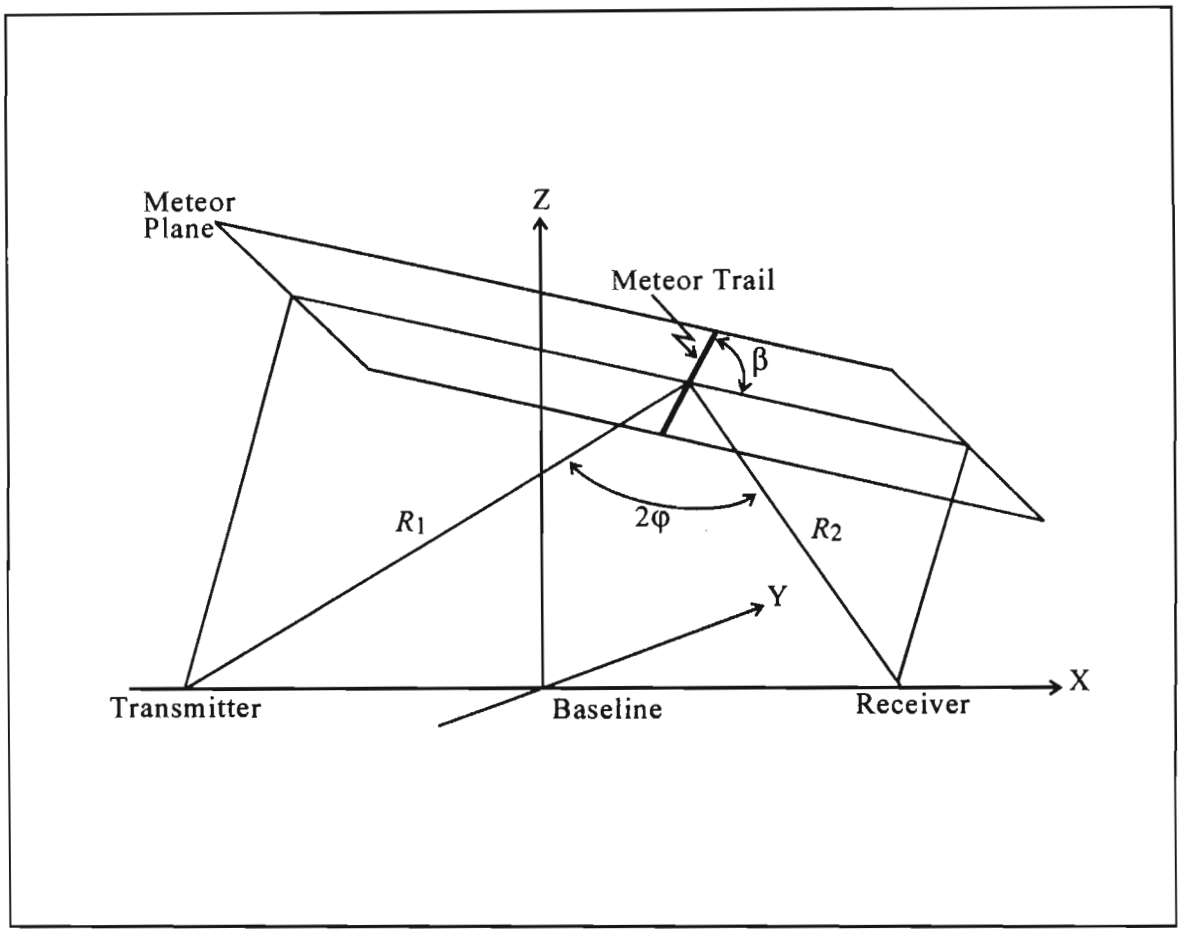

Figure 4-2 Forward-scatter meteor trail reflection geometry

Until the principal Fresnel zone is formed, a weak reflection comes from the part of the incomplete trail that corresponds to the shortest transmission path at that instant. This reflection is usually from the meteor at the head of the trail causing a shift in frequency due to the motion of the effective reflecting point. As the meteor

approaches the principal Fresnel zone, the frequency shift tends to zero and the received frequency decreases with time.

A secondary effect which occurs early in the lifetime of underdense trails is resonance which is caused by the restoring force of the electrons displaced from equilibrium to positions normal to the trail [*Kaiser*, 1953a, 1953b, 1955]. However *Greenhow & Neufeld* [1956] showed that this effect is infrequent and can be neglected.

Of all the effects that occur before principal Fresnel zone formation, the dominant effect is that of reflection from the meteor itself at the head of the meteor trail. The effect of a "moving head" comes from small near-spherical regions of intense ionization surrounding the ablating meteoroid.

4.2.2 Determination of Early Fast Doppler

Determination of early fast Doppler is based upon the length of the principal Fresnel zone (see Figure 4-30 and the velocity of the meteor. The length of the principal Fresnel zone is also a function of the link geometry. By the time the principal Fresnel zone has been established, early fast Doppler ceases to exist. The frequency spread caused during principal Fresnel zone formation is thus [*James & Meeks*, 1956], [*Weitzen*, 1983]:

$$f_{EFD} = \frac{V_m}{2L} = \frac{V_m}{2\left[\dfrac{\lambda R_1 R_2}{(R_1 + R_2)\,(1 - \sin^2\varphi \cos^2\beta)}\right]^{\frac{1}{2}}} \quad [s^{-1}] \tag{4-4}$$

where

V_m is the meteor velocity [m/s]
L is the half length of the principal Fresnel zone [m]
λ is the wavelength [m]
β is the angle between the trail axis and the plane containing the transmitter, receiver and trail [rad]
R_1 and R_2 are the distances from Tx and Rx to the trail [m]
φ is the half-angle between R_1 and R_2

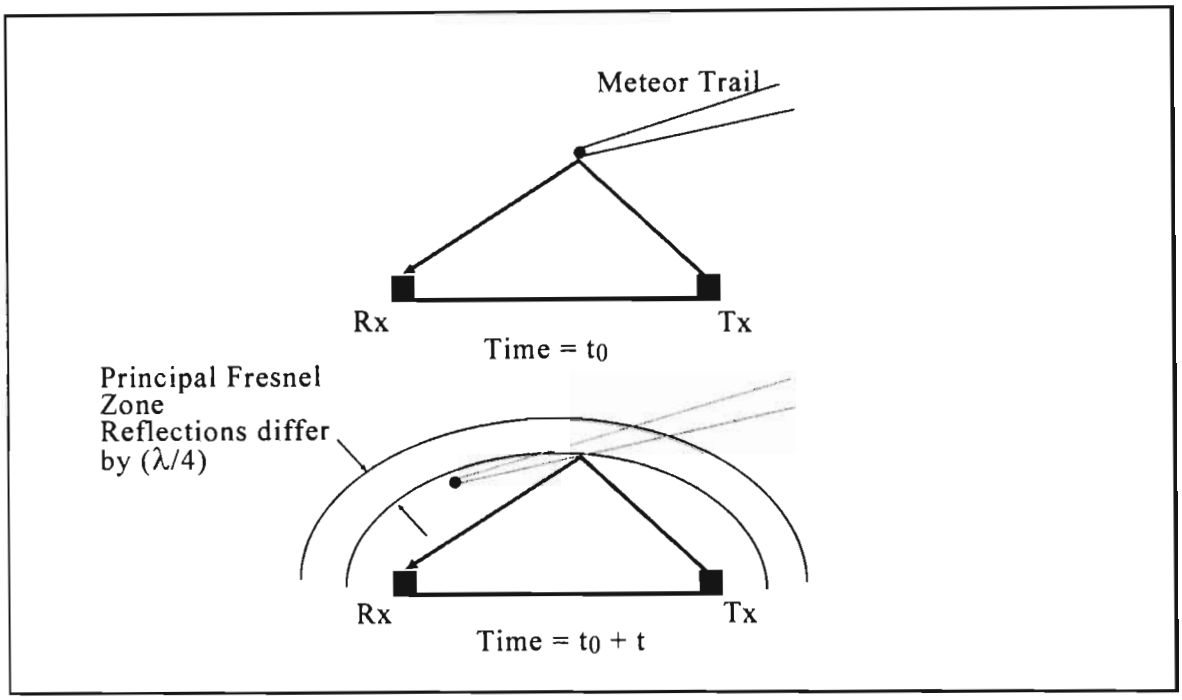

Figure 4-3 a) Meteoric head reflection, b) Meteoric trail reflection after principal Fresnel zone

The system parameters which were used to estimate early fast Doppler and body Doppler spread are given in Table 4-1. They represent the mean geometrical values for a mid-path forward-scatter link between Pretoria and Durban. A spread in values is expected owing to the velocity distribution of the meteors and changes in path length geometry. Figure 4-4 shows a meteor velocity profile as a percentage of meteor trails.

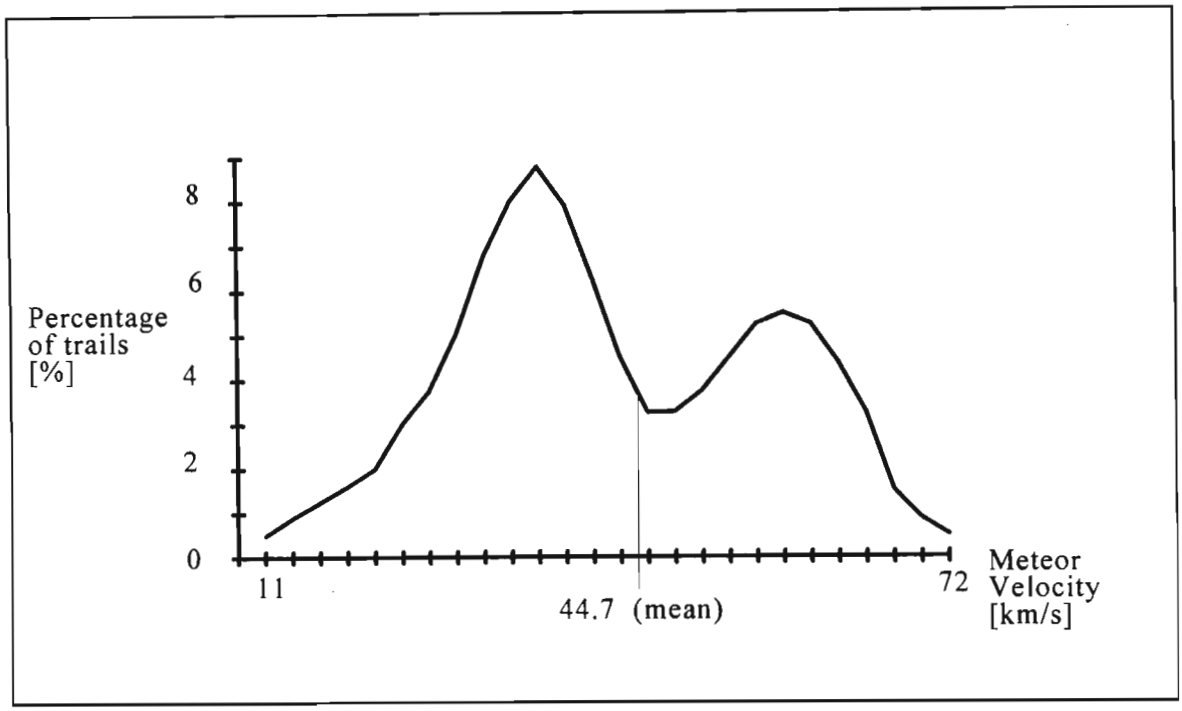

Figure 4-4 Meteor velocity profile, after *McKinley*, [1961]

4.3 Predicted & measured early fast Doppler results

The results of the comparison between predicted and measured early fast Doppler results are found in Table 4-1 for the mean path parameters of the Pretoria to Durban midpath link, [*Fraser* 1991a, 1991b, 1991c, *Fraser & Broadhurst* 1993b]. The results confirmed the findings of previous researchers and revealed interesting properties of early fast Doppler.

The spread in received early fast Doppler frequencies about the 38.7 Hz mean due to the velocity distribution of sporadic meteors can be expected. The measured body Doppler spread of 1.5 Hz (mean) is of minor importance to meteor-burst communications in comparison with early fast Doppler [*Weitzen et al.*, 1983], [*Weitzen*, 1986], [*Fraser*, 1991a, 1991b, 1991c]). Early fast Doppler and body Doppler measurements correlated closely with the values predicted.

Table 4-1 Results of early fast Doppler measurement for the mean link

Path geometry parameters for the mid-path forward-scatter test link			
Receiver position - Durban, South Africa			29.5° S 31.0° E
Transmitter position - Pretoria, South Africa			25.6° S 28.0° E
Mean normal distance from Tx to meteor - R_1			256 km (mid-path)
Mean normal distance from Rx to meteor - R_2			256 km (mid-path)
Mean half internal angle between Rx & Tx to meteor - φ			71°
Mean angle between trail axis and plane containing Tx, Rx & trail - β			56°
Mean meteor velocity - V_m			35 km/s
Mean meteor height - h			95 km
Radio wavelength - λ			6 m
Measured and predicted early fast Doppler for the mid-path forward-scatter test link			
		Measured	**Predicted**
Peak early fast Doppler deviation	mean	38.7 Hz	33.9 Hz
	std. dev.	17.6	-
Early fast Doppler duration	mean	89.3 ms	76.4 ms
	std. dev.	51.4	-
Early fast Doppler slope	mean	433.3 Hz/s	-
	std. dev.	292.4	-
Peak signal amplitude of trails exhibiting early fast Doppler	mean	-103.9 dBm	-
	std. dev.	5.9	-
Total duration of trails exhibiting early fast Doppler	mean	1597.6 ms	-
	std. dev.	961.4	-
Early fast Doppler duration as a % of total trail duration in trails exhibiting early fast Doppler	mean	5.6 %	-
% of trails per hour exhibiting early fast Doppler	9.04 %		
%of long trails with early fast Doppler (>500 ms)	30.2 %		

4.4 Heuristic analysis of early fast Doppler for trail parameter prediction

The purpose of this section is to examine the use of early fast Doppler parameters e.g. frequency spread and duration to give an indication of the type of trail to follow, its peak amplitude and its duration. This basis of the analysis is heuristic, i.e. learning by observation. This work is documented by the author in [*Fraser*, 1991d, 1992, 1993, *Fraser & Broadhurst* 1993b]

4.4.1 Early fast Doppler occurrence and hourly meteor-burst communication duty cycle

The sample set of trails (100000 in total) consisted of 9.04 % trails which exhibited early fast Doppler and 90.96% trails without early fast Doppler. However, when comparing the trails which exhibit early fast Doppler to those which do not, it was

found that the trails in which early fast Doppler occurs are generally long-duration and/or large amplitude trails. This means that out of the sample of long trails (arbitrarily defined as being 500 ms or longer in duration), 30.2 % of these contain some early fast Doppler at their commencement. To determine whether early fast Doppler gave any indication of trail parameters, distributions of these parameters were plotted for trails exhibiting early fast Doppler phenomena.

4.4.2 Trail amplitude distribution

The peak amplitude for trails in the data sample exhibiting early fast Doppler is shown in Figure 4-5.

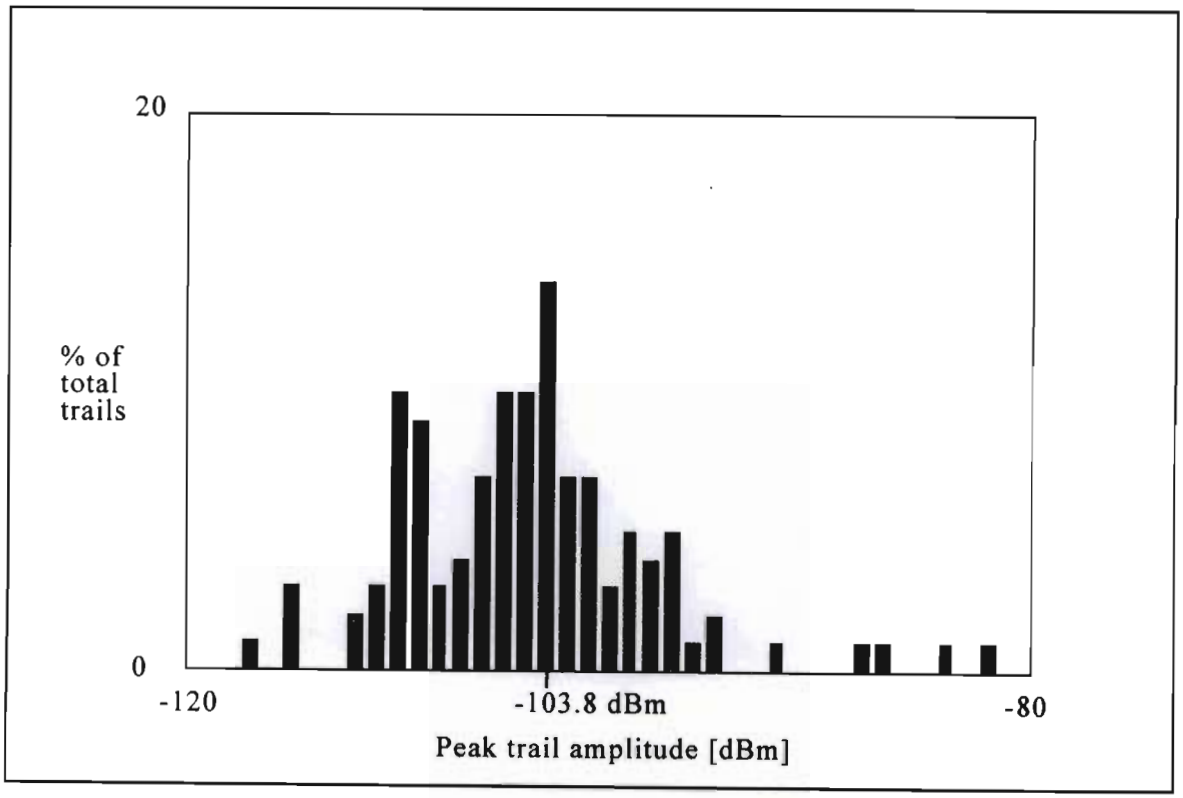

Figure 4-5 Peak trail amplitude distribution in trails exhibiting early fast Doppler, mean = -103.8 dBm, horizontal step size 1 dB

It was found that the mean of the amplitude distribution was -103.9 dBm with a standard deviation of 5.9. The significance of this is that when early fast Doppler is detected, irrespective of its frequency spread or duration, a peak signal amplitude of about -104 dBm can be expected. This distribution of meteor amplitudes is Gaussian with a dB scale. The distribution for underdense trails was first described by *Weitzen* et al. [*Weitzen* et al. 1990] and the distribution of underdense trail durations by *Ralston* et al. [1993]. The findings presented here include both overdense and underdense distributions.

The effects of the standard deviation of 5.9 are reduced when considered against the mean background noise, which varied between 14 and 32 dB above the noise floor of -146.3 dBm [*Fraser*, 1991a]. With a typical mean background noise level of -128 dBm, the signal-to-noise ratios of the large trails exhibiting early fast Doppler would be about 25 dB (mean).

The peak received amplitude normally occurs at the termination of early fast Doppler effects [*Stone & March*, 1975]. This condition occurs when the reflection off the moving meteoric head becomes insignificant in comparison to the reflection from the trail body, which will reach a peak at the time of formation of the principle Fresnel zone (see Figure 4-3).

4.4.3 Trail duration distribution

For all trail types exhibiting early fast Doppler, there is a very wide distribution of values for trail duration (see Figure 4-6). From this there appears to be little significance in the use of early fast Doppler to predict trail length for all trail types. However, comparison between early fast Doppler presence and trail durations for specific trail families may be significant. It is still significant though, that early fast Doppler does not occur in small-amplitude, short duration trails but generally in those of 300 ms to 2500 ms duration. This is not to say that they do not occur in trails of greater than 2500 ms, only that in the dataset used, the longest trail with early fast Doppler was 2500 ms long.

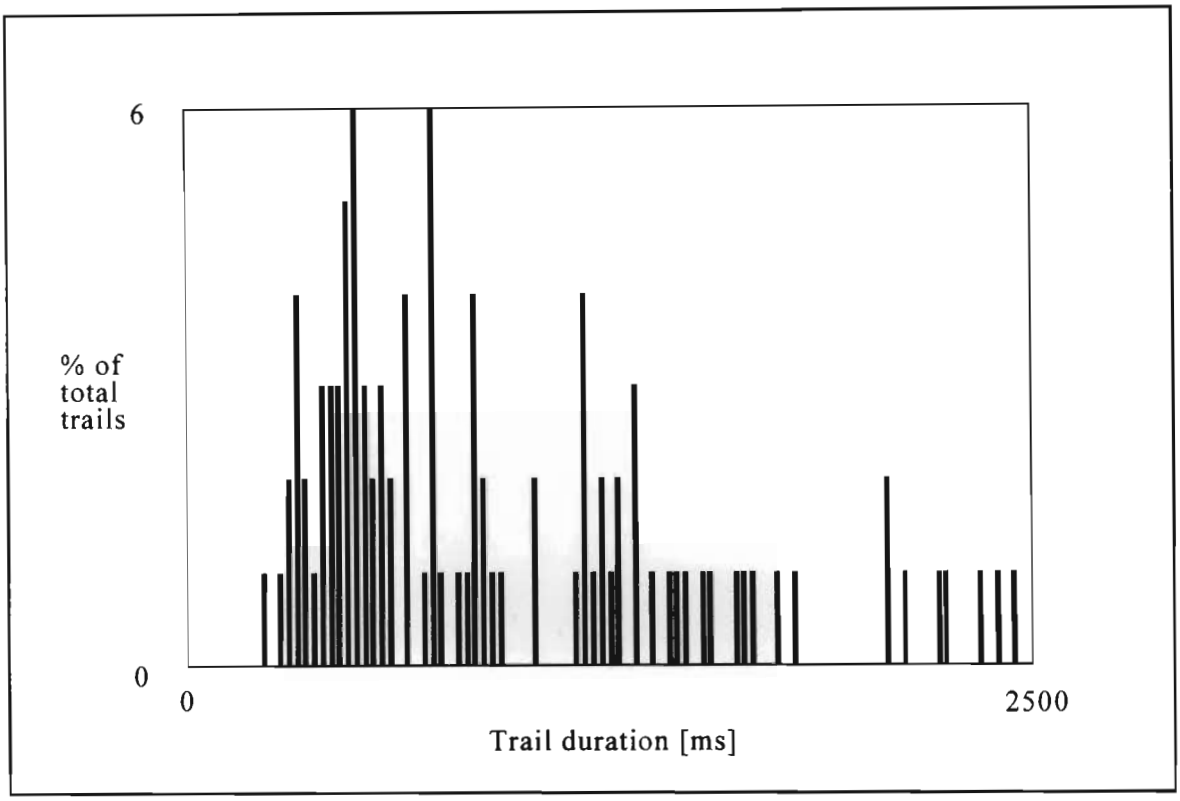

Figure 4-6 Trail duration distribution in trails exhibiting early fast Doppler, mean = 1597 ms, horizontal step size 25ms

4.4.4 Early fast Doppler frequency spread distribution

Early fast Doppler frequency spread is defined as the range of frequency deviation from the carrier centre frequency. Most times, the frequency offset due to early fast Doppler commences at a large deviation, say 30 Hz, and reduces with time till the deviation from the carrier is zero (ignoring body Doppler of 1-2 Hz). Thus the range or spread of early fast Doppler is said to be 30 Hz.

The recorded data has a mean early fast Doppler spread of 38.7 Hz and a standard deviation of 17.6. There is a band of frequencies between which the values fall. Referring to equation (4-4), the lower and upper bounds of the band are governed by meteors traveling at the escape velocity of the earth (approximately 11 km/s) and the escape velocity of the solar system (42 km/s at one A.U.) respectively.

In equation (4-4), for a fixed link geometry, φ, R_1 and R_2 can be assumed to be fixed. The values for V_m and β are however dependent on the meteor velocity and trajectory respectively. The variation in the early fast Doppler spread can be accounted for by variations in both of these parameters as will be shown in section 4.6. Figure 4-7 shows that the range of early fast Doppler values is wide and that there appears to be no significant shape to the distribution.

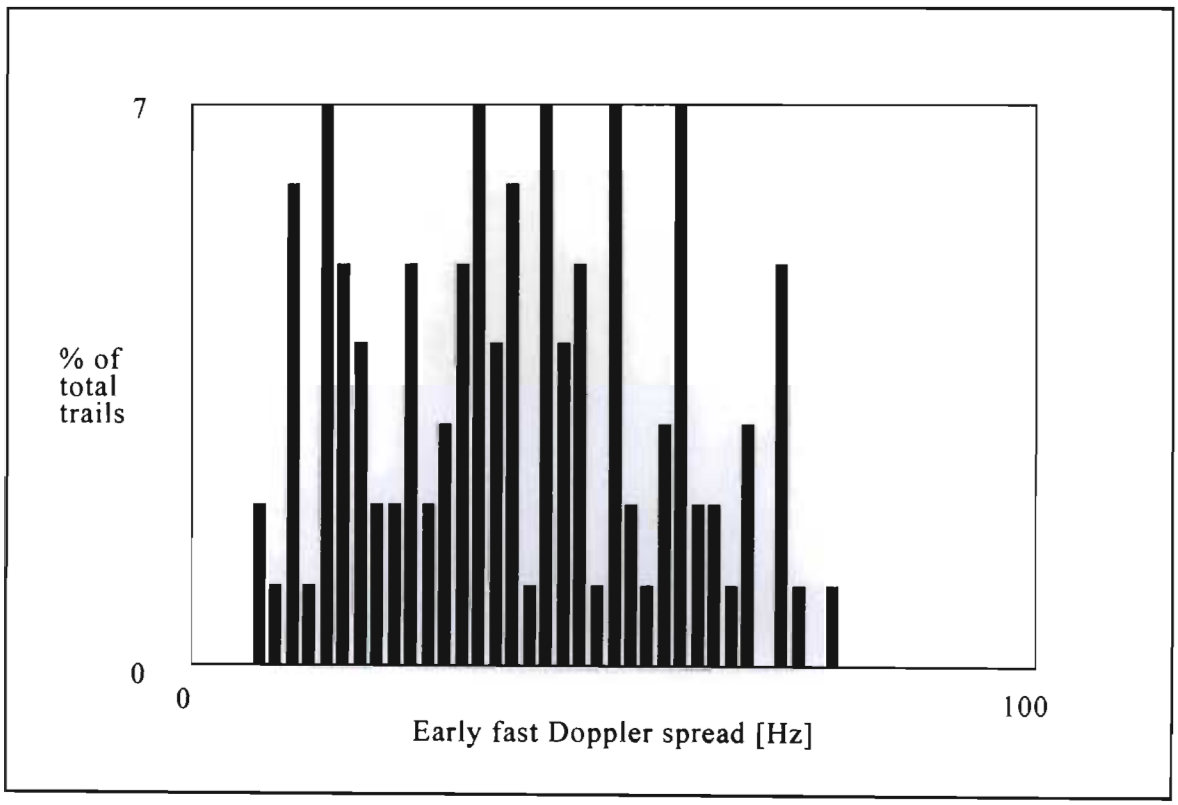

Figure 4-7 Early fast Doppler frequency spread, mean = 38.7 Hz, horizontal step size 2 Hz

4.4.5 Early fast Doppler duration distribution

The early fast Doppler duration is given as the time from trail commencement to formation of the principle Fresnel zone. Thus for a given geometry, the length of the principal Fresnel zone can be calculated using (4-4). The time for the meteor to transit this region is then simply given as the ratio of the length of the principal Fresnel zone to the meteor velocity. The distribution of early fast Doppler duration for the trails measured yielded a mean of 89.3 ms with a standard deviation of 51.4 (Figure 4-8). As with early fast Doppler frequency spread, the early fast Doppler duration is dependent on V_m and β. With early fast Doppler duration and early fast Doppler spread, the standard deviations are both approximately 50% of the mean, indicating a similar statistical dependence on V_m and β.

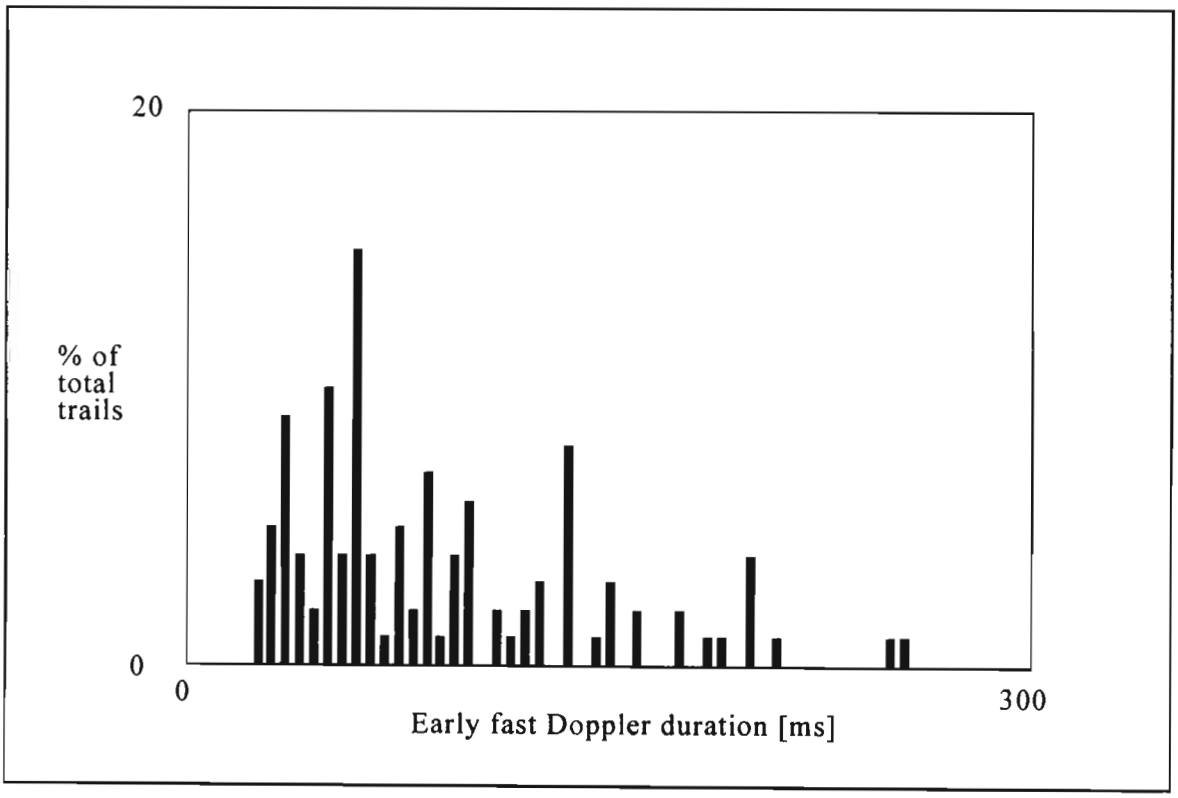

Figure 4-8 Early fast Doppler duration, mean = 89.3 ms, horizontal step size 5 ms

4.4.6 Early fast Doppler slope distribution

The ratio of the early fast Doppler spread to the early fast Doppler duration is termed the early fast Doppler slope (in Hz/s). It is an indication of the rate of change with time of the received frequency with respect to a stable carrier frequency. This distribution has a mean of 433.3 Hz/s and a standard deviation of 292.4 (Figure 4-9). Once again, there is a wide range of early fast Doppler slopes in trails exhibiting this phenomenon.

Despite the wide range of early fast Doppler slopes, it is important to note that the slope generally does not change significantly for the period of early fast Doppler presence (see Figure 3-6). Thus it could be safely predicted that the slope measured during the first few milliseconds will be the same as that at the end of early fast Doppler. This implies that it may be possible to use the slope of the early fast Doppler to pre-categorize trails prior to the formation of their peak amplitude.

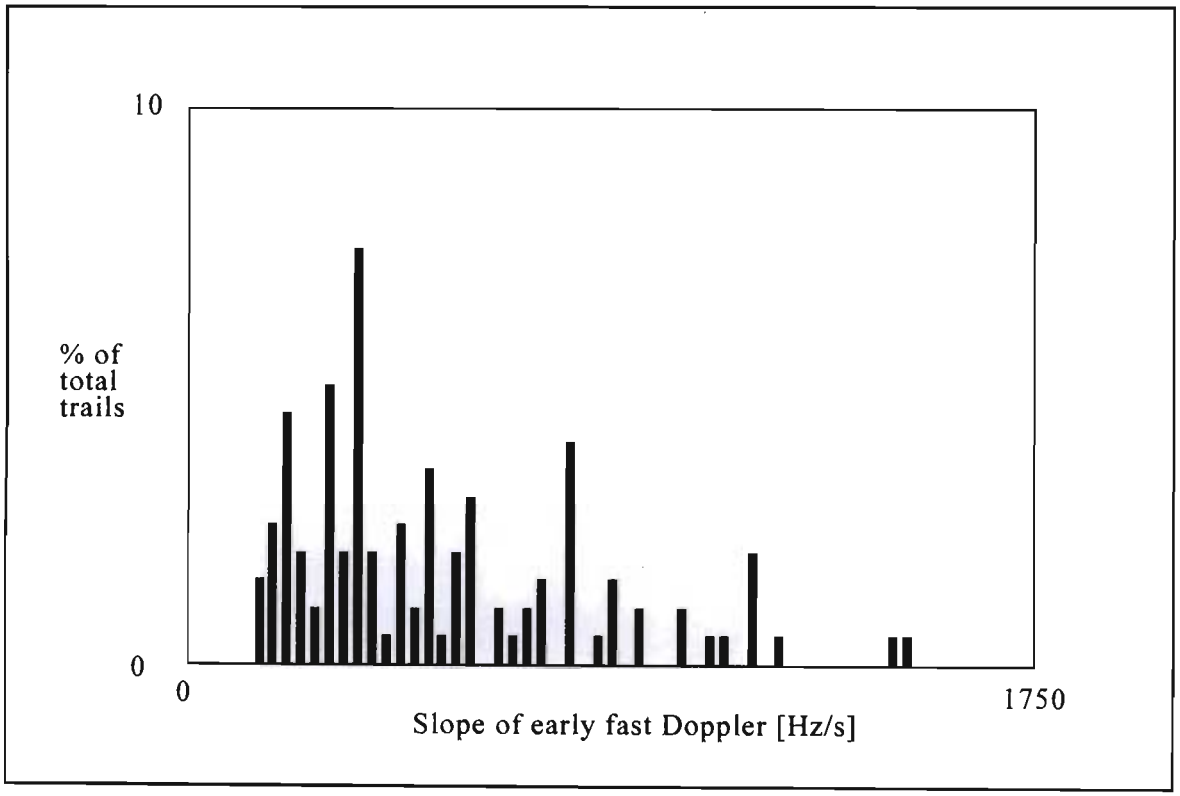

Figure 4-9 Early fast Doppler slope distribution, mean = 513.9 Hz/s, horizontal step size 25 Hz/s

4.4.7 Conclusion

From an heuristic point of view, early fast Doppler provides a rough estimation of the the peak amplitude of the trail that it precedes. As such the presence or non-presence of early fast Doppler could be used as a toggle in real-time decision processes such as adaptive data rates (see section 4.7). The following section investigates whether any good statistical correlations between early fast Doppler and subsequent trail characteristics exist.

4.5 Statistical analysis of early fast Doppler for trail parameter prediction

The purpose of the statistical correlation of early fast Doppler to trail parameters is to see whether early fast Doppler parameters can statistically predict either the types of trails to come or some parameter which may be used to increase data throughput. Scatter plots of the correlation between early fast Doppler and trail parameters were made and the correlation coefficient calculated. Only a representative sample of the total database of trails is shown on the scatter plots.

4.5.1 Early fast Doppler spread and trail duration correlation

Correlation between the early fast Doppler frequency spread (in Hz) and the total trail duration (in ms) was performed to see whether trail duration was predictable from early fast Doppler. The correlation coefficient was particularly low at 0.112 indicating very little dependence of trail duration on early fast Doppler spread (see Figure 4-10).

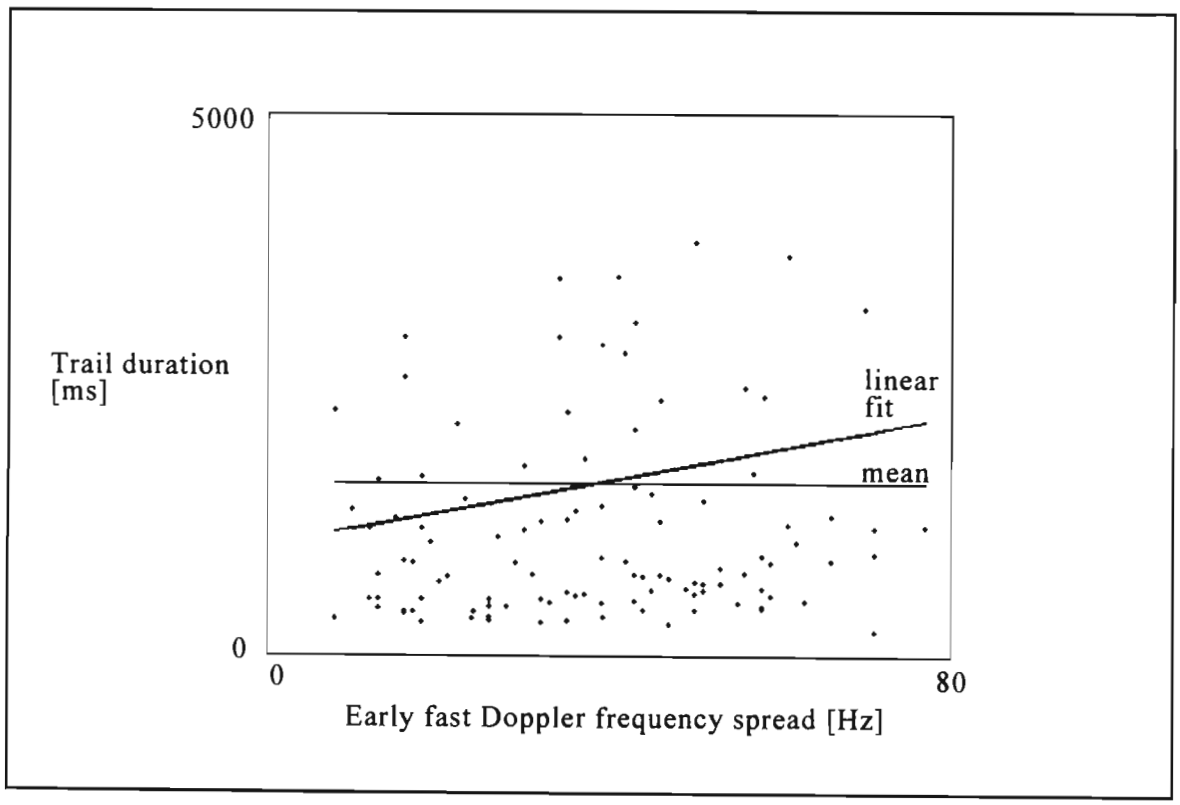

Figure 4-10 Correlation between early fast Doppler frequency spread and trail duration

One of the most obvious reasons for the poor correlation is the fact that the early fast Doppler spread is based primarily on the meteor velocity and entry geometry whilst the trail duration is mainly dependent on the meteor mass or size [*McKinley*, 1961]. Momentum of meteoric particles ($M \times V_m$) is not constant, since not all large particles travel slowly nor do all small particles travel at high speed. Thus the correlation between meteor velocity V_m and meteoric mass M is poor and cannot be used for prediction of trail duration.

4.5.2 Early fast Doppler duration and trail duration correlation

Similarly it was found that there exists a correlation of only 0.44 between the early fast Doppler duration and the trail duration, (see Figure 4-11). Thus early fast Doppler duration appears to be unsuitable as a predictor of trail duration.

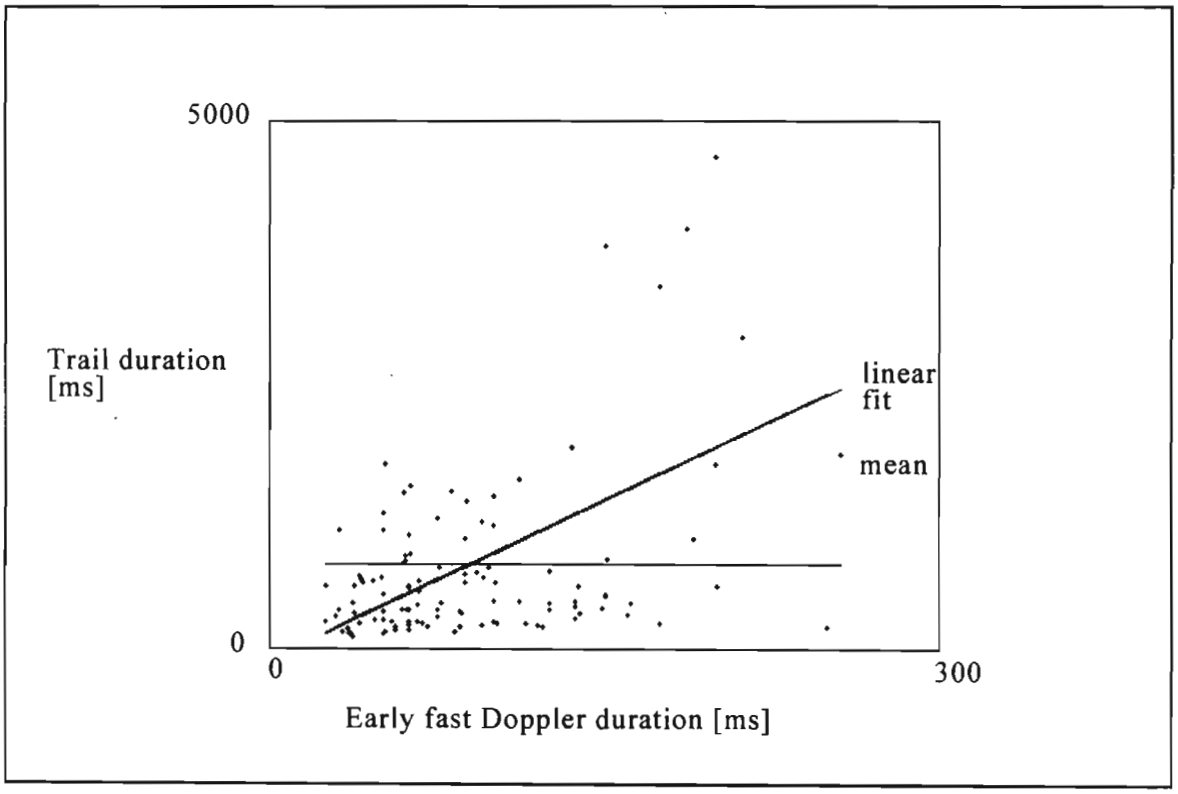

Figure 4-11 Correlation between early fast Doppler duration and trail duration

4.5.3 Early fast Doppler spread and trail peak amplitude correlation

The relationship between early fast Doppler frequency spread and peak trail amplitude shows an even poorer correlation of around 0.429 (see Figure 4-12). It seems too that early fast Doppler spread cannot be used for peak amplitude prediction.

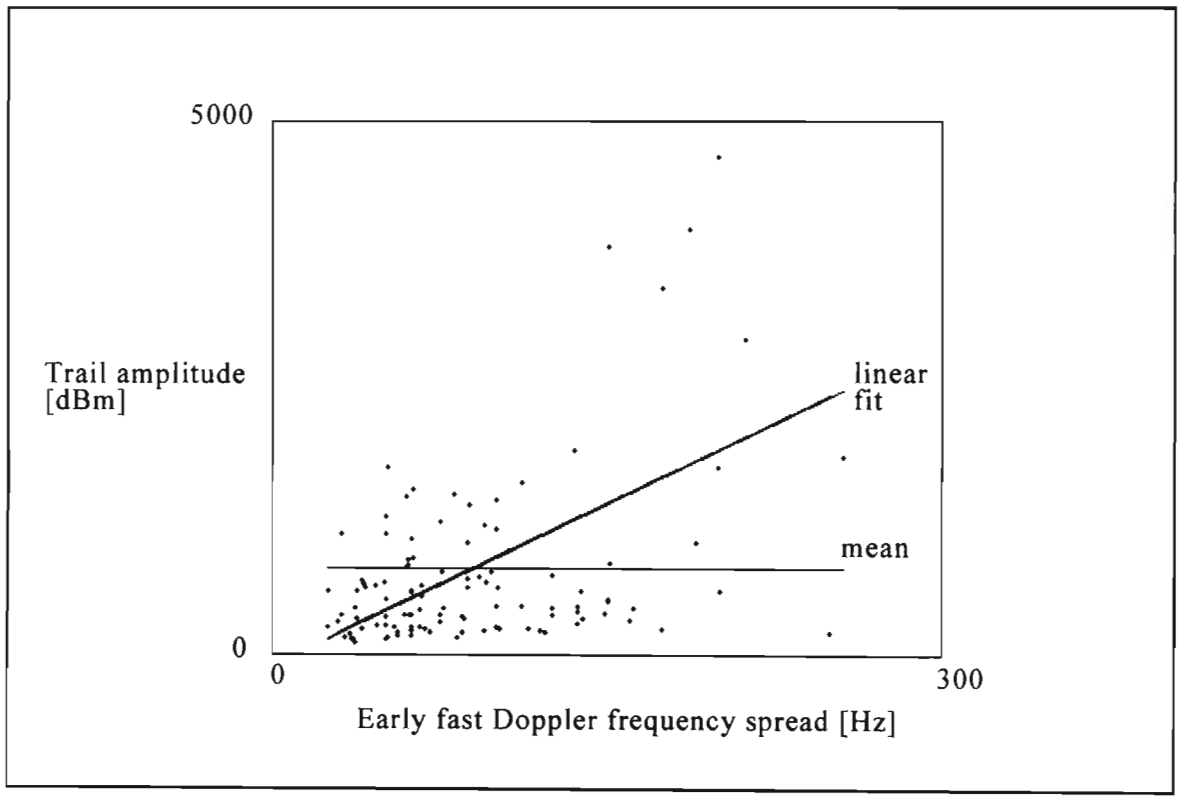

Figure 4-12 Correlation between early fast Doppler frequency spread and peak trail amplitude

4.5.4 Early fast Doppler duration and trail peak amplitude correlation

This comparison yields the best correlation compared with the previous three at a figure of 0.51 (see Figure 4-13). Though not statistically significant, there does appear to be an increase in trail amplitude with increased early fast Doppler duration in the sample data.

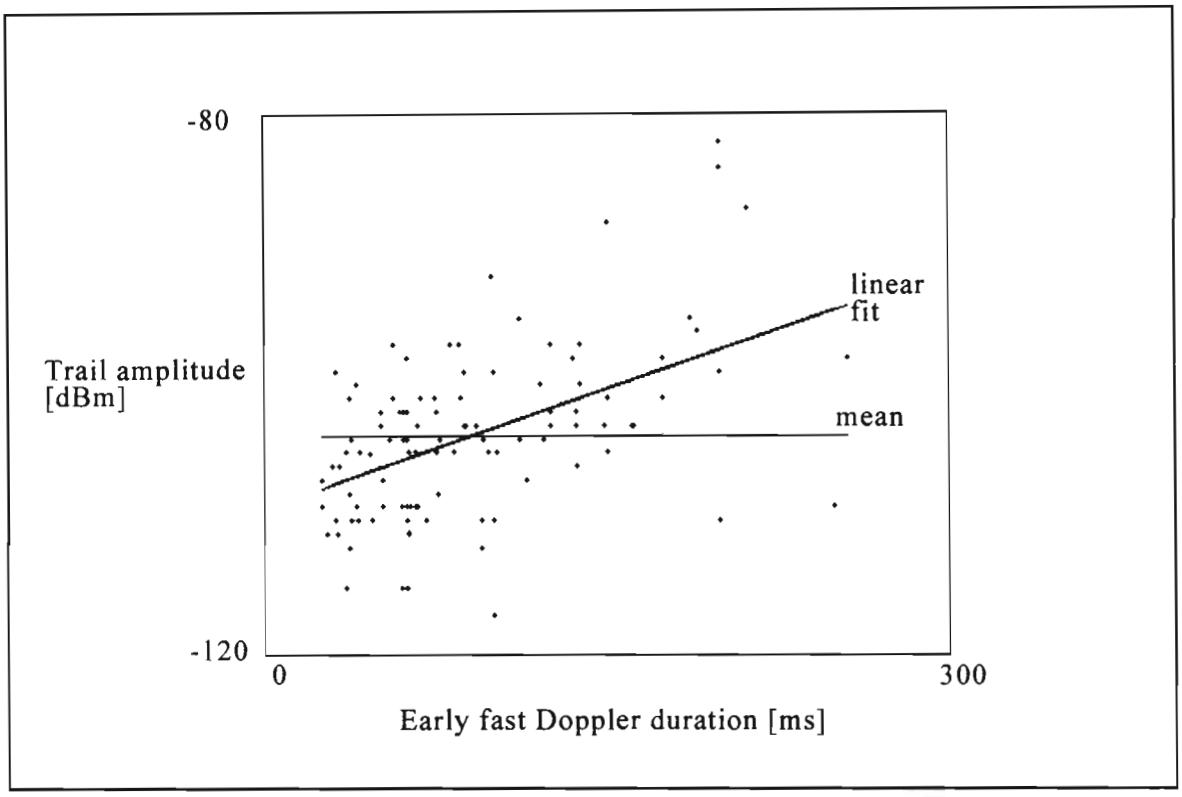

Figure 4-13 Correlation between early fast Doppler duration and peak trail amplitude

This is not entirely unexpected since the optimal geometrical trail orientation for longest principle Fresnel zone (and hence longest early fast Doppler duration) is the same as that for the optimal signal amplitude from an overdense meteor trail under forward scatter conditions.

For example, assuming a mid-path link with $R_1=R_2$, then the early fast Doppler duration will be large when:

$$\tau_{EFD} = \frac{1}{f_{EFD}} = \frac{2L}{V_m} = \frac{2}{V_m}\left[\frac{\lambda (R_1 R_2)}{(R_1+R_2)(1-\sin^2\varphi \cos^2\beta)}\right]^{\frac{1}{2}} \text{ [s]} \qquad (4\text{-}5)$$

is large. This occurs in the limit when:

$$\lim_{\varphi \to 90, \beta \to 0} (1-\sin^2\varphi \cos^2\beta) \to 0$$

The approximate power available to a receiver on the ground from an overdense trail is given by the following equation [*Hines & Forsyth*, 1957]:

$$P_R = \frac{P_T G_T G_R \lambda^2 S_p^2}{32 \pi^2 R_1 R_2 (R_1 + R_2)(1 - \sin^2\varphi \cos^2\beta)} \cdot \left[\frac{4 d t + r_0}{sec^2\varphi} \ln \tau_0 \right]^{\frac{1}{2}} [W] \qquad (4\text{-}6)$$

$$\text{where } \tau_0 = \frac{r_e q \lambda^2 sec^2\varphi}{\pi^2 (4dt + r_0^2)}$$

The condition for maximum reflected power occurs in the limit when:

$$\lim_{\varphi \to 90, \beta \to 0} (1 - \sin^2\varphi \cos^2\beta) \to 0 \qquad \text{when } \varphi < 90°$$

This is the same condition for both early fast Doppler duration and trail peak amplitude. It is noted however that the early fast Doppler duration has a dependency on meteor velocity, which is itself, a non-normal distribution (see Figure 4-4).

4.5.5 Conclusion

The results of the four statistical correlations performed show no meaningful direct relationships which could be used to estimate trail parameters based on information derived from early fast Doppler alone. Apart from the low correlation, there is a great degree of variation in the parameters involved, such as meteor velocity and trail orientation. These distributions greatly reduce the significance of statistically based predictions of peak trail amplitude and trail duration based on either early fast Doppler frequency spread or duration. It appears that the use of early fast Doppler in prediction is limited to the heuristic approach of section 4.4 in which the presence of early fast Doppler is simply used to indicate a large amplitude trail being formed. In addition, because the slope of the early fast Doppler [Hz/s] is nearly constant, measurements of early fast Doppler made early on in trail lifetime can provide a good estimate of when the early Fast Doppler would cease and hence when maximum trail amplitude would occur.

4.6 Physical factors influencing early fast Doppler

If early fast Doppler is to be used as an heuristic estimator of trail type, trail duration or peak trail amplitude, there are several factors that must be investigated including meteor ionization height, velocity and path geometry that have a direct bearing on early fast Doppler properties, [*Fraser & Broadhurst*, 1992b].

4.6.1 The influence of ionization height and velocity

The height at which a trail forms depends on meteor mass, velocity, and path orientation, as well as on the atmospheric density. *McKinley* [1961] has shown that radio echo heights increase with higher meteor velocities. This is because meteors of higher velocity will impart more energy to the particles in the upper atmosphere causing higher levels of ionization at greater heights, than meteors of a similar mass but traveling at lower velocities. Using back-scatter radar a velocity profile is shown in Figure 4-4 and a height profile in Figure 4-14.

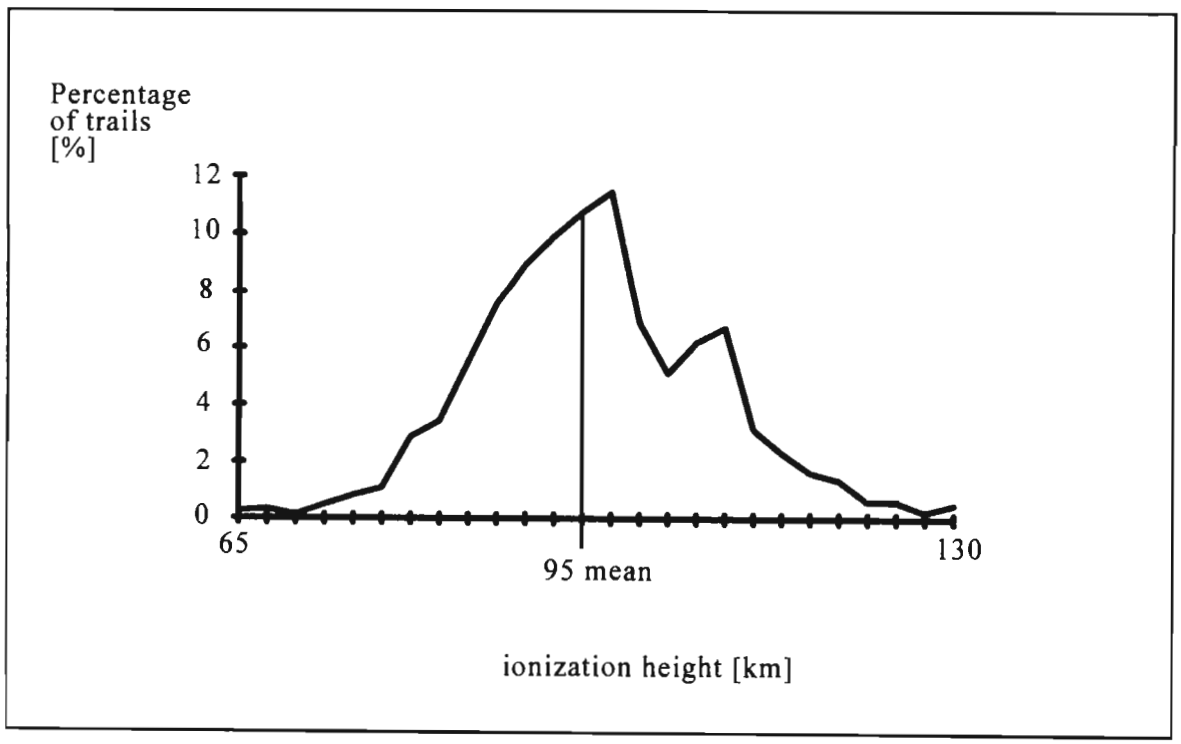

Figure 4-14 Meteor ionization height profile given as a % of trails, after *McKinley*, 1961.

It is interesting that both curves yield a similar shape and reveal a "saddle-point" just off centre. For stations in the middle latitudes of the earth, even a theoretically uniform radiant distribution will yield a "double-humped" type velocity distribution, due to the apex and antapex effects [*McKinley*, 1961]. Furthermore, there are small areas of the celestial sphere which are necessarily deficient in meteor radiants because the corresponding orbits pass so close to the sun that the meteoroids are vaporized accentuating the "double-hump". An ecliptic concentration of orbits will also accentuate this feature (Figure 4-15).

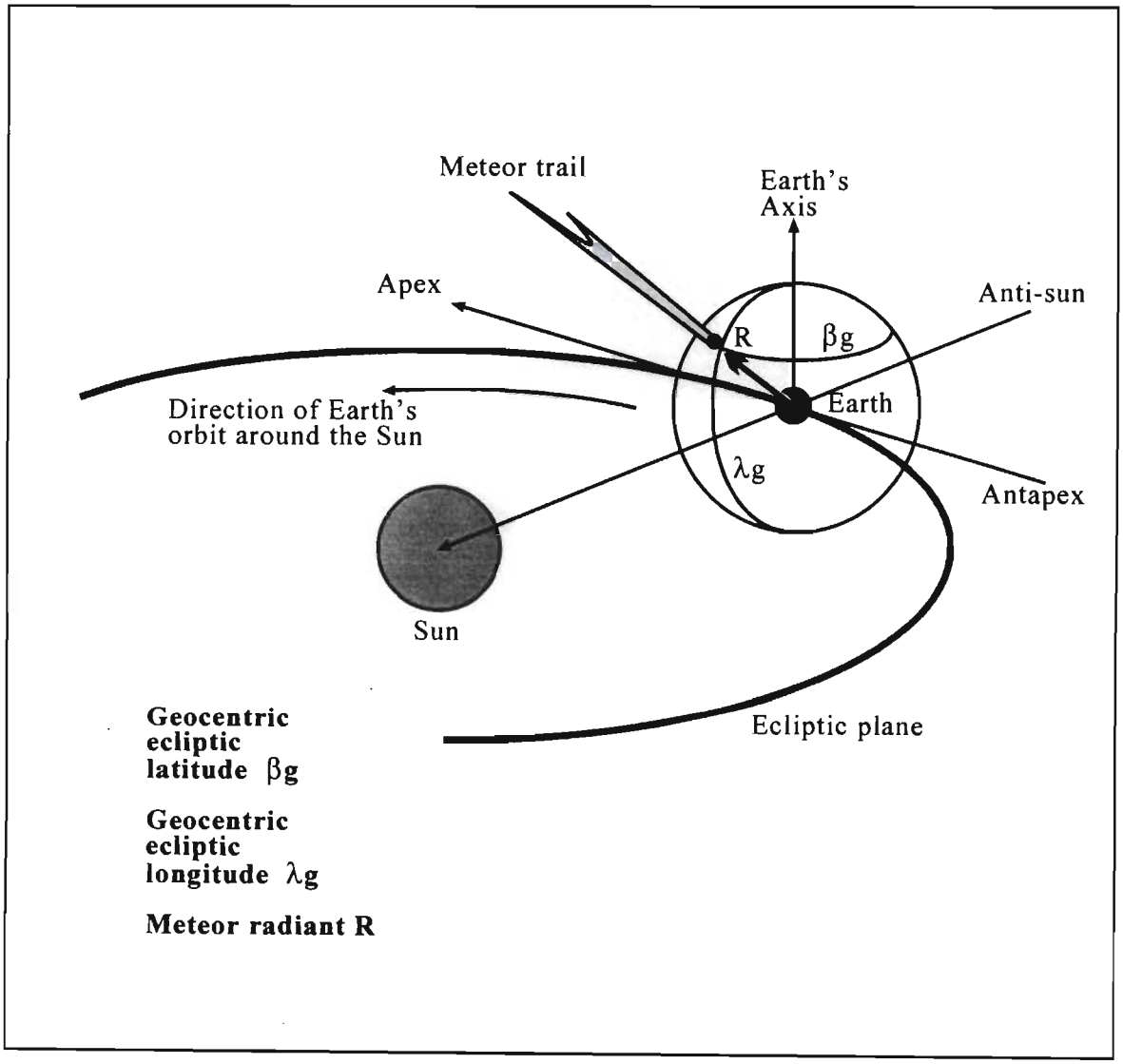

Figure 4-15 Geometric orientation of the earth with respect to the sun and meteors, after *Mawrey*, 1990

Meteor velocity directly influences the height at which ionization begins. Both meteor velocity and ionization height affect early fast Doppler duration and spread (equations 4-4, 4-5). However, a dominant effect on peak trail amplitude is ionization height (equations 4-3, 4-6).

The height at which ionization occurs is influenced by the trajectory of the meteor (R_1, R_2, and φ for the path). This path geometry has a direct influence on the early fast Doppler spread and early fast Doppler duration as equations 4-4, 4-5 show. However, this influence is small.

Consider a hypothetical meteor with fixed velocity and trajectory. A change in ionization height say from 65 km to 130 km (see Figure 4-14), would change the early fast Doppler frequency spread and duration by only about 4.5%. Thus in most considerations of the effects influencing early fast Doppler, changes in height can be neglected and the mean of 95 km (for meteoric head echoes) can be assumed.

4.6.2 The influence of β

As shown in Figure 4-2, β is defined relative to the earth as the angle between the trail axis and the plane containing the transmitter, receiver and trail. This together with the distribution of velocities between 11 and 71 km/s yields the family of curves in Figure 4-16 as plotted for a 550 km mid-path link, [*Fraser* 1991d, *Fraser & Broadhurst* 1992b].

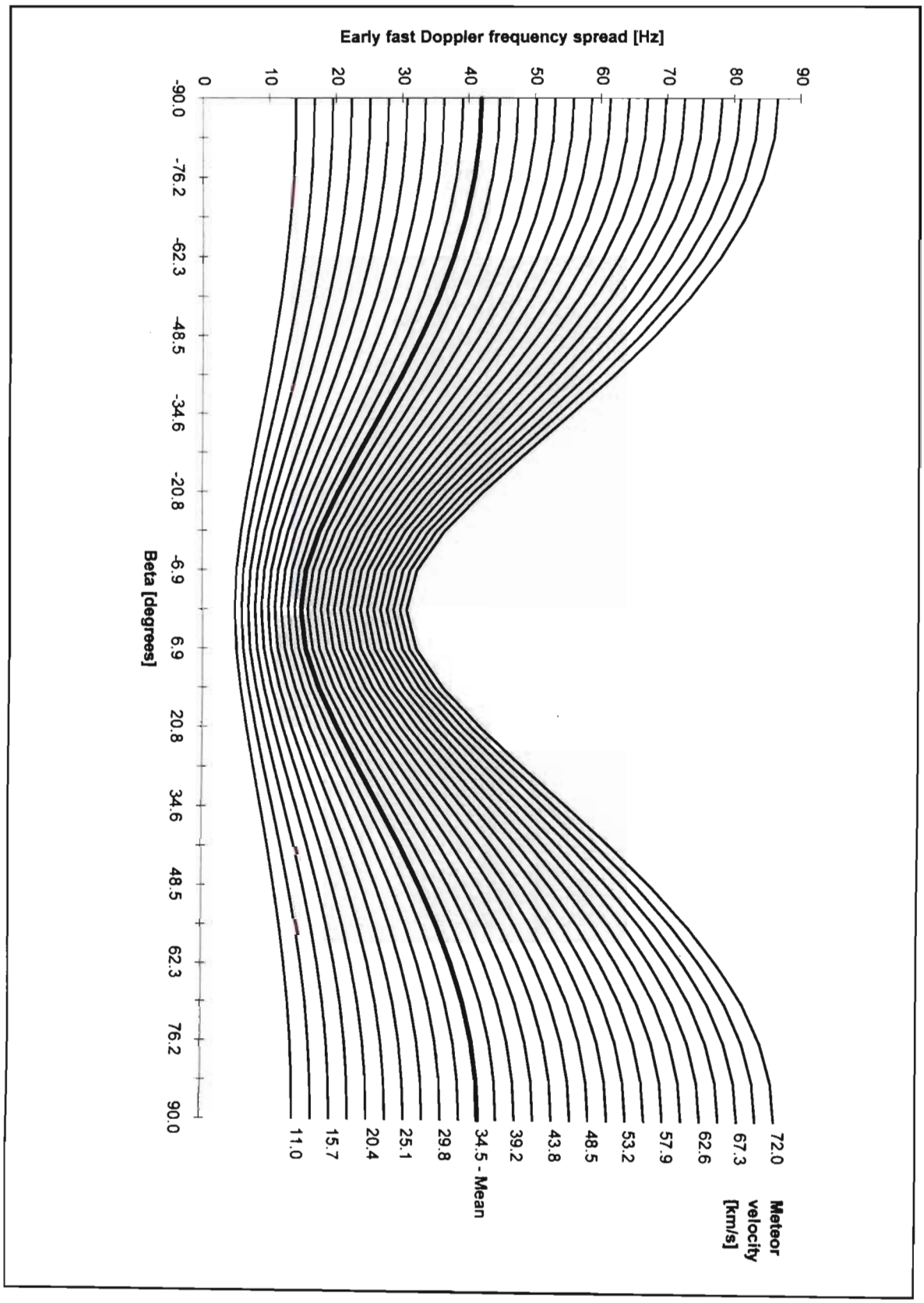

Figure 4-16 Early fast Doppler frequency spread on a 550 km mid-path link as a function of β and meteor velocity, [*Fraser*, 1991d].

As can be seen, both meteor velocity and β play a large role in the early fast Doppler spread that is produced at the receiver. The ratio of maximum to minimum early fast Doppler spread for velocities of 72, 35 and 11 km/s are 2.7:1, 2.4:1 and 2.3:1 respectively. This indicates that the higher velocity meteors show a greater variation in early fast Doppler spread than those of lower velocity. In comparison to the results of Table 4-1, the values from these nomographs compare very favourably with the measured early fast Doppler mean over the test link ($\beta_{link} = 56° \approx 45°$ for equations to be valid).

It must also be borne in mind that the velocities depicted on the graph do not occur with the same probability but should be scaled in significance by the factors given in Figure 4-4.

4.6.3 Path configuration and path length

Figure 4-17 shows a family of curves plotted under similar conditions to those of Figure 4-16 but in a 550 km end-path configuration. In this case, the percentage change in early fast Doppler spread due to β is far smaller than that of the 550 km mid-path link but the figure shows a proportionately larger early fast Doppler spread for a similar meteor velocity.

A comparison between short and long mid-path links is also useful as Figure 4-18 shows. The longer path lengths show a greater variation in early fast Doppler spread with β, but a lower average value of early fast Doppler spread than the shorter paths. Figure 4-19 gives curves for two commonly used links, Pretoria to Durban and Pretoria to Cape Town.

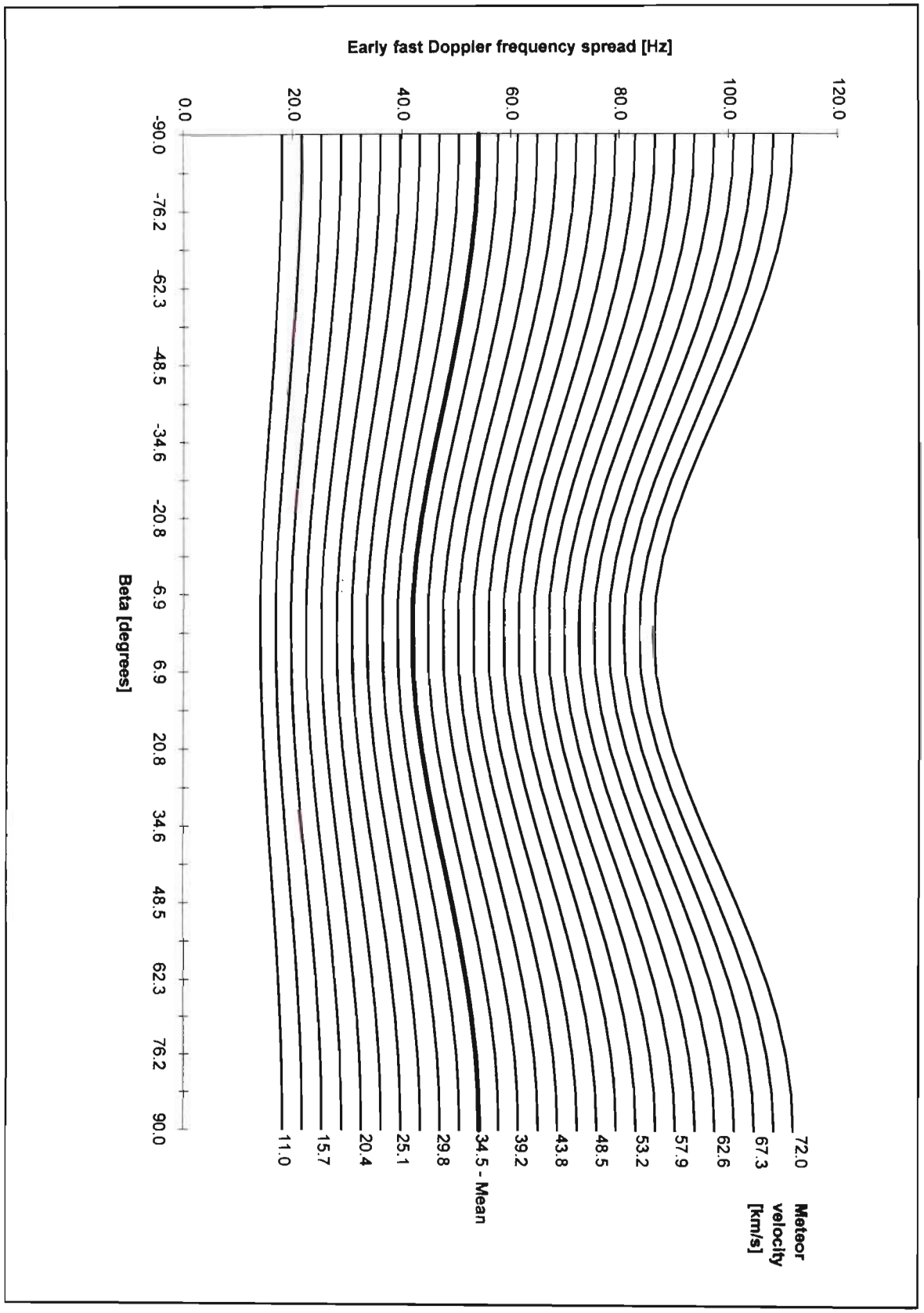

Figure 4-17 Early fast Doppler frequency spread on a 550 km end-path link as a function of β and meteor velocity, [*Fraser*, 1991d].

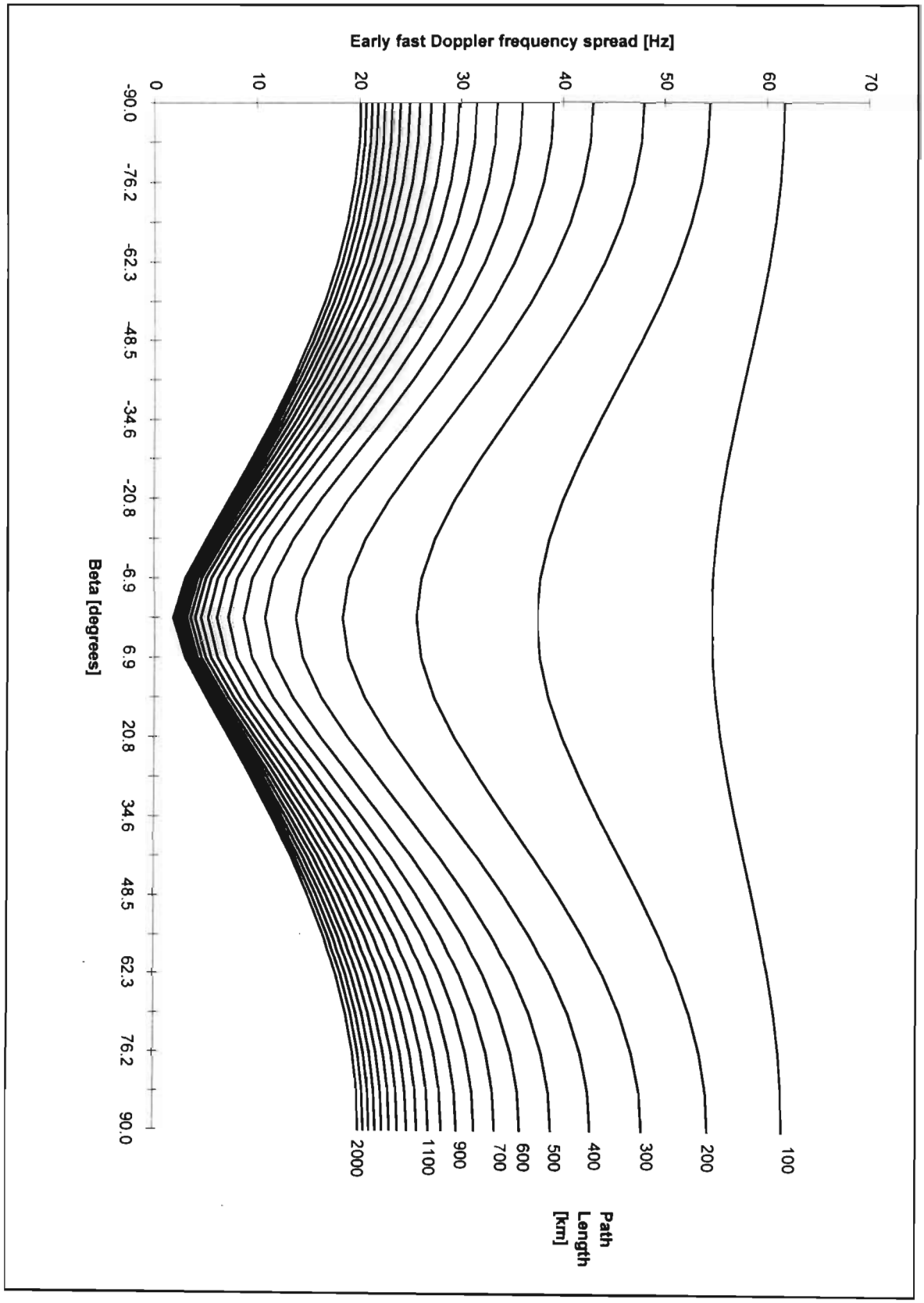

Figure 4-18 Early fast Doppler frequency spread on paths of varying length link as a function of β, (mean velocity of 34.5 km/s), [*Fraser*, 1991d].

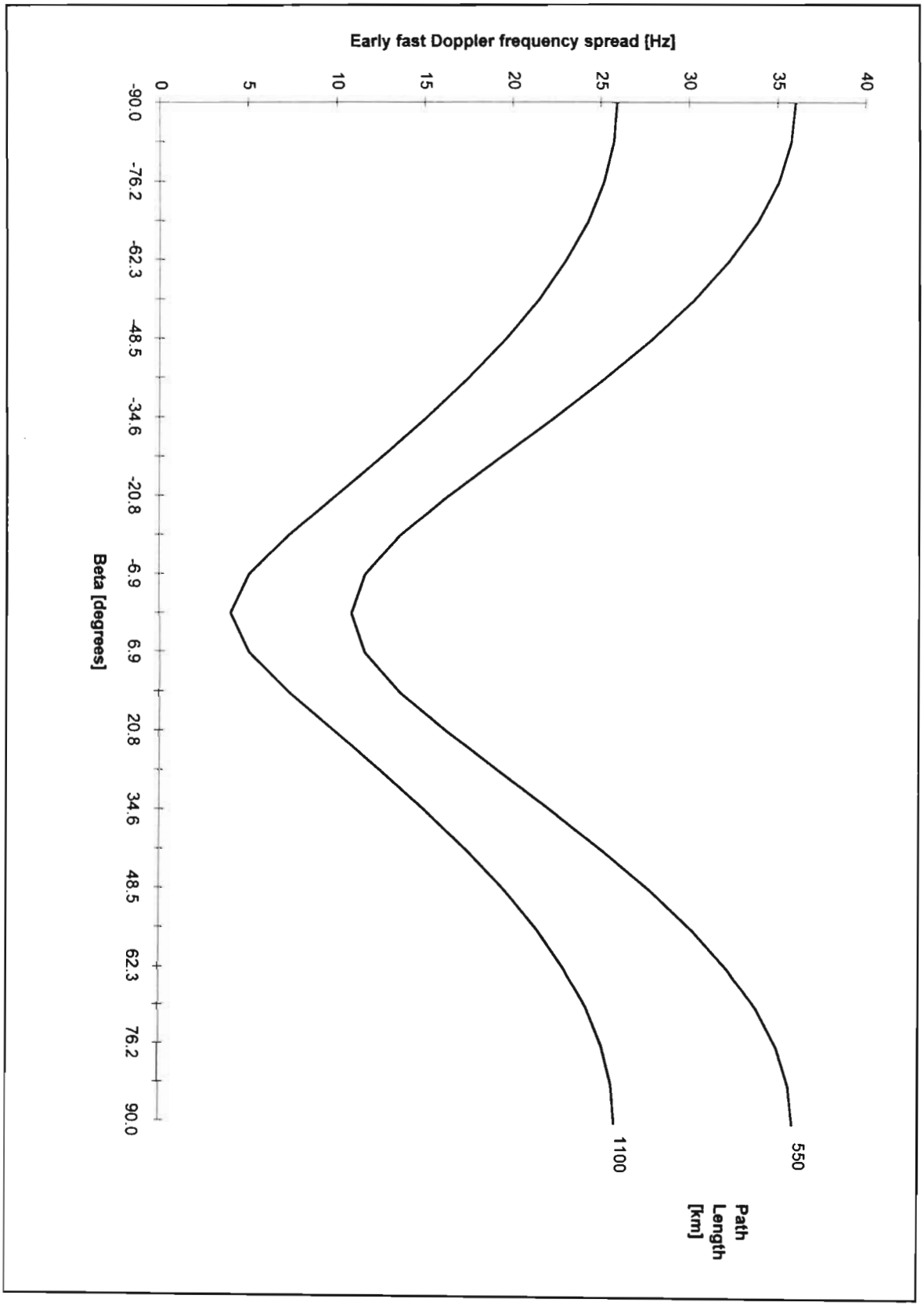

Figure 4-19 Early fast Doppler frequency spread on typical short and long paths as a function of β, medium link - Pretoria-Durban, long link - Pretoria-Cape Town, mean velocity = 34.5 km/s, [*Fraser*, 1991d].

4.7 Early fast Doppler as an heuristic in a simple adaptive data rate system

In a simple adaptive data rate system, the presence of early fast Doppler is used as a toggle to a higher data rate on the pretext that early fast Doppler will precede a high signal-to-noise ratio long duration trail. If no early fast Doppler is detected, a lower data rate would be used. The lower rate would apply whenever there was no clear indication that early fast Doppler was present. The following brief comments give an estimate of the throughput improvements of such a system.

4.7.1 Trail count and duration by trail type

Histograms compiled of trail count and trail duration for each trail category using the captured data reveal certain facts that may not be immediately apparent (Figures 4-20 and 4-21). Category definitions are given in [*Melville & Larsen*, 1992].

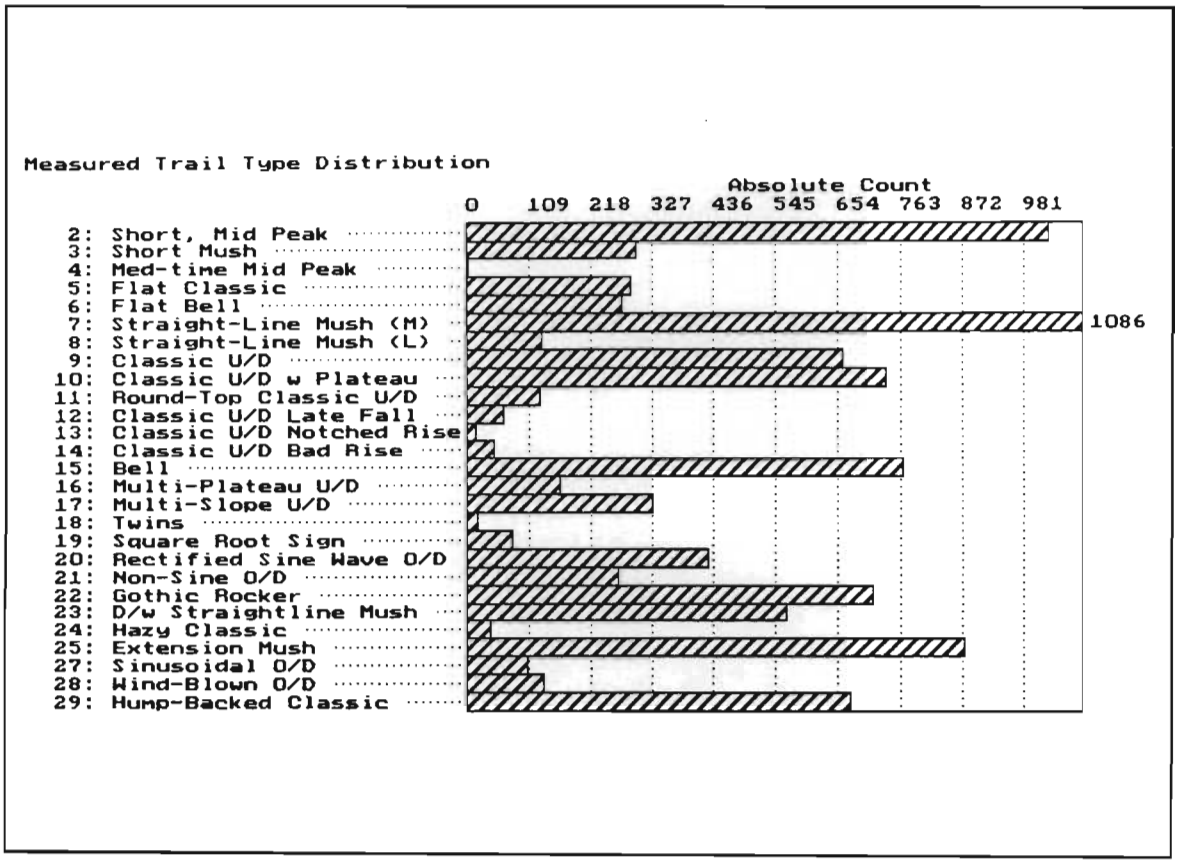

Figure 4-20 Histogram representation of the percentage of trail counts for each particular trail type classified over a period of a day, [*Melville & Larsen*, 1992]

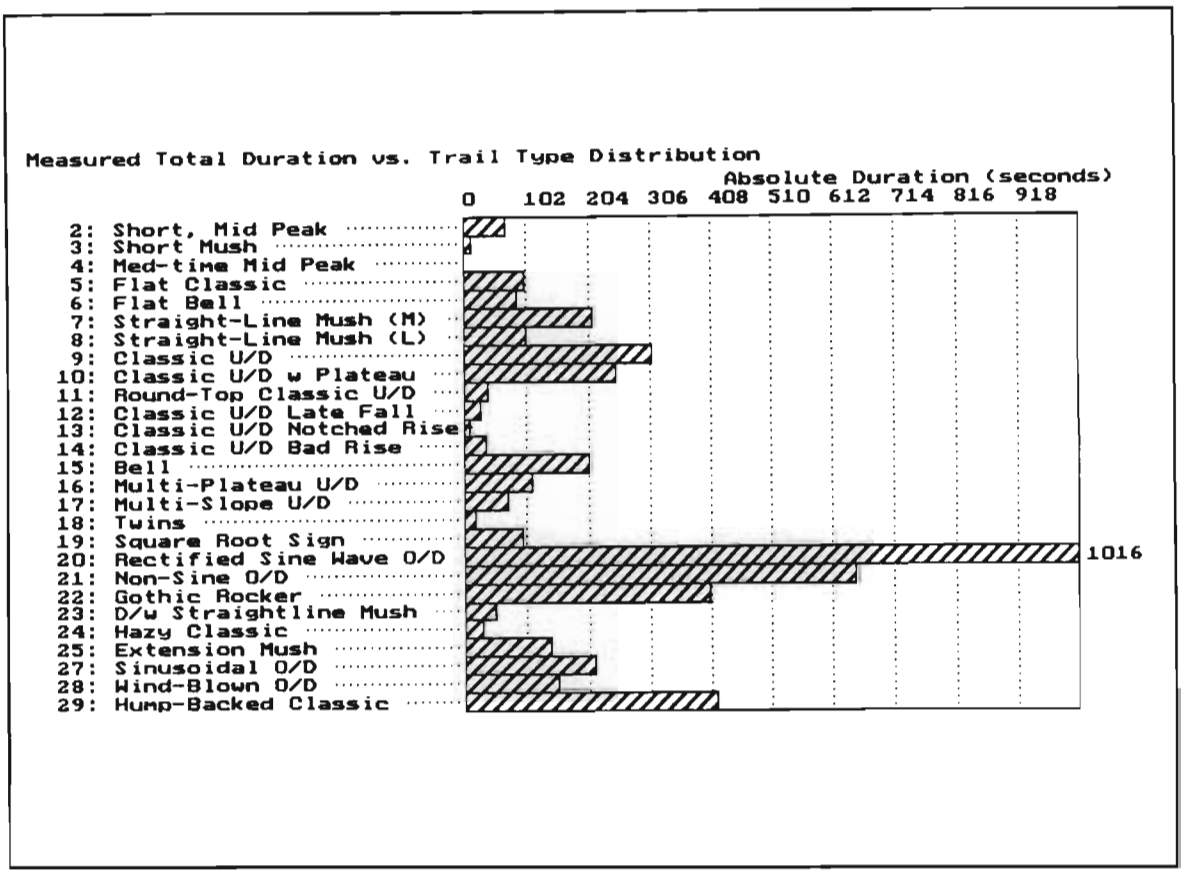

Figure 4-21 Histogram representation of the percentage of trail durations for each particular trail type classified over a period of a day, [*Melville & Larsen*, 1992]

It can be seen from Figure 4-20 that the short, "mid-peak" trails, "extension mush" trails and "classic underdense" trails represent the greatest percentage of the total number of trails seen. However, the duty cycle of these trails (i.e. their total duration per hour) is not significant as Figure 4-21 shows. This makes them less suitable than the overdense trails mentioned for data transmission.

The trails of particular importance to meteor-burst communication are "rectified sine" overdense and "non-sine" overdense types since they comprise the greatest useful duration even though fewer in number than the underdense type. The trails which carry the greatest amount of data per hour are the trails with the largest signal-to-noise ratios and durations. These trails also exhibit the greatest phase effects such as early fast Doppler and fading (see section 4.4.1 and Table 4-1).

4.7.2 Early fast Doppler occurrence and duty cycle

Of the sample set of trails measured, 10-20 % exhibited early fast Doppler. However, in comparing the trails which exhibit early fast Doppler with those which do not, it is found that the trails in which early fast Doppler occurs, are often long-duration or large-amplitude trails or both. This means that out of a sample of long trails (previously defined as being 500 ms or greater in duration), 30.2 % of these contain early fast Doppler at their commencement. Considering that the large overdense trails (e.g. "sinusoidal overdense", "rectified sine" and "Gothic rocker") make up some 60 % of the hourly duty-cycle (Figure 4-19) for meteor-burst communication, the fact that early fast Doppler gives prior indication of their occurrence with a probability of 0.302 is highly significant, [*Fraser*, 1991d, 1992, *Fraser & Broadhurst*, 1992a, 1993a]. If large overdense trails constitute around 60% of the hourly meteor duration and some 30 % of those contain early fast Doppler, it means that around 20% (1/3 of 60%) of the hourly duty cycle can benefit from the use of the early fast Doppler to toggle between a lower base rate and a higher data rate.

4.7.3 An estimate of the improvement in data throughput

If a simple bi-rate adaptive data rate system is implemented based on the early fast Doppler toggle heuristic, an estimate of the improvement in data throughput is obtainable by considering the hourly duration that can make use of early fast Doppler prediction:

$$d_{EFD} = \eta\,\hat{e} = 1 - d \tag{4-7}$$

where:

d_{EFD} is the fraction of the hourly duration using early fast Doppler heuristic

η is the ratio of the duty cycle of high signal-to-noise ratio, long duration trails to the total duration per hour

$\hat{e}$ is the estimate of the fraction of the high signal-to noise-ratio, long duration trails that exhibit early fast Doppler

d is the fraction of the hourly duration not using the early fast Doppler heuristic

The average data rate D for the bi-rate system is then given by:

$$D_{ave} = [d_{EFD} \cdot b_2 + d \cdot b_1]$$

$$= d_{EFD}(b_2 - b_1) + b_1 \qquad (4\text{-}8)$$

where:
D_{ave} is the average data rate [kb/s]
b_1 is the base data rate [kb/s]
b_2 is the higher data rate [kb/s]

If, for example the base data rate was 8 kb/s and the higher data rate was 32 kb/s, the improvement in the average data rate using this simple scheme could be as much as 60%. There would of course be losses for "false" triggers and for the parts of the trail where the signal-to-noise ratio dropped beneath that required to sustain the higher bit rate. There is good potential for significant throughput enhancement in a half-duplex system using this scheme.

4.8 Conclusion

Based on the experimental results, the following deductions are a summary of the use of early fast Doppler for trail prediction:

- The occurrence of early fast Doppler at the commencement of large amplitude and long duration trails is significant.
- The trails in which early fast Doppler occurs are of major importance to the duty cycle of data throughput.
- Trails which exhibit early fast Doppler have a mean amplitude -104 dBm with a standard deviation of 5.
- Trails which exhibit early fast Doppler have widely varying durations and exhibit little correlation between either early fast Doppler spread or early fast Doppler duration and trail duration.

- Early fast Doppler slope (early fast Doppler frequency spread / early fast Doppler duration) is constant and can be extrapolated linearly from 2-3 initial data points.

- Statistical use of early fast Doppler as a predictor is not useful owing to poor correlation between early fast Doppler parameters and subsequent trail parameters.

- Heuristic use of early fast Doppler as a predictor by detecting early fast Doppler at trail commencement and using that knowledge in a decision process appear to have merit.

- Any practical application of early fast Doppler predictors must take accomodate the effects of velocity and path configuration and to a much lesser extent meteor ionization height.

In conclusion, the best use of early fast Doppler to improve data throughput appears to be heuristic rather than statistical. The correlations between early fast Doppler parameters and trail metrics such are amplitude and duration are poor. However, the mere presence or absence of early fast Doppler gives useful knowledge about the developing trail very on in its lifetime. The presence of this phenomenon is linked most closely to large amplitude, long duration trails. Therefore, its presence at their commencement serves as a useful indicator which may toggle data rates between a low rate (for underdense and non-early fast Doppler trails) and a higher rate (for long/large overdense trails). This heuristic toggle would aid around a third of the 10-20% large trails seen every hour. In numerical terms this would only be 3-6% of all trail types, but these large trails constitute a significant percentage of the total hourly duty cycle. This novel technique can provide a considerable data throughput enhancement to the smaller half-duplex systems.

Chapter 5

Introduction to neural networks for meteor-burst communications

5.1 Introduction

Neural networks have several properties which make them ideally suited to the tasks of prediction and classification. As such, they are useful tools in communications [*Cichocki & Unbehauen*, 1993], [*Yuhas & Ansari*, 1994], [*Alspector* et al., 1993]. This introductory chapter on neural networks lays the foundation of the application of neural networks to meteor-burst communications presented in chapter 6. The reader who is familiar with neural networks may omit sections 5.1 to 5.4, but should include section 5.5 as this introduces the terminology of the specific neural network development environment used by the author.

Artificial neural networks have evolved from mainstream artificial intelligence as an attempt at modeling learning in biological neural systems. Whereas rule-based expert systems, fuzzy logic and case-based reasoning rely on logical syntax for decision making (syntactical artificial intelligence), neural networks depend on a more abstract symbolic representation of data. Whereas traditional artificial intelligence rests heavily on a rigorous set of *IF-THEN* rules, historical precedents or partial set membership, neural networks attempt to learn the underlying relationships present in data without such formalism. They rely on the recognition of patterns latent in the data without being explicitly shown which patterns or which inputs to use in the association.

There are several distinguishing features of neural computing which differs from other artificial intelligence methods and more traditional techniques:

Learning by example

Neural networks generate their own rules by learning from examples which they have been shown.

Distributed associative memory

Neural networks store their information in a distributed way. This leads to an important capability of neural networks namely generalization of input data. Generalization allows "intelligent" responses to novel stimuli.

Fault tolerance

Unlike traditional systems which are rendered useless by even a small amount of damage to memory, neural networks are much more robust and fault tolerant. Fault tolerance extends to graceful degradation with increased neural network corruption.

Relative noise immunity

The generalizing ability of neural networks allows a certain amount of tolerance to noisy, missing or incomplete data.

Pattern recognition

Neural networks are much more adept at pattern recognition tasks than traditional techniques. Their ability to deduce complex relationships between data give them an edge of expert systems.

Functional synthesis

Certain neural networks are able to learn complex continuous non-linear mappings from one or more inputs to one or more outputs.

Other advantages

Certain neural networks are capable of adaptive learning which is useful in dynamically varying environments. neural networks are often cheaper and quicker to develop than other artificial intelligence techniques. A typical development cycle for neural networks is shown in Figure 5-1.

5.1.1 Biological neurological basis for neural networks

Animal brains consist of billions of neurons connected in a massively parallel manner. Each neuron, for example, typically has 10 thousand connections to its neighbours. The speed of signal propagation in the connections is around 1-100 m/s, not fast by digital computing standards. Similarly, the speed of each neuron

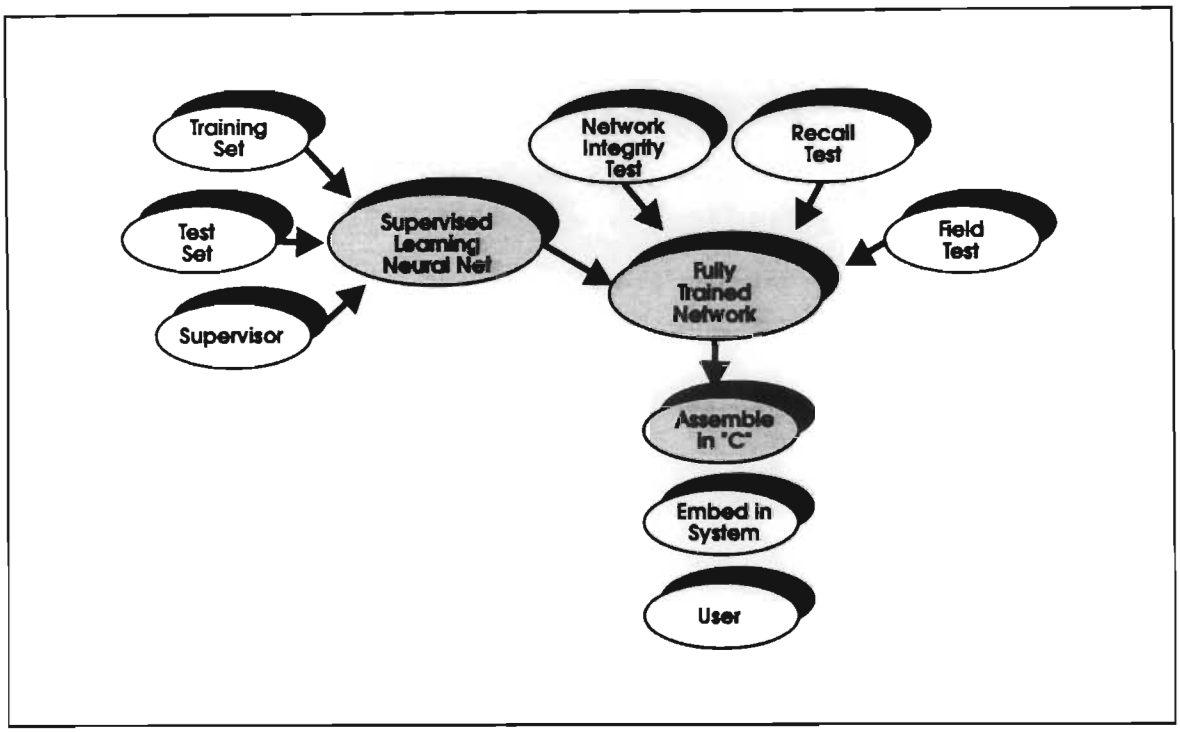

Figure 5-1 Neural Network development cycle

in processing incoming data is relatively low. It can calculate the weighted sum of the signal strengths on these inputs in around 5 ms. The performance of a biological brain is therefore dependent more on its parallel architecture than its elemental processing speed.

An example of a simplified biological neuron is shown in Figure 5-2. The connections from thousands of neighbouring neurons enter through the axons which connect to the cell body. The output of the neuron is via the dendrite to its other neural neighbours. Neurons trigger or "fire" in response to the relative strength of the excitatory (+ve) or inhibitory (-ve) signals on its input. The decision whether to trigger or not is not based on a single event or a occurrence, but on the cumulative response of a network of neural elements to a stimulus. It appears that learning in biological systems takes place in the adjustment of the relative strengths of the incoming connections to each neuron; the greater the connection strength, the more important or influential that particular input is. Learning in which similar

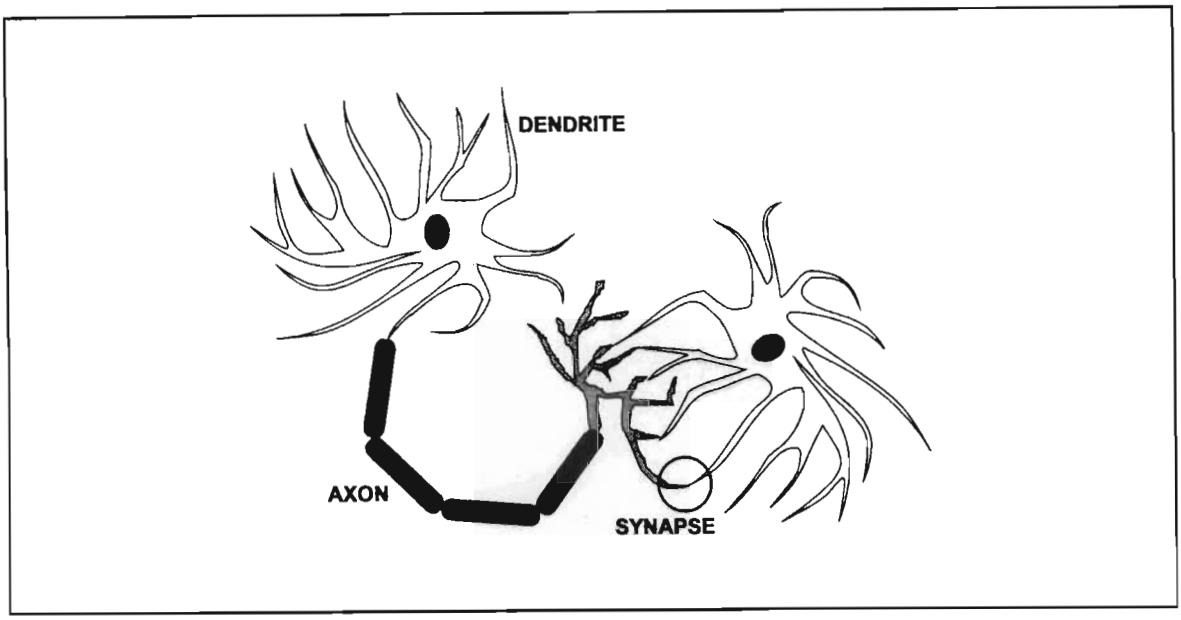

Figure 5-2 Simplified biological neuron

patterns strengthen connections is termed Hebbian learning after its discoverer Donald Hebb.

Thus information in neural networks is stored in the connection strengths between the neurons and not in discrete locations. This distributed representation of the information learned represents a departure from localised knowledge and a greater level of knowledge abstraction than is found in other artificial intelligence methods.

Artificial neural networks attempt to model biological neural systems in a very loose way. The biological metaphor is carried through into a multiplicity of highly interconnected artificial neurons. Each neuron provides the simple function of summing the input signals in proportion to their connection strength and passing this weighted sum through a non-linear transfer function. The processing power of artificial neural networks, like their biological prototypes, is found in their highly connected, massively parallel network structure. Artificial neural networks, however, differ considerably from biological neural networks in practical implementation.

5.2 Neural network structures

5.2.1 Microstructure

The microstructural basis of neural networks is the neuron, also known as the processing element. The neuron structure used in most synthetic neural networks is given in Figure 5-3. The incoming signals, called activations are either from preceding neurons or from the data source directly. Each activation is multiplied by its connection strength, or weight, and then summed. This weighted sum is then passed through a transfer function, the output of which connects to subsequent neurons.

A bias signal is usually added to the weighted sum to provide a fixed-level signal useful for shifting the operating point on the transfer function on all neurons equally, [after *Maren* et al., 1990].

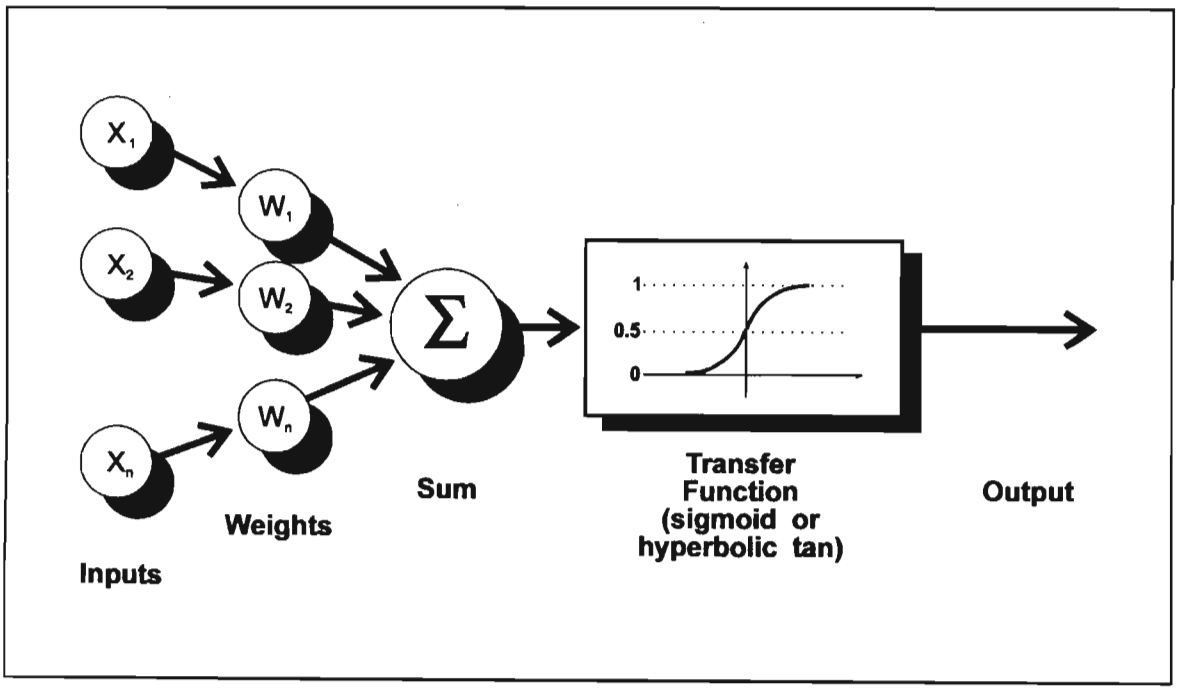

Figure 5-3 Artificial neuron microstructure

$$A_j = f\left[\sum_{i=1}^{n} w_{ij} A_i + \theta_j\right] \tag{5-1}$$

where
A_j is the output activation of neuron j
w_{ij} is the weight between neuron i and neuron j
A_i is the incoming activation of neuron i
θ_j is the bias signal for neuron j

Several functions are useful as the neuron transfer function. Non-continuous functions are shown in Figure 5-4 (threshold logic) and Figure 5-5 (hard limit). The threshold logic is of limited use in neural networks, but the linear function with hard limits is useful in neural networks where a continuous-valued output is a required, such as general regression analysis:

$$y = 0 \quad (x < -\theta) \tag{5-2a}$$

$$y = \frac{x}{2\theta} + \frac{1}{2} \quad (-\theta \le x \le \theta) \tag{5-2b}$$

$$y = 1 \quad (x > \theta) \tag{5-2c}$$

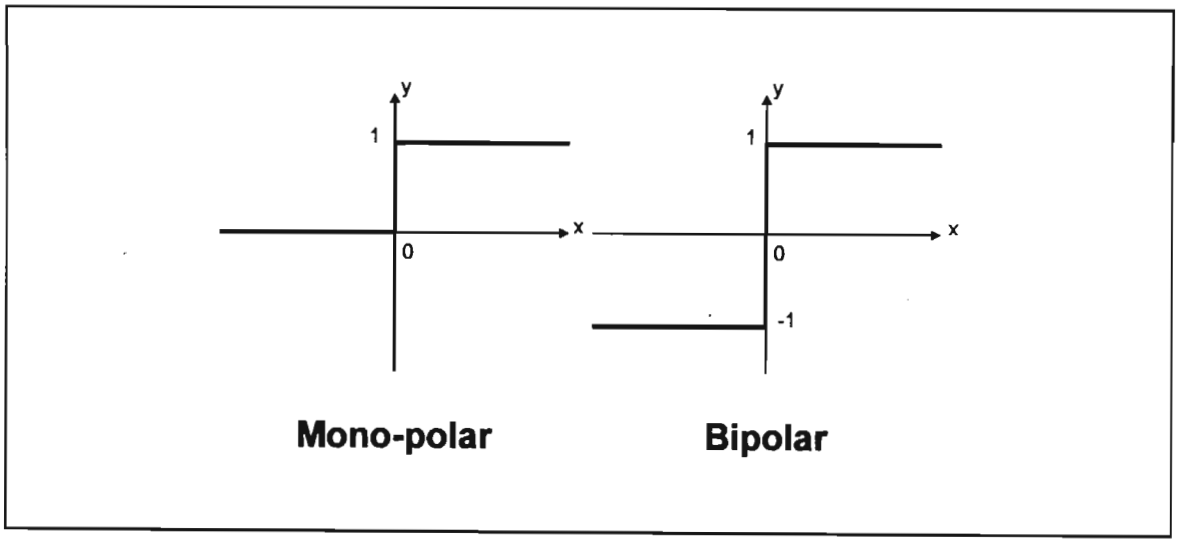

Figure 5-4 Threshold logic neuron transfer function

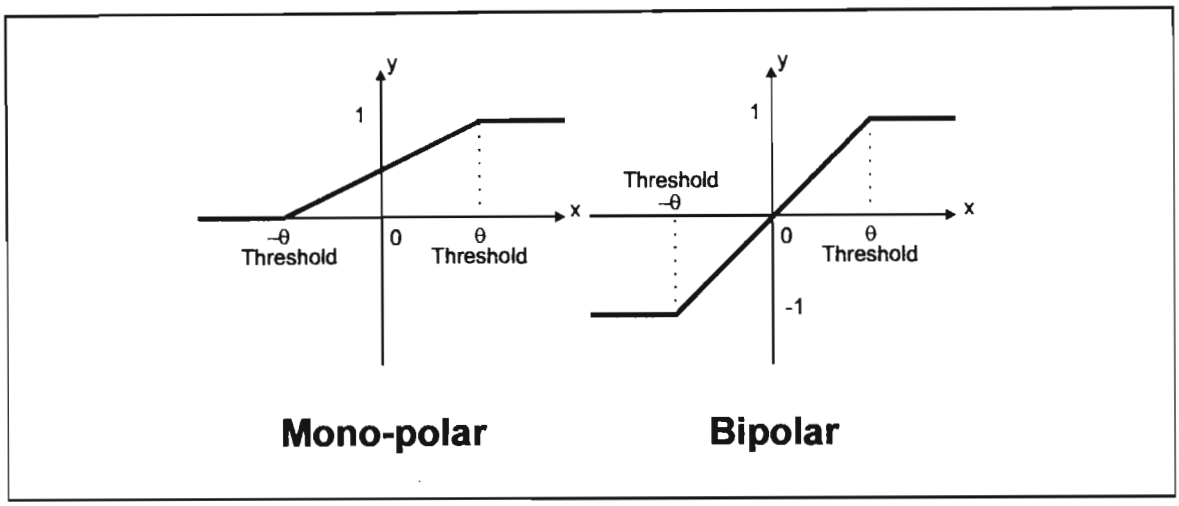

Figure 5-5 Hard-limit neuron transfer function

Continuous functions are much more useful and provide non-linearity to the neurons. They are smooth over $-\infty$ to $+\infty$ and are in general monotonically increasing. In addition, they must be asymptotic to limits in the extremes. The two most common functions are the sigmoid and the hyperbolic tangent shown in Figure 5-6 and 5-7. The sigmoid is used for monopolar inputs scaled to be between 0 and 1, and the hyperbolic tangent for bipolar inputs scaled between -1 and +1:

Sigmoid:

$$f(x,\alpha) = \frac{1}{1 + \exp^{-\alpha x}} \tag{5-3}$$

Hyperbolic Tangent:

$$f(x,\alpha) = \frac{\exp^{\alpha x} - \exp^{-\alpha x}}{\exp^{\alpha x} + \exp^{-\alpha x}} \tag{5-4}$$

where α is the slope variable

For the majority of input values, the functional output is near the asymptotes, i.e. either inhibitory or excitatory. The greatest effect of the functional non-linearity is on the small range of values clustered about zero.

The derivative of these functions yields a maximum at zero and a minimum at the extremes. This characteristic allows training of neurons as shown in section 5.3.

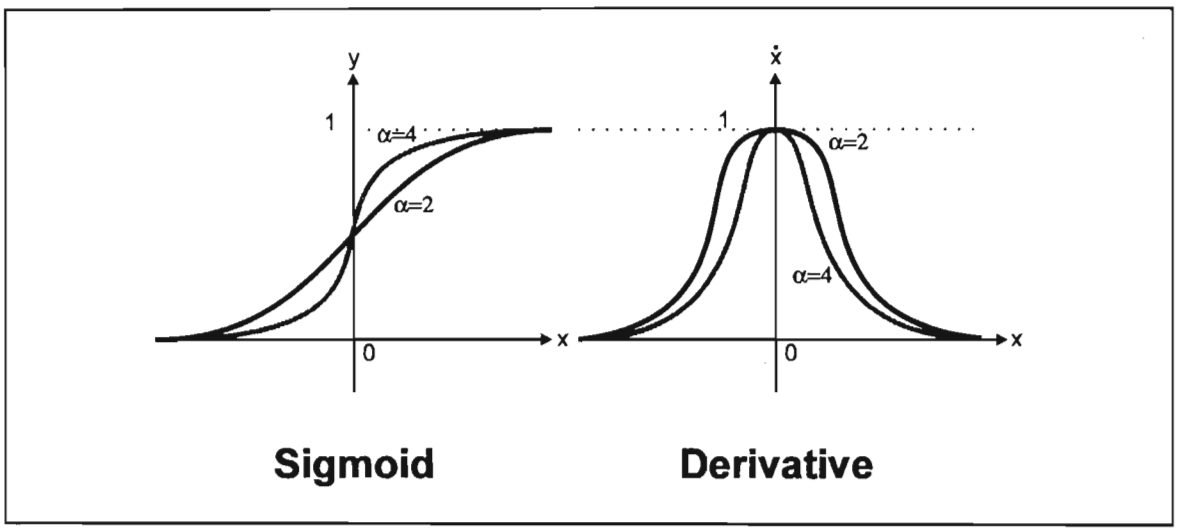

Figure 5-6 Sigmoidal neuron transfer function and its derivative

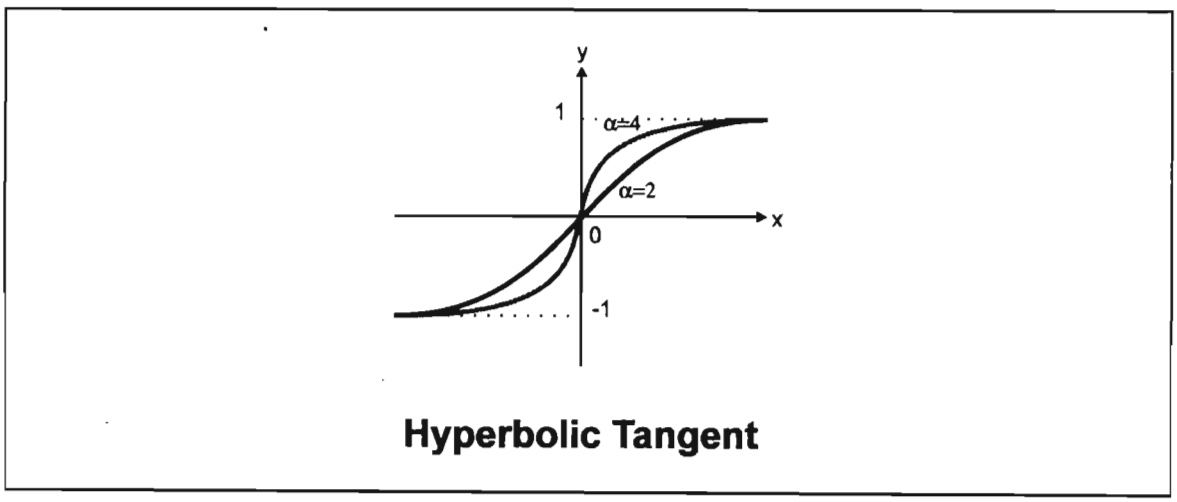

Figure 5-7 Hyperbolic tangent neuron transfer function

5.2.2 Mesostructure

The meso-structure of neural networks relates to their physical organization and the arrangement and connection of neurons. The mesostructure is the primary distinguishing feature of classes of neural network. Neural networks are classified by the following characteristics:

- number of layers (also called slabs)
- number of neurons (also called processing elements) per slab
- the type of connections (forward, backward, lateral, implicit)
- the degree of inter-neuron connectivity

Based on these parameters, there are five major classes of structurally related neural networks.

Multilayer feedforward neural network

In multi-layer networks the inputs to the neural network are passed through a layer known as the input layer which merely serves to connect each input to every neuron in the subsequent layer. The input layer performs no operation on the data. The output layer is a fully-functional layer of neurons whose outputs indicate the output vector in response to an input vector. Between the input and output layers there are several layers of neurons called hidden layers. There is usually one and very rarely more than three hidden layers.

As indicated in Figure 5-8, signals propagate in the forward direction only. There are no feedback connections for each neuron, nor lateral or backward connections. The flow of information for decision making is in the forward direction only. The most famous and widely used neural network is the back-propagation neural network. Back-propagation refers to the method of training the neural network and not the direction of information flow. It is still a feedforward neural network. General applications of feedforward neural networks include system modeling, prediction through non-linear general regression analysis, classification by pattern recognition and filtering. Details of the back-propagation neural network are given in section 5-3.

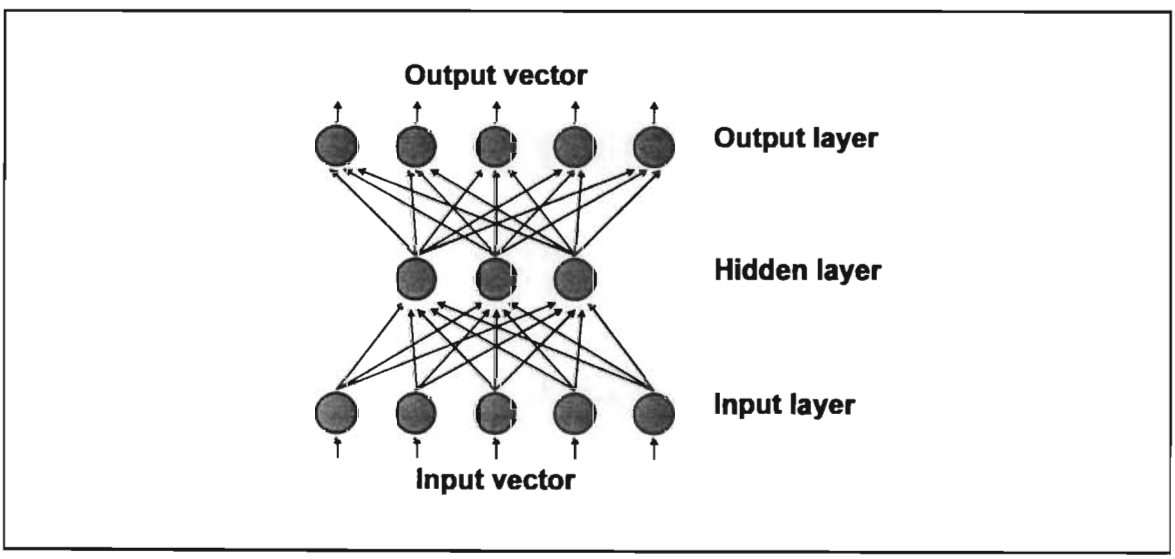

Figure 5-8 Feedforward neural network structure.

Single layer laterally connected neural network

These neural networks consist of a single layer of neurons with bi-directional lateral connections (Figure 5-9). They are mainly used in auto-associative applications where the neural network is outputs a stored pattern in response to the same pattern appearing at its inputs most often partially complete or noisy. If the desired neural network output is the same as the input for all the input patterns it is termed auto-associative. If, however, the desired output is different to the input patterns it is termed hetero-associative. Single layer neural networks are sometimes provided with feedback on themselves via closed loops. This gives rise to a sub-class named recurrent neural networks. Examples of this class include the Hopfield neural network and the Brain-State-in-a-Box neural network.

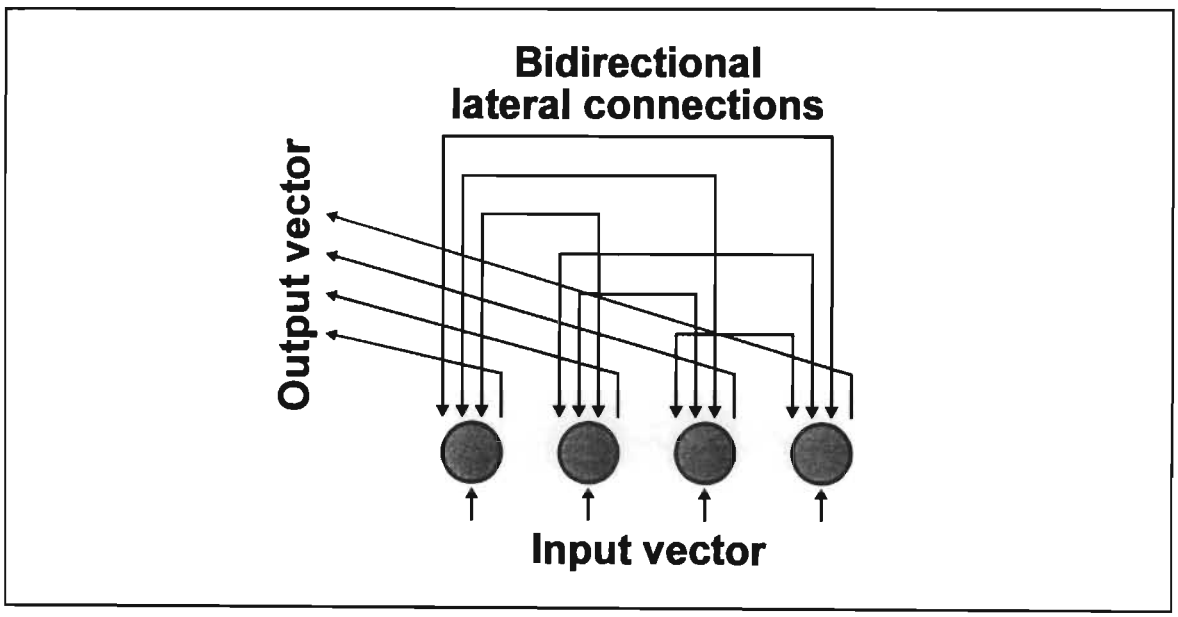

Figure 5-9 Single-layer neural network structure (explicit connections), after *Maren* et al. [1990]

Single layer topographically ordered neural network

This neural network has no explicit connections as in the previous neural network and is used in cases where distinct categories of classification are already known. Inputs to the neural network are grouped as vectors called neurodes. Each neurode represents a an individual from a representative selection of training vectors. They are topographically ordered with respect to one another by comparing their relative Euclidean vector distances in vector space. The shape of the neighbourhood of comparison and measures of distance are two prime parameters in designing these neural networks (Figure 5-10).

Once the neurodes are organized according to their categorical similarity or dissimilarity, a new vector, when presented to the neural network, will result in a projection into a region of vector space (category) with which it is most similar. This allows robust classification of data. Specific details of this method are contained in the section on Learning Vector Quantization (section 5-4).

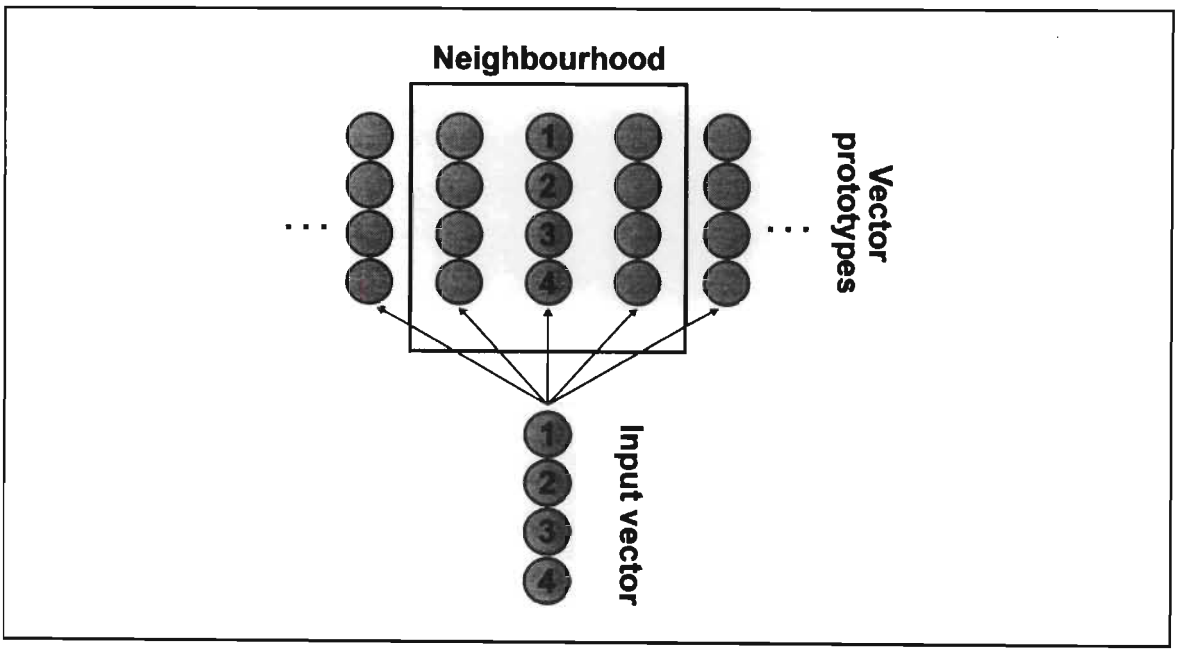

Figure 5-10 Single-layer neural network structure (implicit connections), after *Maren* et al. [1990]

Bilayer feedforward/feedback networks

These neural networks contain both feedforward and feedback connections in a multi-layer structure. A simplified generic structure of these neural networks is shown below (Figure 5-11). In these neural networks, the forward and reverse connections are not just the transpose of one another but usually have different connection strengths (weights) in each direction. Because of the bi-directional flow of information in these neural networks, they are also known as resonating neural networks. Patterns in each layer stimulate patterns in one another in a state of resonance until a stable state exists in each layer.

The prime application of this class of neural network is in pattern recognition. Their advantage over other architectures used in pattern recognition is the ability to learn new patterns without losing memory of or degrading the recall performance of previously stored patterns. Examples of these neural networks are the Adaptive Resonance Theory (ART) networks of *Carpenter and Grossberg* [1987a, 1987b, 1988], and the Bi-directional Associative Memory (BAM) of *Kosko* [1987].

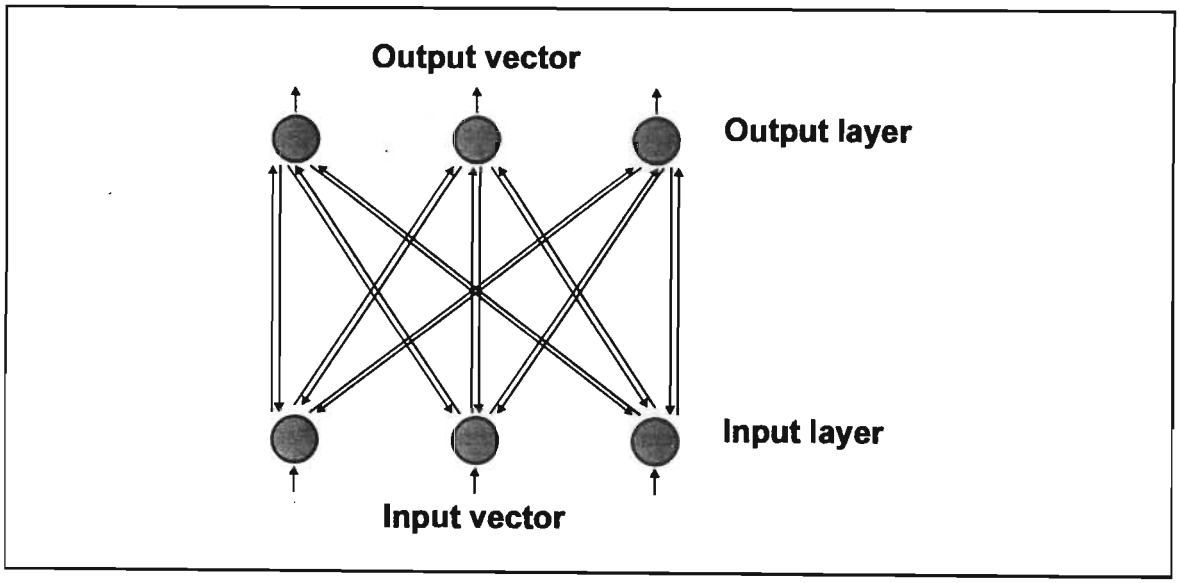

Figure 5-11 Bilayer feedforward/feedback neural network structure (resonating neural networks), after *Maren* et al. [1990]

Multilayer co-operative/competitive neural networks

Figure 5-12 shows schematically that these networks have lateral connections in addition to feedforward and feedback connections. The lateral connections allow individual neurons in the neural network to compete/co-operate for the opportunity of passing information. The competitive (inhibitory) and co-operative (excitatory) nature of these neural networks improves classification ability where a winner-takes-all strategy suppresses spurious classifications and enhances most-likely classifications. Examples of these networks include the Probabilistic Neural Network of *Specht* [1988, 1990].

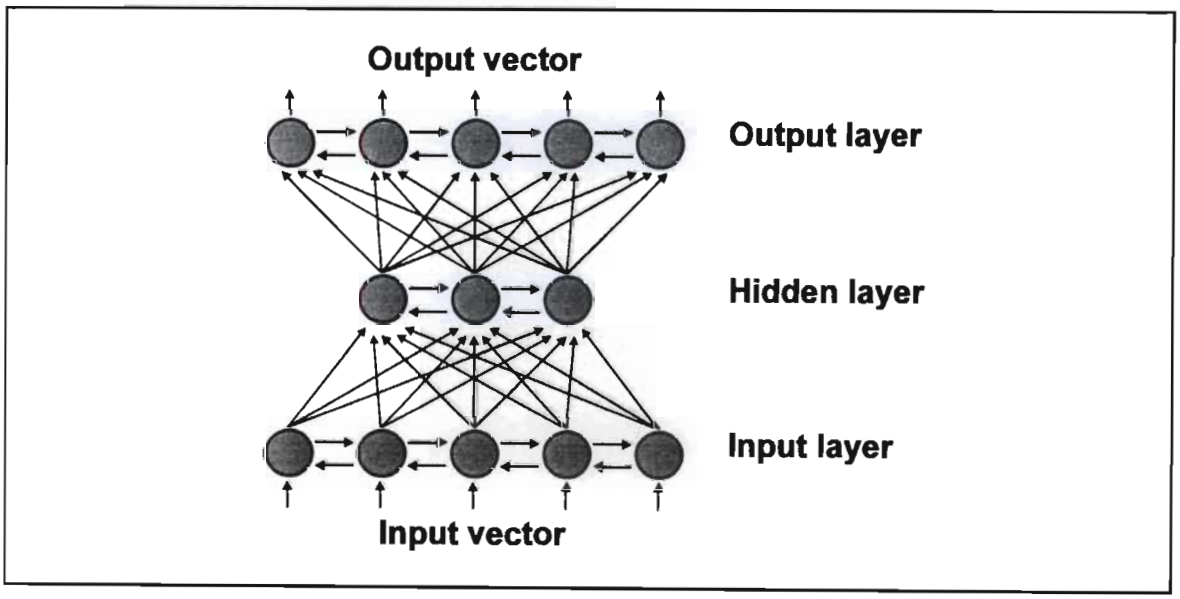

Figure 5-12 Multilayer cooperative/competitive neural network structure, after *Maren* et al. [1990]

5.2.3 Macrostructure

Often a single neural network is incapable of solving all aspects of a problem owing to the nature of the data and the problem involved. The solution is found in segmenting the problem into several neural networks each apportioned a separate task. This allows the neural networks to act independently yet combine their results either through a neural network or a logical function. In solving large problems, this "panel of experts" approach is often the only way of ensuring cohesive data processing, analysis and decision making. The parameters involved in the choice of macrostructure include, the number of neural networks, the sizes of these networks, the types of inter-neural network connection (feedback, feedforward, lateral etc.), the degree of connectivity and the logical gating or non-linear neural network-based opinion fusion.

A generic structure of a multi-neural network system is shown in Figure 5-13. When designing such systems of neural networks the emphasis is to highlight the positive contributions of individual neural networks and reduce the effect of their weaknesses. Examples of these networks are the Hamming Network and the Counter-propagation Network.

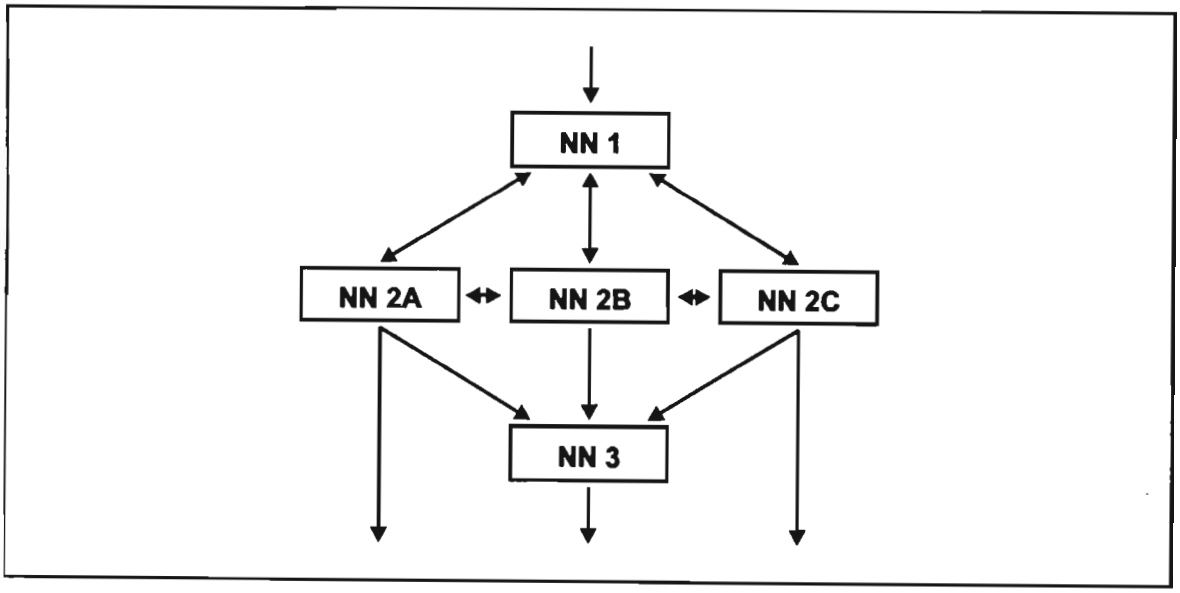

Figure 5-13 Multi-neural network structure (macrostructure), after *Maren* et al. [1990]

5.2.4 Neural network learning

The Brittanica Dictionary defines learning as:

> "*the modification of behaviour following upon and induced by interaction with the environment and as a result of experiences leading to the establishment of new patterns of response to external stimuli*"

The ability to learn is what differentiates neural networks from other signal processing techniques and statistical methods. Learning in a network of neurons is an extension of the process of adjusting weights of individual neurons to meet a global criterion. The regime used to adjust the individual neuron weights in response to a target is called the learning rule or paradigm.

The process of learning commences with randomization of the neural network weights to small values around zero according to a Gaussian density function. The learning rule dictates the method of adjusting individual weights to minimize the global error between desired and actual response to input stimuli. In order to learn, training data must be presented to the neural network, so that it may extract the underlying relationship between the input and output vector.

The training data are selected from the training data set randomly without replacement. After several cycles of training data presentation and weight adjustment, target performance criteria are met and the weights stored. These represent the "knowledge" of the neural network. Once training is complete, the neural network may be tested on a separate set of test data with which it has not been presented before.

Performance tests on the novel data reveal whether the neural network has sufficiently abstracted the underlying relationships in the data or whether it has merely learnt the training data set. More on performance measures in sections 5-5 and 5-6.

There are three classes of learning in neural network, supervised, reinforcement and unsupervised learning:

Supervised learning

Supervised learning requires a teacher, that is a set of input-output pairs that represent the desired response of the neural network to particular input vectors. This data may be measured, or derived from a human (or rule-based) expert. In the first instance, historical (input) data with its resultant (output) effect are used. For the second case, a human or a rule-based expert system may arbitrate on the correct action to take as a target response to a set of inputs. The first method is most frequently used when dealing with problems when it is known or suspected that there is some deterministic relationship between several inputs and the neural network output.

In many cases, it is not possible to obtain input-output pairs of data, for example when one is unsure how many and how different categories of data should be. Figure 5-14 gives a schematic representation of supervised learning. The most famous supervised learning technique is the back-propagation paradigm.

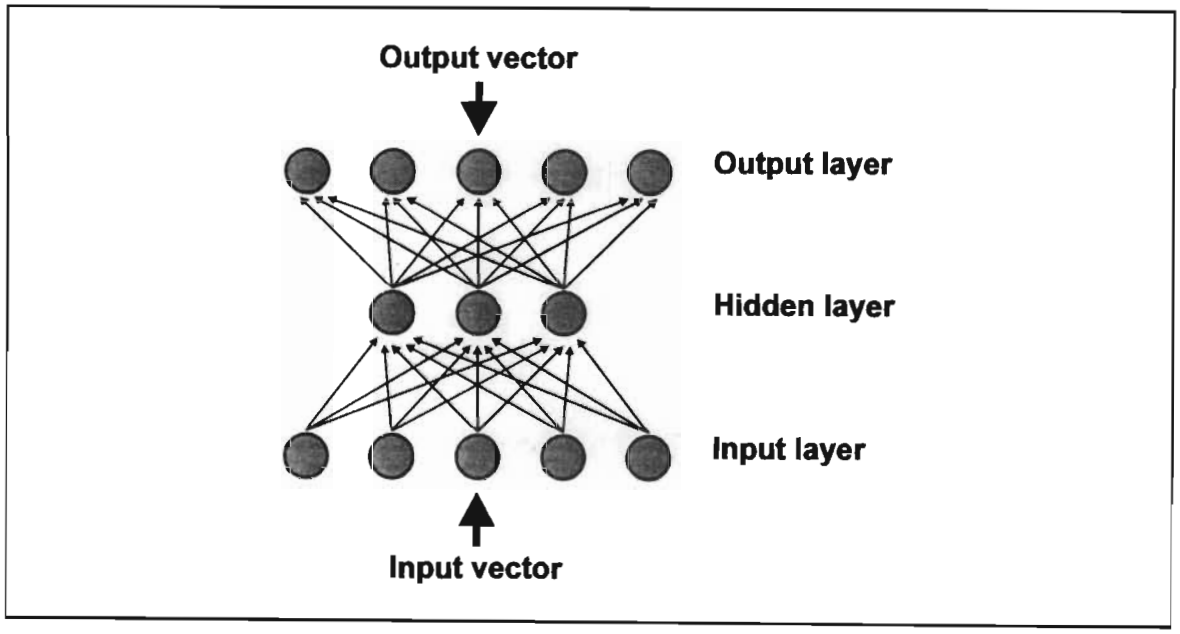

Figure 5-14 Supervised learning paradigm

Reinforcement learning

Although similar to supervised learning, reinforcement learning is much slower. Reinforcement learning (also called Hebbian learning) attempts to emulate the biological method of global reward/punishment in response to inputs. Instead of showing the target response at the output of the neural network to aid learning, this process merely assigns a reward or punishment to the network as a whole. Many training trials are required for the neural network to assign the weights correctly. Compared to the supervised learning case where the learning process is more directed, the reinforcement paradigm is more akin to a directed random search. Figure 5-15 indicates diagramatically how reinforcement learning works. An example of this technique is the Directed Random Search paradigm and Genetic Algorithm enhanced learning.

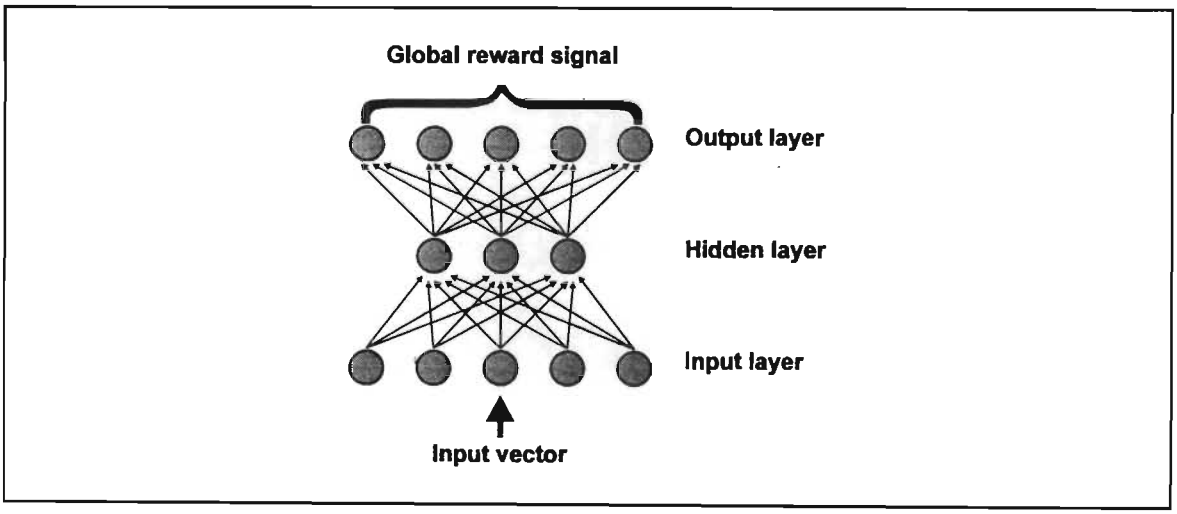

Figure 5-15 Reinforcement learning paradigm

Unsupervised learning

Also known as self-supervised learning, this method allows the data to organize itself into regions of similar characteristics. Thus input vectors that were similar would be projected onto a common classification region, those that were dissimilar onto different classification regions. The two-dimensional plane containing these classification regions is commonly known as the Kohonen layer after its originator Tuevo Kohonen. Kohonen's neural networks are known as self-organizing-maps or simply Kohonen neural networks. A related technique, though not totally unsupervised is the learning vector quantization paradigm where the "regions" of simi-

larity are uni-dimensional. Figure 5-16 shows a simple self-organising map neural network where similar and dissimilar vectors are matched to separate regions on the Kohonen layer.

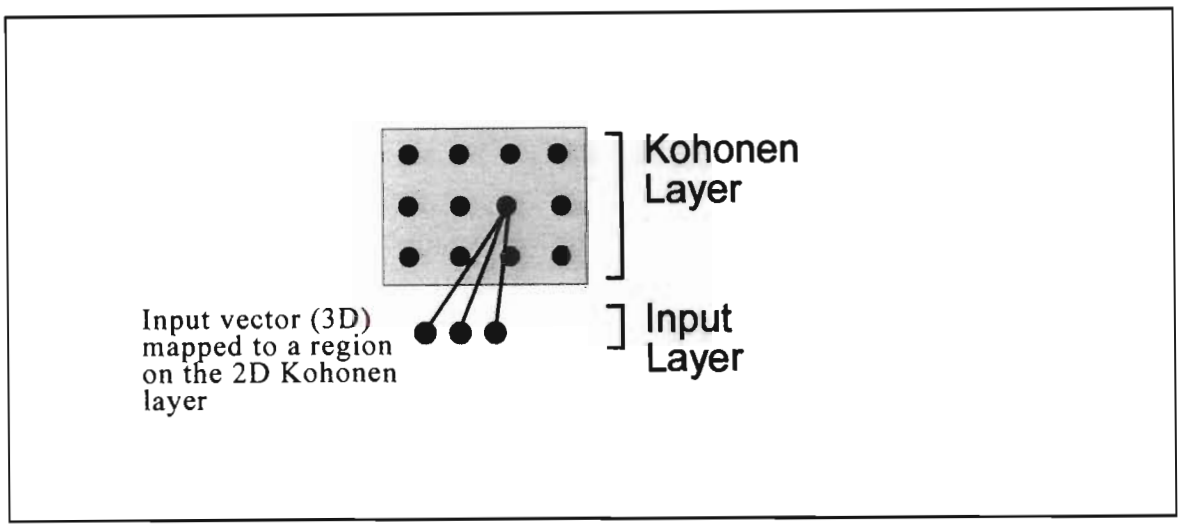

Figure 5-16 Unsupervised (self-supervised) learning paradigm

5.3 Back-propagation neural networks

Back-propagation neural networks are feedforward multilayer type networks. The back-propagation relates to the method of learning. Back-propagation neural networks rely on supervised training where the training set consists of discrete pairs of input-output vectors. Back-propagation neural networks form a mapping of the input vector to the output vector, the features of this mapping and the relationship between the input variables is learnt by the hidden layer/s. The layers in a back-propagation neural network are usually fully connected.

The back-propagation paradigm in a multi-layer neural network was co-invented by several researchers in the 1970's and 1980's, [*Werbos*, 1974, 1988], [*Rumelhart & McClelland*, 1986], [*Parker*, 1985]. Back-propagation neural networks are currently the most popular neural network paradigm for real-world applications. Also see *Neural Computing* [1993].

5.3.1 Learning in back-propagation neural networks

Back-propagation learns by calculating an error between the desired and the actual neural network output in response to an input. This error is propagated backwards through the network to every neuron. The back-propagated error is used to drive the learning (i.e. weight adaptation) at each neuron.

The rate at which these errors modify the weights is referred to as the learning rate or learning coefficient. Figure 5-17a shows a typical back-propagation neural network structure and Figure 5-17b the notation used for each neuron in the back-propagation neural network analysis.

Considering the Figures 5-17a and 5-17b, the output of an individual neuron is given by [*Werbos*, 1988]:

$$x_j^{[s]} = f\left[\sum_i w_{ji}^{[s]} x_i^{[s-1]}\right]$$

$$= f(I_j^{[s]}) \qquad (5\text{-}3)$$

where

[ ] indicate the layer under consideration

$x_j^{[s]}$ is the output activation of current neuron j in layer [s]

$w_{ji}^{[s]}$ is the weight on the connection between the ith neuron in layer [s-1] to the jth neuron in layer [s]

$x_i^{[s-1]}$ is the incoming activation of neuron i in the previous layer [s-1]

$I_j^{[s]}$ is the weighted sum of the input to the jth neuron in layer [s]

f is the transfer function $f(z) = (1 + \exp^{-z})^{-1}$ for a sigmoid

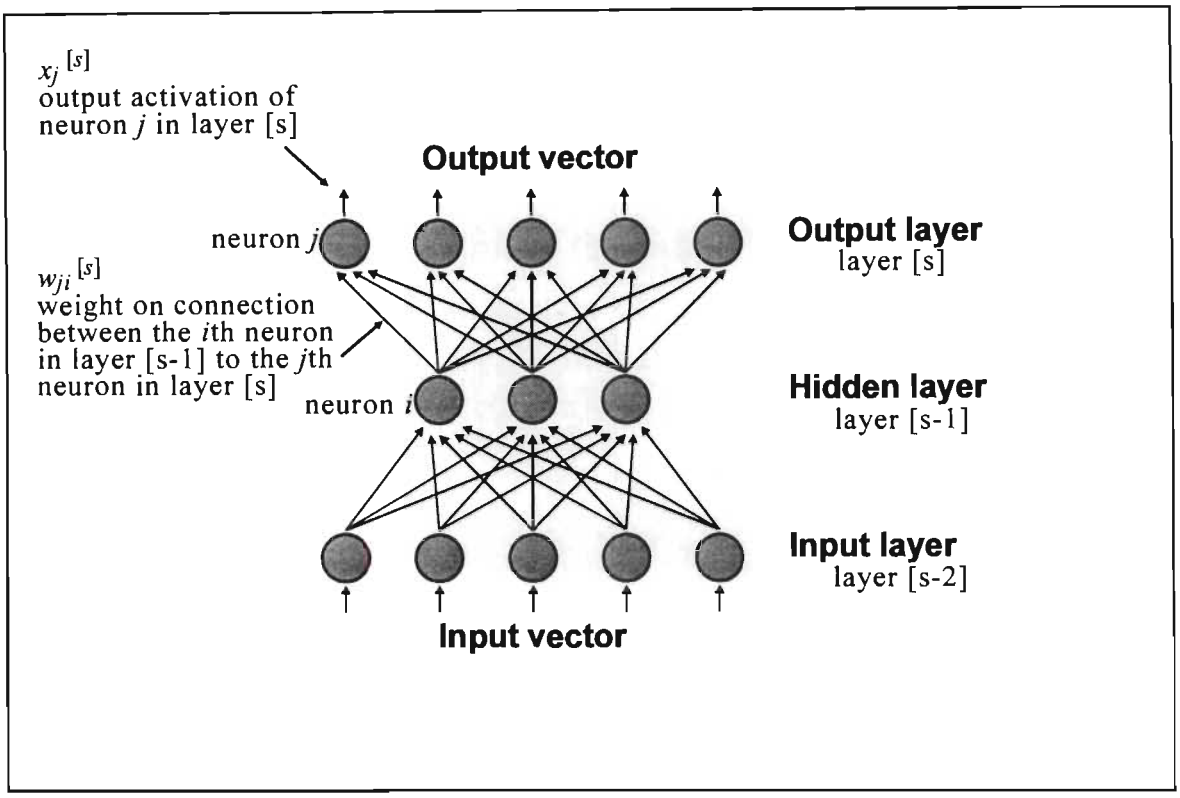

Figure 5-17a Back-propagation neural network nomenclature

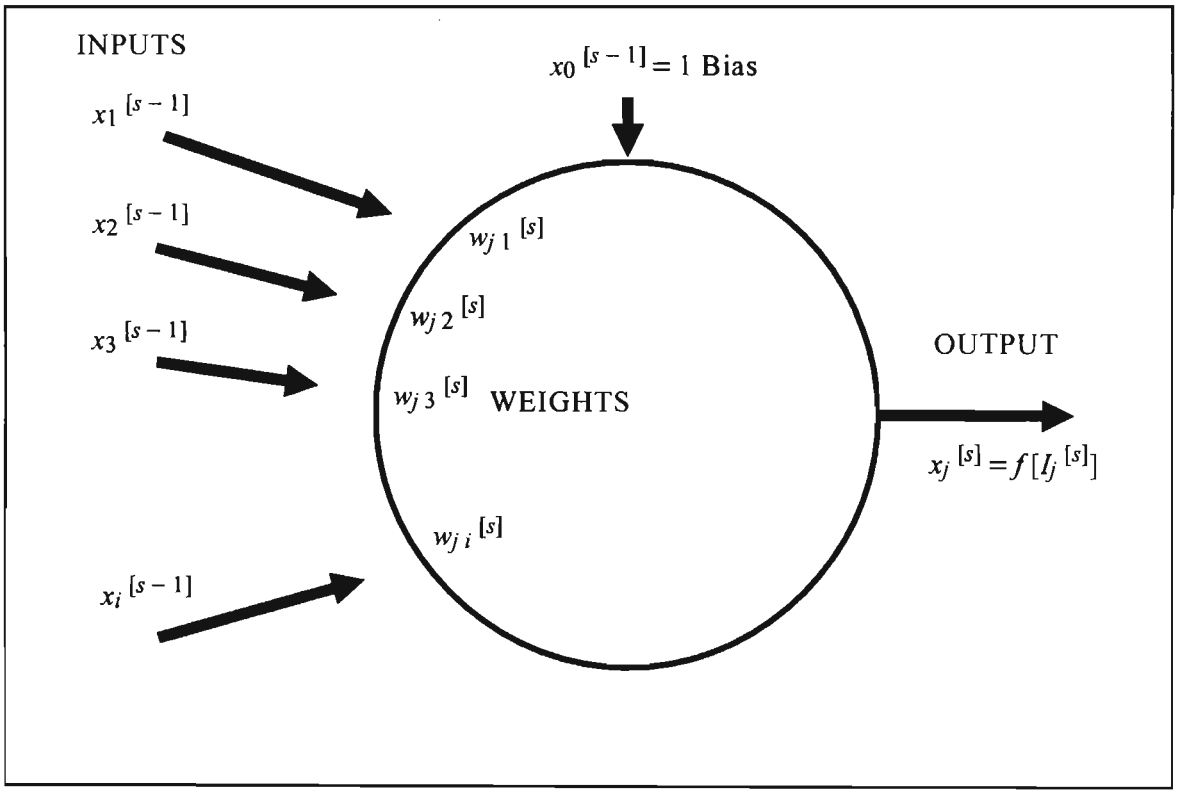

Figure 5-17b Back-propagation neuron nomenclature

5.3.2 Back-propagating the local error

The neural network has a global error function E associated with it which is a differentiable function of all the connection weights of the neural network. The parameter that is passed back through the layers is:

$$e_j^{[s]} = \frac{-\partial E}{\partial I_j^{[s]}} \tag{5-4}$$

where

$e_j^{[s]}$ is a measure of the local error at neuron j in layer [s]

Using the chain rule twice gives a relationship between the local error at a particular neuron in layer [s] and all the local errors at in the following layer [s+1]:

$$e_j^{[s]} = f'\left(I_j^{[s]}\right) \cdot \sum_k \left(e_k^{[s+1]} \cdot w_{kj}^{[s+1]}\right) \tag{5-5}$$

Note: this is used in all layers except the output layer (since it has no [s+1] layer).

If the sigmoid transfer function is used in equation (5-5), then the derivative of the sigmoid is a simple function of itself:

$$f'(z) = f(z) \cdot (1 - f(z)) = \frac{\exp^{-z}}{\left[1 + \exp^{-z}\right]^2} \tag{5-6}$$

If the derivative is near zero (when $f(z)$ is near 0 or 1), then the change in weights is small. These are two stable states. When the derivative is not near zero, there is a corresponding increase in weight change.

If the transfer function is a hyperbolic tangent function, then its derivative may also be expressed with respect to itself:

$$f'(z) = (1 + f(z))(1 - f(z)) \tag{5-7}$$

Using this equation (5-5) would be modified to:

$$e_j^{[s]} = (1 + x_j^{[s]})(1 - x_j^{[s]}) \cdot \sum_k \left(e_k^{[s+1]} . w_{kj}^{[s+1]} \right) \tag{5-8}$$

Continuing with the sigmoid transfer function, using (5-6), (5-5) can be re-written as follows (provided f is a sigmoid):

$$e_j^{[s]} = x_j^{[s]}(1 - x_j^{[s]}) \cdot \sum_k \left(e_k^{[s+1]} . w_{kj}^{[s+1]} \right) \tag{5-9}$$

The summation term in (5-9) is which is used to back-propagate errors is analogous to the summation term in (5-3) which is used to forward propagate the input through the network. Thus the main mechanism is to forward propagate the input and then back-propagate the errors from the output to the input using (5-9) or more generally (5-7).

5.3.3 Minimizing the global error

To fulfill the aim of minimizing the global error E by modifying the weights, use is made of the local error at each neuron.

Given a current set of weights $w_{ji}^{[s]}$, we need to determine how to increment or decrement them in order to decrease the global error E. This error E may be visualized as a multi-dimensional surface in n-dimensional space. This may be achieved by using a gradient descent method of searching for an optimal minimum. There are several other rules and heuristics which may be used in place of the gradient descent method to improve learning. These will be discussed shortly as improvements to the back-propagation algorithm.

The gradient descent method gives a measure of changing the individual weights in response to the global error. This equation shows that weight changes are made in response to the size and direction of the negative gradient of the error surface:

$$\Delta w_{ji}^{[s]} = - l_{coef} \left(\frac{\partial E}{\partial w_{ji}{}^{[s]}} \right) \tag{5-10}$$

where l_{coef} is a learning coefficient

The partial derivatives in (5-10) can be calculated directly from the local error values. Using the chain rule and (5-4):

$$\frac{\partial E}{\partial w_{ji}{}^{[s]}} = \left(\frac{\partial E}{\partial I_j{}^{[s]}} \right) \cdot \left(\frac{\partial I_j{}^{[s]}}{\partial w_{ji}{}^{[s]}} \right)$$

$$= - e_j{}^{[s]} x_i{}^{[s]} \tag{5-11}$$

Combining (5-10) and (5-11):

$$\Delta w_{ji}{}^{[s]} = l_{coef} e_j{}^{[s]} x_i{}^{[s-1]} \tag{5-12}$$

5.3.4 The global error function

This function is needed to specify the local errors at the output layer so that they can be propagated backwards. Suppose vector i is presented to the input and vector d presented to the output as a training data pair. Let o denote the actual output produced by the neural network with its current set of weights. Then a measure of the error in achieving the desired output is given by the square of the Euclidean distance between the two vectors (also known as the mean-squared error):

$$E = \frac{1}{2} \sum_k \left[(d_k - o_k)^2 \right] \tag{5-13}$$

where k indexes the components of d and o

Here the raw local error at each neuron of the output layer is:

$$e_k^{[o]} = \frac{-\partial E}{\partial I_k^{[o]}}$$

$$= \frac{-\partial E}{\partial o_k} \cdot \frac{\partial o_k}{\partial I_k^{[o]}}$$

$$= (d_k - o_k) f'(I_k^{[o]})$$

$$e_k^{[o]} = (d_k - o_k) x_k^{[o]} (1 - x_k^{[o]}) \qquad (5\text{-}14)$$

Other error functions may be substituted for this standard one:

$$E = \frac{1}{3} \sum_k \left| (d_k - o_k)^3 \right| \qquad (5\text{-}15)$$

$$E = \frac{1}{4} \sum_k \left[(d_k - o_k)^4 \right] \qquad (5\text{-}16)$$

These give local errors of:

$$e_k^{[o]} = (d_k - o_k)^2 f'(I_k^{[o]}) \qquad (5\text{-}17)$$

(quadratic error function)

$$e_k^{[o]} = (d_k - o_k)^3 f'(I_k^{[o]}) \qquad (5\text{-}18)$$

(cubic error function)

(5-13) is for the global error for a *particular* (*i*,*d*). An overall global error can be defined as the sum of all the specific error functions. Then each time a particular (*i*,*d*) is shown, the back-propagation modifies weights to reduce that particular component of the overall error function.

5.3.5 Summary of the standard back-propagation algorithm operation

Given an input vector $\underline{i}$ and a desired output vector $\underline{d}$ do the following:

- Present $\underline{i}$ to the input and propagate it through the neural network to the output obtaining vector $\underline{o}$
- As $\underline{i}$ propagates through neural network, it will set all the summed inputs I_j and output states x_j for each neuron
- For *each* neuron in the output layer, calculate the scaled local error as given in (5-14) and then calculate the delta weight using (5-12)
- For each layer [s], starting at the layer prior to the output layer and moving to the layer after the input layer, and for each neuron in [s] calculate the scaled local error as given by (5-9) then calculate the delta weight using (5-12)
- Update all weights in the network by adding the delta weights to the corresponding previous weights.

5.3.6 Enhancements to the back-propagation algorithm

Cumulative weight update

In cumulative (batch) mode, back-propagation neural networks accumulate their weights over an epoch before they are applied to the neural network. The epoch size is a number less than or equal to the number of training vectors. Standard back-propagation uses an epoch size of one, i.e. the weight changes are applied as soon as they are calculated. Cumulative back-propagation may aid learning by "filtering out" minor changes in weights and updating general weight change trends instead.

Momentum

The difficulty with the gradient descent method is the setting of the learning coefficient. This is because changing weights as a linear function of the partial derivative makes the assumption that the error surface is locally linear. While this assumption may hold in general, in regions of high curvature it does not and may lead to divergent behaviour if the learning coefficient is not sufficiently small. The drawback with a small learning coefficient is slow learning, therefore the concept of momentum is added to solve the dichotomy. Momentum simply indicates that if weights are changing in a certain direction, there should be a tendency for them to continue changing in the same direction.

The delta weight is modified so that a proportion of the previous delta weight is fed through to the current delta weight:

$$\Delta w_{ji}{}^{[s]}\,(\text{current}) = l_{coef}\, e_j{}^{[s]}\, x_i{}^{[s-1]} + \text{momentum}\,\Delta w_{ji}{}^{[s]}\,(\text{previous}) \tag{5-19}$$

Momentum allows for a smaller learning coefficient yet with faster learning.

Saturation and *f'* offset

To improve the learning speed of the standard back-propagation algorithm, a small positive offset is added to the derivative of the sigmoid. The reason is that the incoming weights of a neuron can become so large that the activation values saturate at their limits (either 0 & 1 or -1 & +1). The derivative of these values on the transfer function is very near zero, so training at that neuron effectively stops. By adding the *f'* offset, this saturation problem is alleviated.

Extended-delta-bar-delta learning heuristic

The extended-delta-bar-delta heuristic was developed by *Minai and Williams* [1990] as an extension to the delta-bar-delta heuristic of *Jacobs* [1988]. The delta-bar-delta rule uses past values of the gradient to infer the local curvature of the error surface. This leads to a learning rule in which every connection has a different learning rate which is automatically calculated. The extended delta-bar-delta heuristic also calculates a momentum term for each connection, thus automating both learning rate and momentum choice. This paradigm is the paradigm of choice for back-propagation neural network development, though others such as Cascade Correlation [*Fahlman*, 1988] and the Logicon Projection Network™ [*Wilensky & Manukian*, 1992] have particular strengths in specific applications.

5.3.7 Back-propagation summary

- It is a general purpose non-linear regression technique which attempts to minimize global error.
- Any multi-dimensional can theoretically be synthesized by a back-propagation neural network.
- It can provide a very compact distributed representation of complex data sets

5.4 Learning vector quantization neural networks

The learning vector quantization neural network was originally suggested by *Kohonen* et al., [1988] to assign vectors to one of several classes. A learning vector quantization network contains a Kohonen layer which learns and performs the classification. Learning vector quantization provides equal numbers of neurons for each class in the Kohonen layer. The basic learning vector quantization neural network trains and then uses the Kohonen layer as follows:

- In the training mode, the distance of a training vector to each neuron is computed and the nearest neuron is declared to be the winner.
- If the winning neuron is in the class of the training vector, it is moved toward the training vector.
- If the winning neuron is not in the class of the training vector, it is moved away from the training vector (called repulsion).
- During this training process, the neurons assigned to a class, migrate to the region associated with their class.
- In the classification mode, the distance of an input vector to each neuron is computed and again, the nearest neuron is declared to be the winner. The input vector is then assigned to the class of that neuron.

The basic learning vector quantization neural network suffers from several shortcomings and variants have been developed to overcome them. These include the addition of a "conscience" mechanism to restrict operation of neurons which win too often and prevent others from participating, a technique to refine the boundaries between classes, a method of including the Bayesian likelihood function and the elimination of the repulsion mechanism. Combined these form a very workable implementation of learning vector quantization. More details of learning vector quantization neural network are found in *Neural Computing* [1993].

5.5 Neural network development environment

The neural network development environment used was produced by *NeuralWare Inc.* of Pittsburgh U.S.A. The environment which allows cross-platform compatibility between IBM-type personal computers and workstations is called *NeuralWorks Professional II+*. This package supports development of 28 major neural network paradigms with several variations on each. The back-propagation and learning vector quantization algorithms required for this thesis, were well supported. *NeuralWorks Professional II+* allows building, training, refining and deployment of neural network's. Several features make it particularly useful in development, viz.:

- *InstaNet* - a menu system to select neural network type and parameters
- *FlashCode* - ANSI standard C code generation of neural network for deployment
- *SaveBest* - facility to prevent overtraining a neural network by regularly saving a neural network (i.e. memorization of training data causing loss of generalization ability with test data).
- *Prune* - facility during training to eliminate neurons that do not contribute to learning
- *ExplainNet* - feature to explain why a neural network made its decisions and which inputs are important

In addition diagnostic tools such as classification rate, RMS error, weight-histogram etc. help in the development phase. All the features of the development environment are available from an intuitive graphical user interface. This eliminates the need to hard-code neural network paradigms and training schedules. An example of the graphical user interface is shown in Figure 5-18.

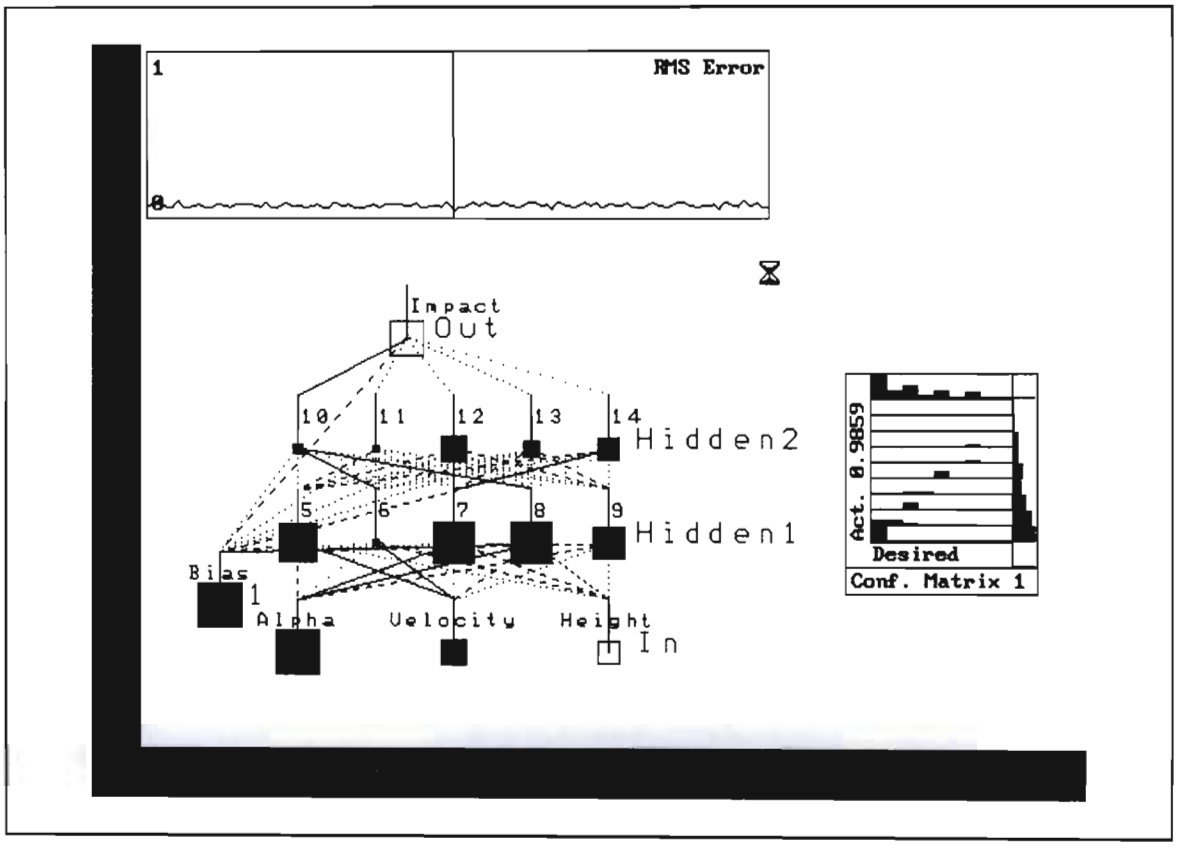

Figure 5-18 *NeuralWorks Professional II+* graphical user interface

There are several instruments available in *NeuralWorks Professional II+* which help in training and testing neural networks. Examples of these instruments are shown in Figure 5-19:

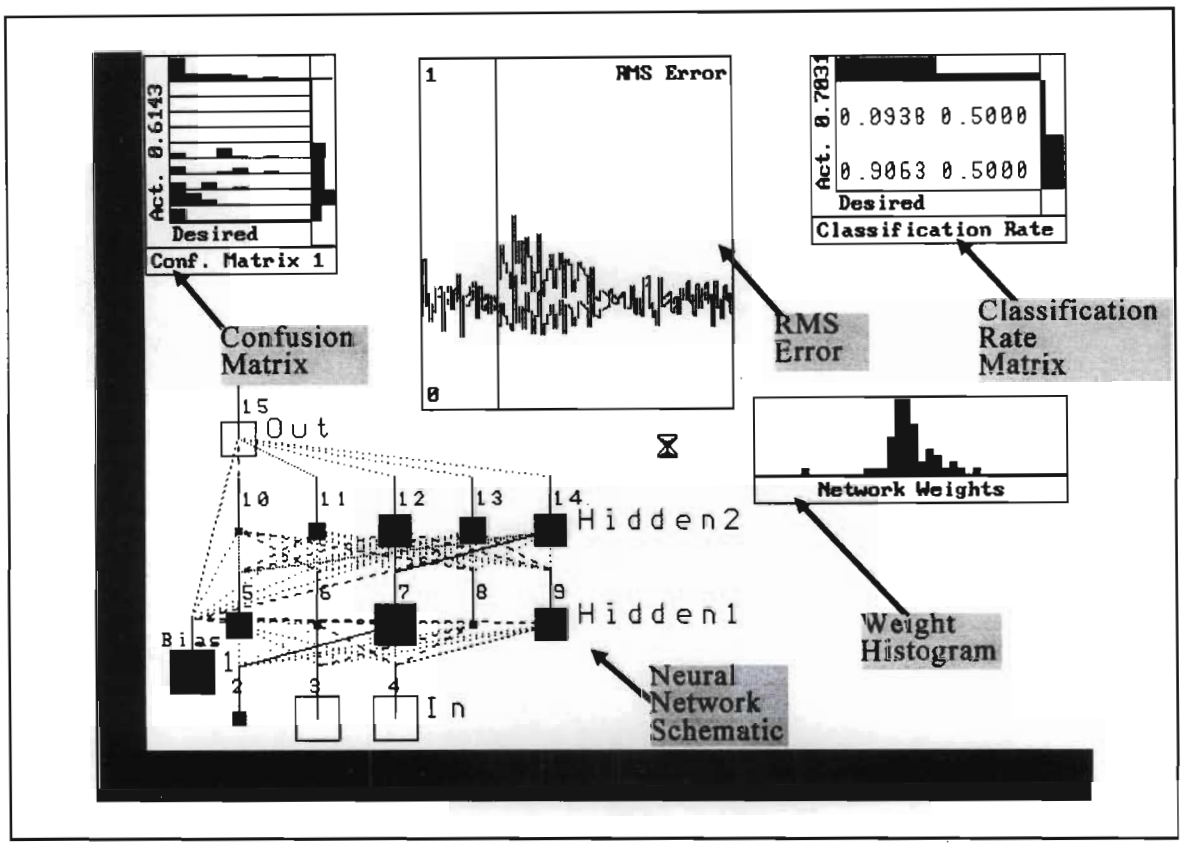

Figure 5-19 *NeuralWorks Professional II+* instrumentation

RMS error

- used in prediction/regression analysis
- indicates the error root-mean-square error of all the neurons in the output layer
- gives a measure of the closeness of fit of desired to actual neural network response

Weight histogram

- used to check condition and spread of neural weights
- provides a measure of the entire network
- the height of the bars represents the number of weights in each weight category
- for a well-trained, non-saturated neural network, the weights should be ideally Gaussian distributed about zero or evenly distributed across the weight range

Confusion matrix

- used in classification/ranking problems
- indicates the correlation of actual to desired to actual results for each category
- the confusion matrix is a analogue of a scatter-plot where the height of the bars in each "bin" represent the number of "hits" within that bin.
- ideally the bars should line up along the diagonal
- the numerical figure indicates the correlation for each matrix

Classification rate matrix

- used in classification/ranking problems
- similar to the confusion matrix, it provides a measure of correlation for the entire network
- the figures on the diagonal represent the fraction of correctly classified training or test cases
- the figure off-diagonal represent the fraction of misclassified classes
- it can provide a measure of which classifications are overlapping or difficult to separate

5.6 Practical issues in developing back-propagation neural networks

Number of input neurons

The number of input neurons is determined by the type of data used. In other words, the more feature descriptors that are used, the larger the input layer will be. Generally it is better to commence with more feature descriptors and selectively delete those which have little or no effect on learning.

Number of hidden neurons

The choice of this number is one of the most debated topics in neural networks. Fundamentally the number of hidden neurons depends strongly on the type of data used. That is, if the data is simple (e.g. easily separable) then fewer neurons are required than in the case of complex data sets. Basically, each hidden neuron provides an extra hyperplane to separate regions in multi-dimensional hyperspace. If the contour of distinction between categories, for example, is complex more hyperplanes will be needed to define it.

Widrow & Stearns [1985] recommend that the number of hidden neurons be related to the number of training samples available. They states that the ratio of the number of weights to the number of training samples should be at most 10%. In most instances, the number of input and output neurons are defined by the type of problem, so calculation of the number of weights in a back-propagation neural network is simple.

Several heuristics exist, but do not take into account a measure of data complexity. A better method is to use the designed experiments technique. This allows a scientific, rigorous approach to choosing this number. A set of experiments is designed, neural networks constructed and tested with different numbers of hidden neurons and the optimal configuration selected. This method was used in neural network development in this thesis.

Number of hidden layers

In general it is advisable to start with a single hidden layer in the back-propagation neural network and only progress to two hidden layers when training became difficult. The need for three hidden layers is rarely found.

Choice of learning paradigm

With back-propagation, it is usually best to use the extended-delta-bar-delta heuristic for learning. It alleviates the need to set the momentum and learning coefficient terms interactively, by automatically selecting these parameters during training. The extended delta-bar-delta heuristic was used in all back-propagation neural networks designed in this thesis.

Epoch size

The number of training data passes that are allowed before cumulative update of weights is termed the epoch size. Ideally this should be as large as the number of training samples, however owing to the extensive training set available, the epoch size was limited, usually between 250 and 1000. The limit was required to improve learning speed and allow the influence of training samples with a lower rate of occurrence to influence the weights. If the full epoch size had been chosen, the rarer data samples would have been eliminated in the generalization that occurs.

Optimal epoch size can be chosen using a designed experiments method in which various sizes are tested for the highest correlation value. This is a more thorough approach yet had little effect on the large data set available for training.

Weight initialization

Weights were initialized randomly within a small range around zero. Typically the values were between -0.2 and +0.2.

Chapter 6

Neural networks for prediction and classification in meteor-burst communications

6.1 Introduction

Meteor-burst systems follow the laws of physics and are deterministic, i.e. they are sufficiently quantifiable to allow modeling and statistical prediction on the macroscopic level. However, individual meteor trails are sufficiently stochastic to defy traditional methods of predicting their attributes on a trail-by-trail basis as is seen in chapters 3 and 4. This characteristic makes meteor-burst communications ideally suited to the application of neural networks. Neural networks are adept at generalising the data with which they are presented and therefore are able to interpolate results when presented with new and unseen data. This makes neural network decision making extremely robust and insensitive to noise. Furthermore, the slight parametric changes that can be expected in data from a natural phenomenon are used constructively in the decision making process to refine predictions, rather than being considered as disturbances.

In this chapter the novel techniques for classification and prediction in meteor-burst communication are presented. Based on the trail amplitude data detailed in chapter 3, methods of data preparation are investigated. In particular meteor-burst communication trail classification by neural network and neural networks for prediction of trail type, peak trail amplitude and trail duration are presented. This work is extensively documented by the author in *Fraser* [1993], *Fraser & Melville* [1992, 1993a, 1993b] and *Goldstein, Melville and Fraser* [1992].

6.2 Data preparation

The raw data was obtained from the measurement system described in chapter 3. The data is stored in a format of header files and sample files. The header file consists of records, each of which contains information about a specific trail. Each record contains the positions in the sample file of the first and last samples of the current trail, background noise level, the time since the previous trail and the time and date. The sample file contains a stream of bytes, where each byte represents the magnitude of the signal at the sampling instant. A sampling frequency of 200 Hz was used (samples spaced at 5 ms intervals). For this application, no early fast Doppler data was used.

Based on the amplitude envelope of the signal received by the measurement system of chapter 3, meteor trails may be classified into different trail families. The classification is based on shape features of the trail amplitude envelope. Classification is an off-line procedure in which the entire trail data is used. The basis of trail classification comparison was the *TrailStar* rule-based expert system developed by *Melville* et al. [1989]. *TrailStar* was used to classify each trail into one of 29 distinct trail categories or classes. Examples of the trail families classified by *TrailStar* are shown in Figures 6-1 to 6-29. The term "trail-type" is used for consistency with previous research by this group. The more correct term as defined by the I.A.U. is "echo-type"

For the purposes of trail classification using neural networks, the classification decision of *TrailStar* was taken as correct, i.e. the classification of *TrailStar* would be the target decision of the neural network when training. The classification neural network may be viewed as a mapping of trail feature descriptors of an entire trail to a particular trail type. Instead of using the entire 29 categories, the data for the neural networks was subdivided into overdense and underdense categories (according to *TrailStar*), bad data (which was discarded) and "other" types (which *TrailStar* could not classify as either overdense or underdense).

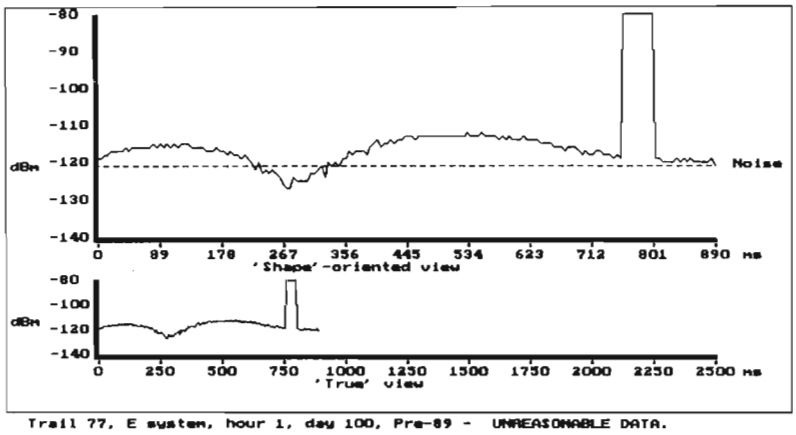

Figure 6-1 Trail type 1 - unreasonable data

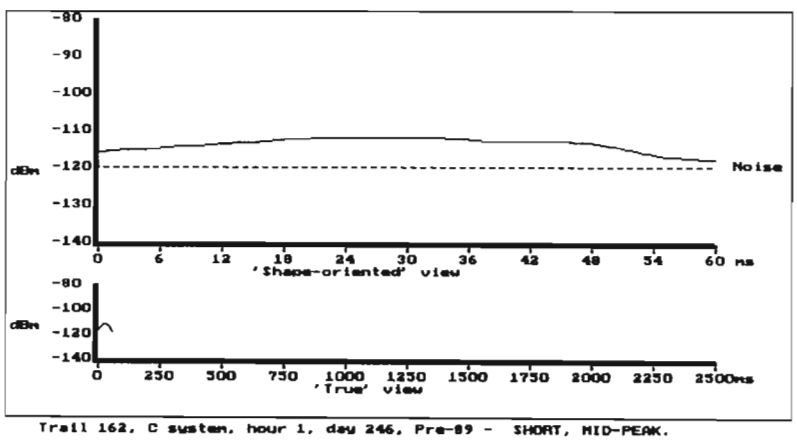

Figure 6-2 Trail type 2 - short mid-peak

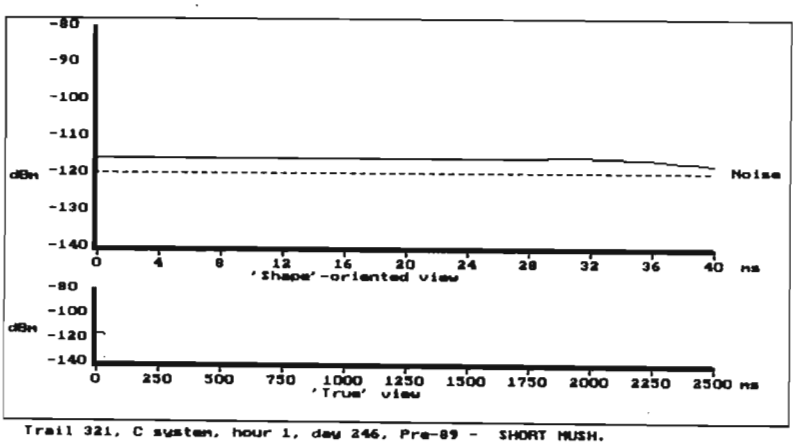

Figure 6-3 Trail type 3 - short mush

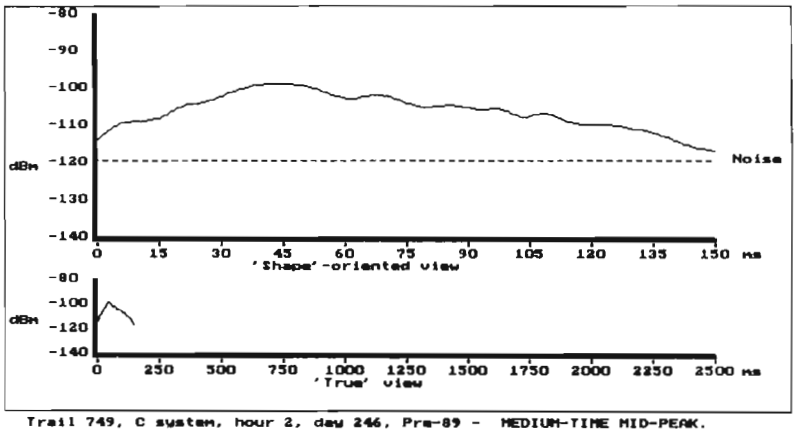

Figure 6-4 Trail type 4 - medium time mid-peak

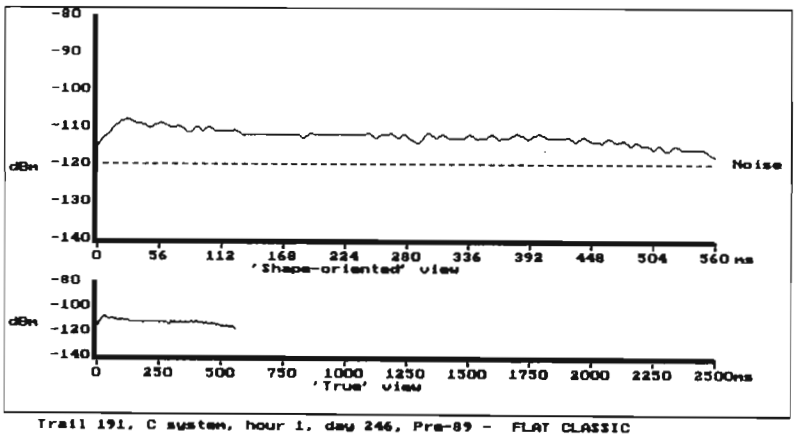

Figure 6-5 Trail type 5 - flat classic

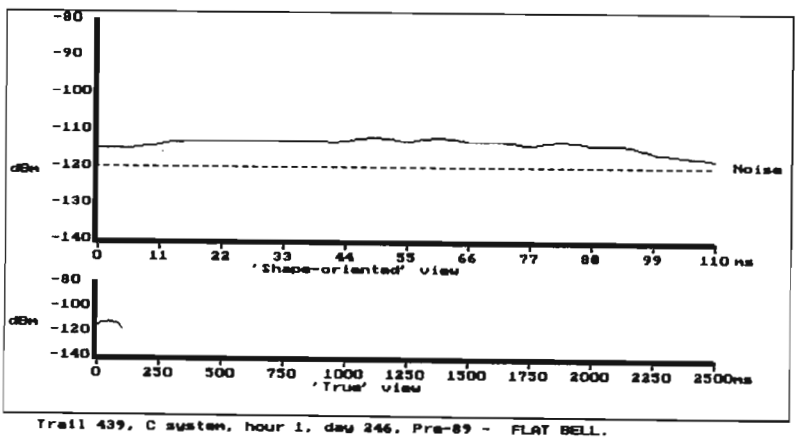

Figure 6-6 Trail type 6 - flat bell

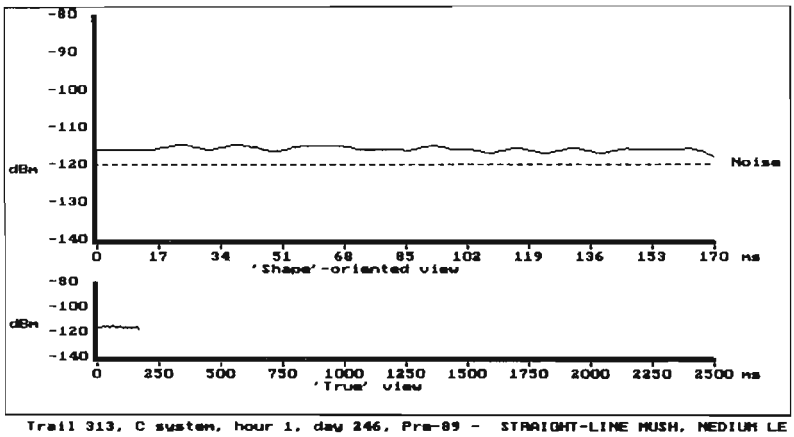

Figure 6-7 Trail type 7 - straight-line mush (medium length)

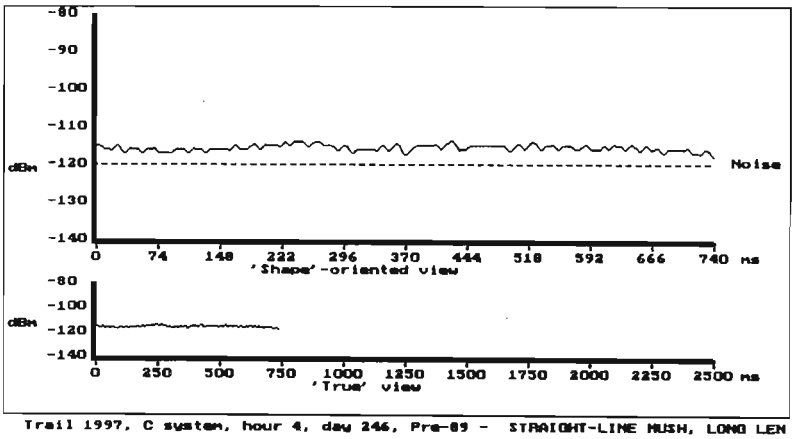

Figure 6-8 Trail type 8 - straight-line mush (long length)

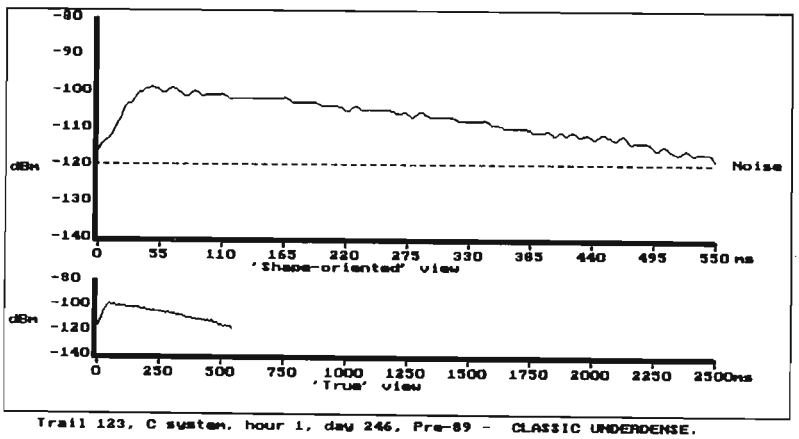

Figure 6-9 Trail type 9 - classic underdense

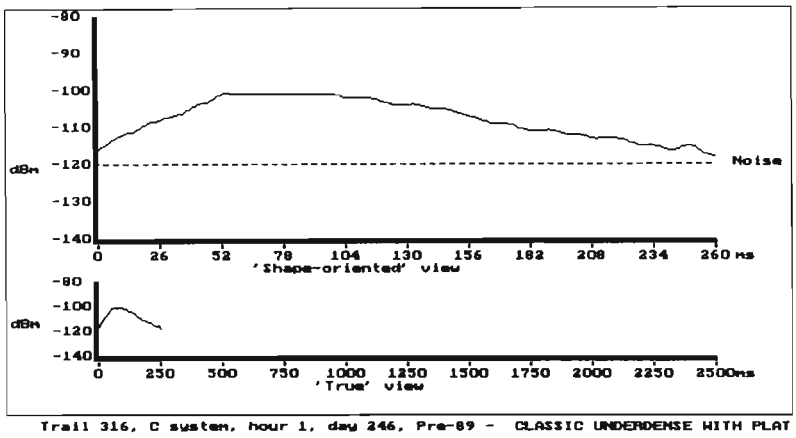

Figure 6-10 Trail type 10 - classic underdense with plateau

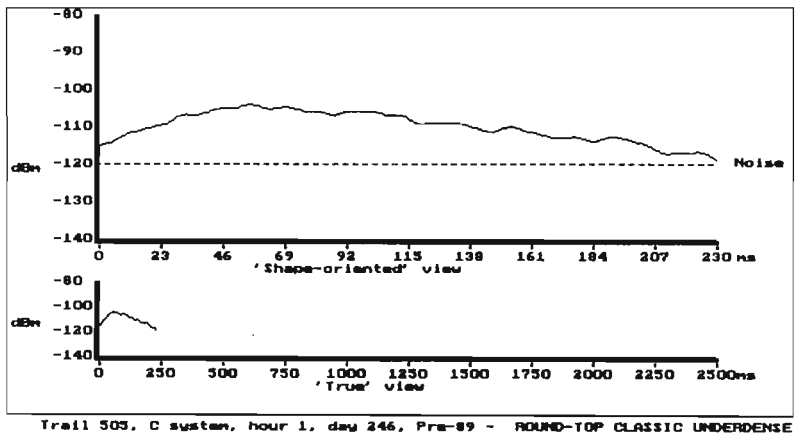

Figure 6-11 Trail type 11 - round-top classic underdense

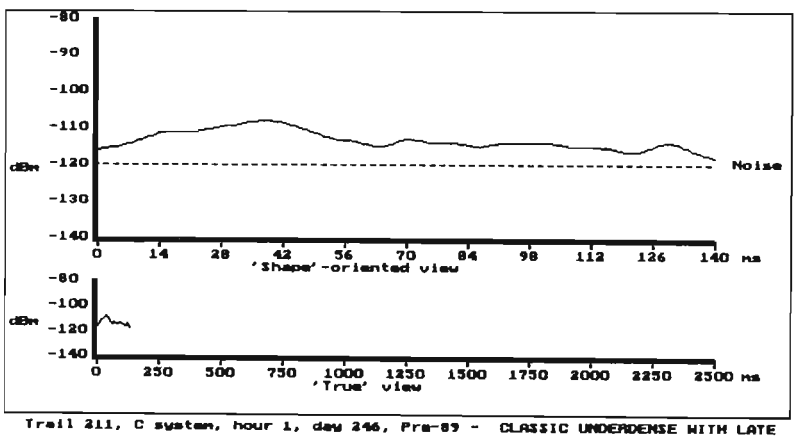

Figure 6-12 Trail type 12 - classic underdense with late fall

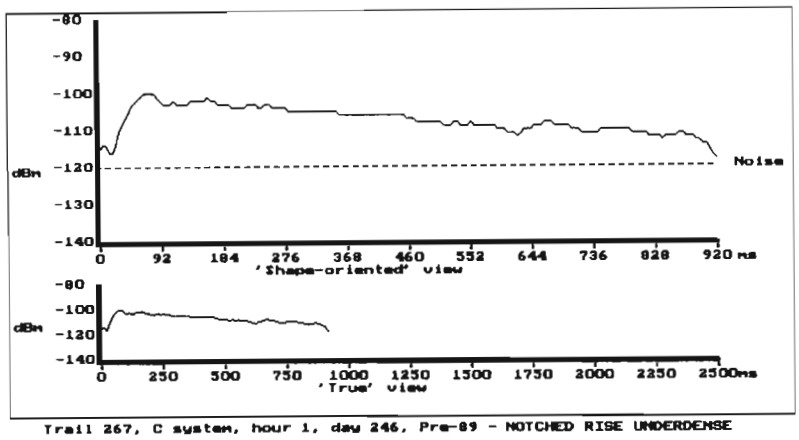

Figure 6-13 Trail type 13 - notched rise underdense

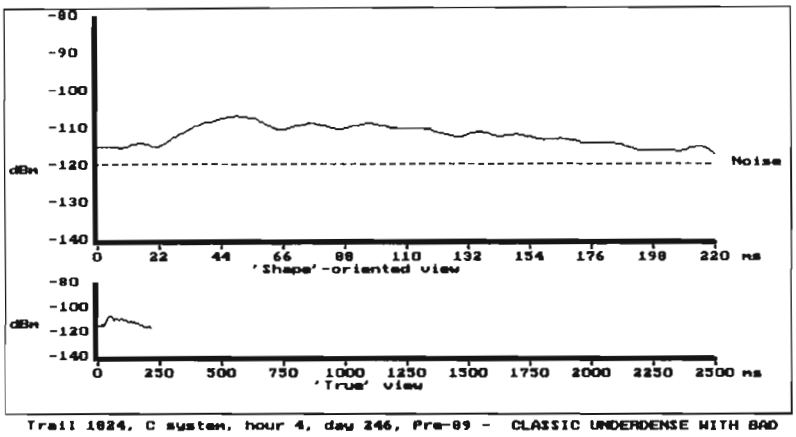

Figure 6-14 Trail type 14 - underdense with bad rise

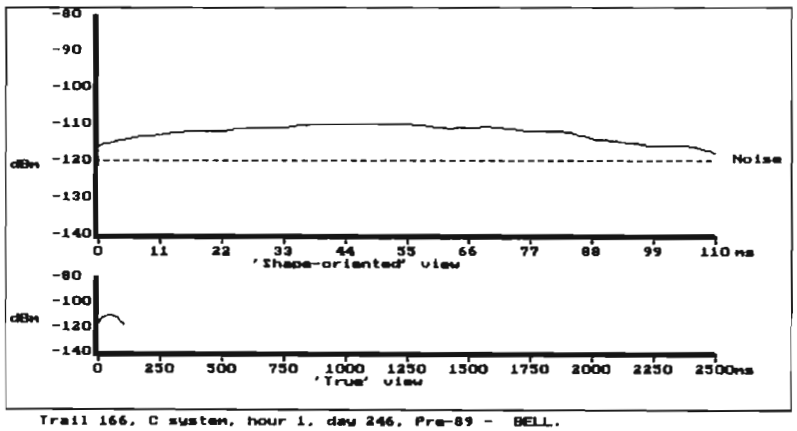

Figure 6-15 Trail type 15 - bell

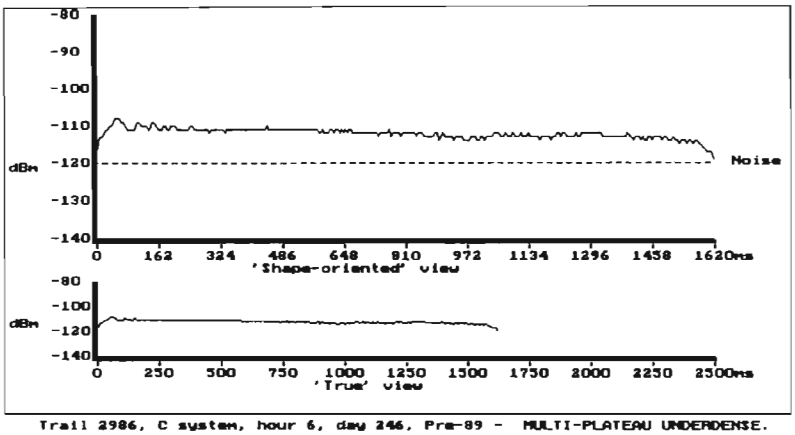

Figure 6-16 Trail type 16 - multi-plateau underdense

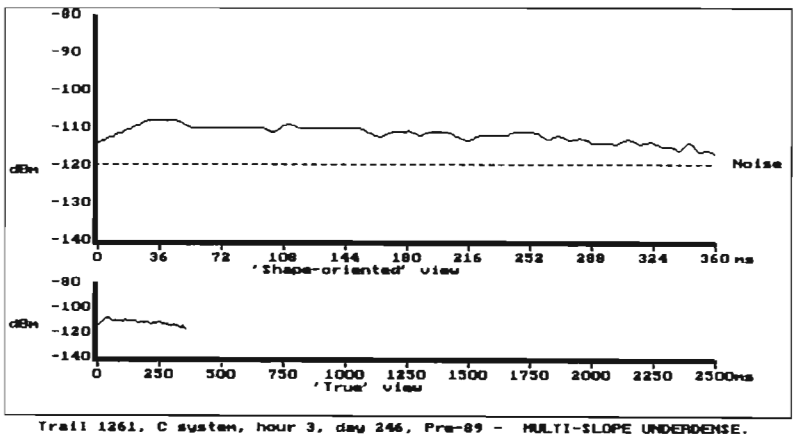

Figure 6-17 Trail type 17 - multi-slope underdense

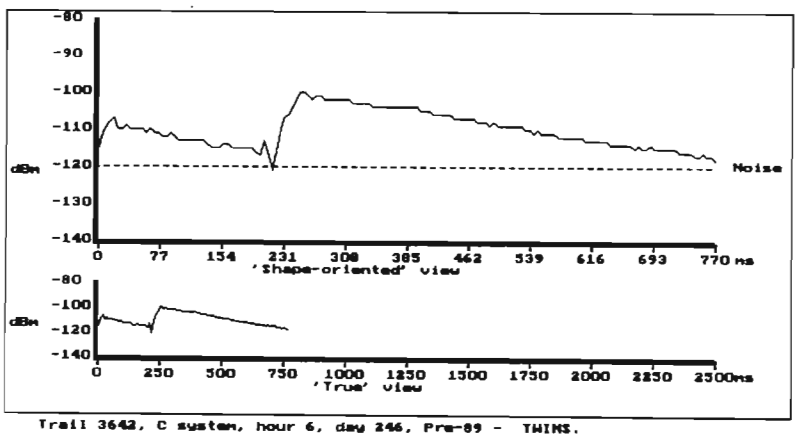

Figure 6-18 Trail type 18 - twins

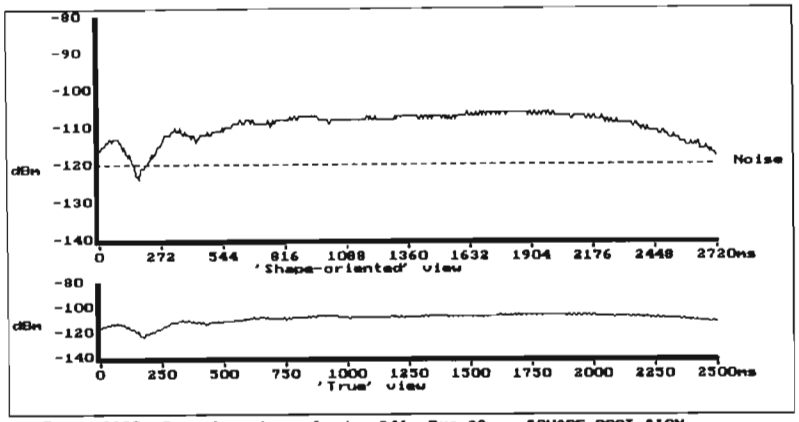

Figure 6-19 Trail type 19 - square root

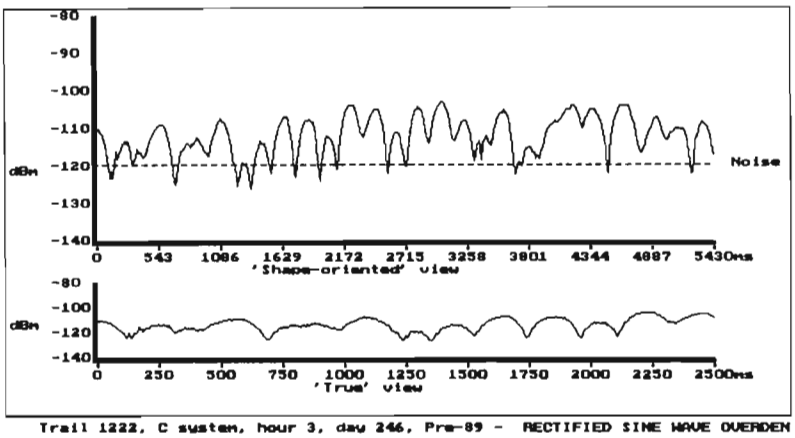

Figure 6-20 Trail type 20 - rectified sine overdense

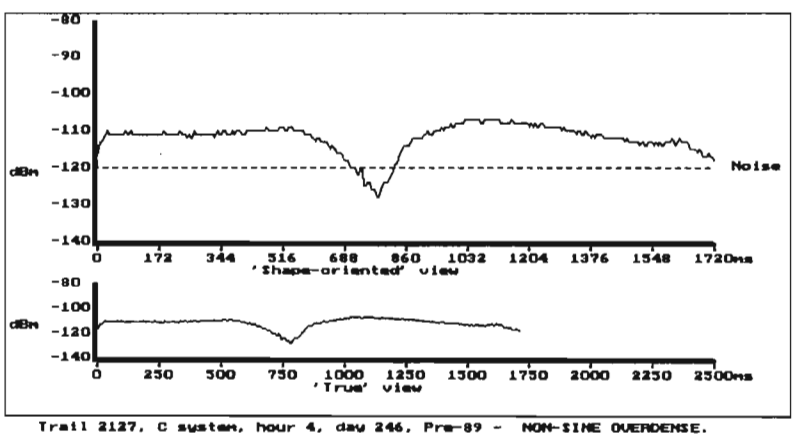

Figure 6-21 Trail type 21 - non-sine overdense

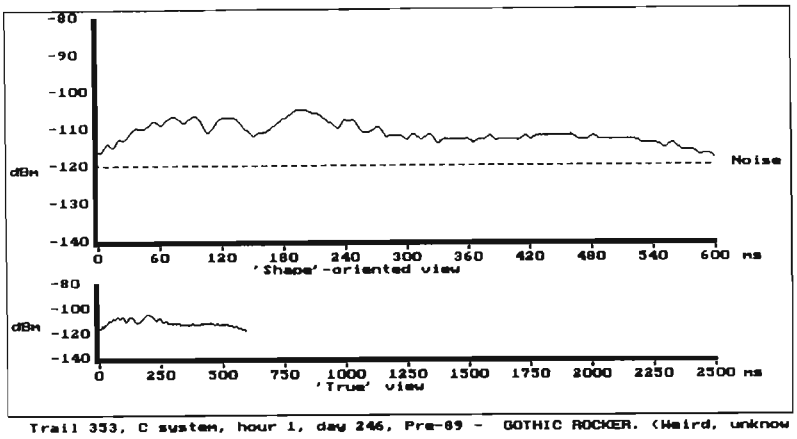

Figure 6-22 Trail type 22 - gothic rocker (unknown/weird type)

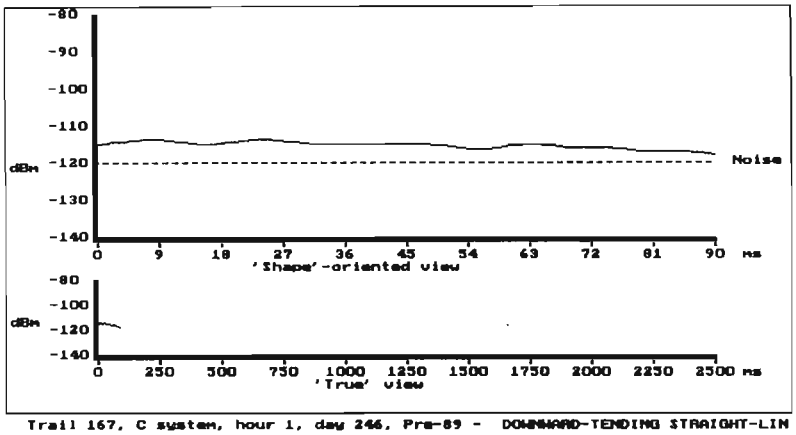

Figure 6-23 Trail type 23 - downward-tending straight-line mush

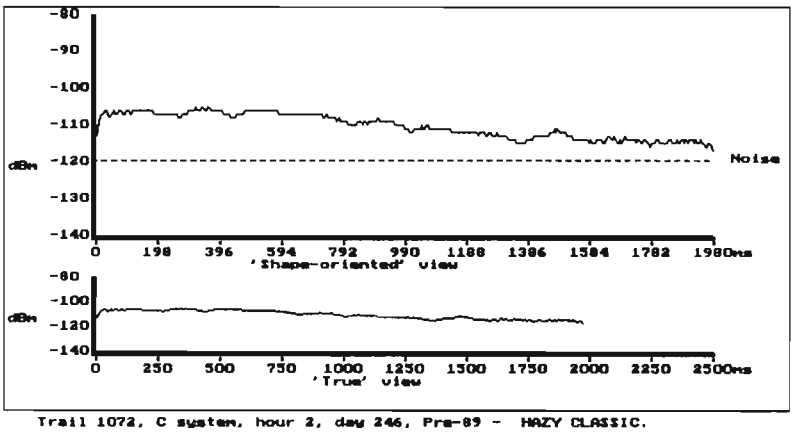

Figure 6-24 Trail type 24 - hazy classic

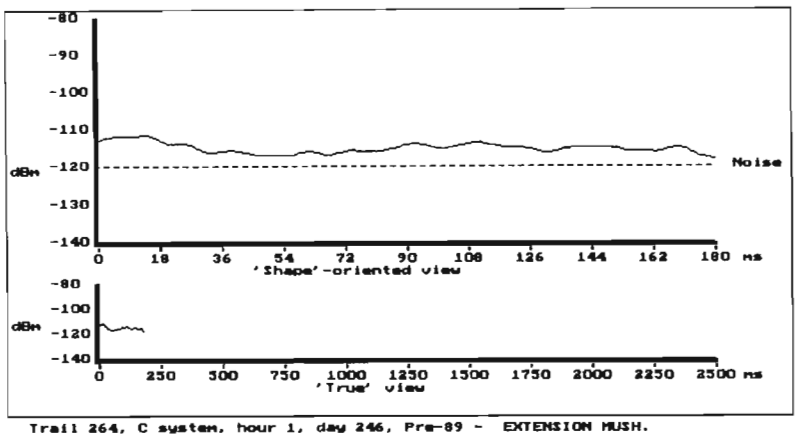

Figure 6-25 Trail type 25 - extension mush

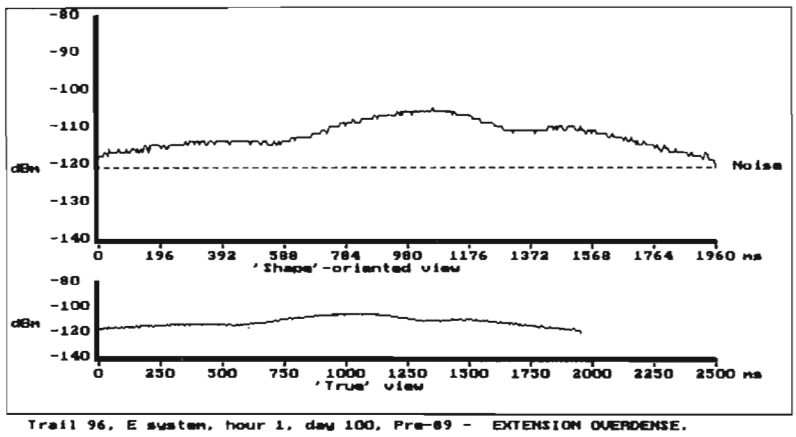

Figure 6-26 Trail type 26 - extension overdense

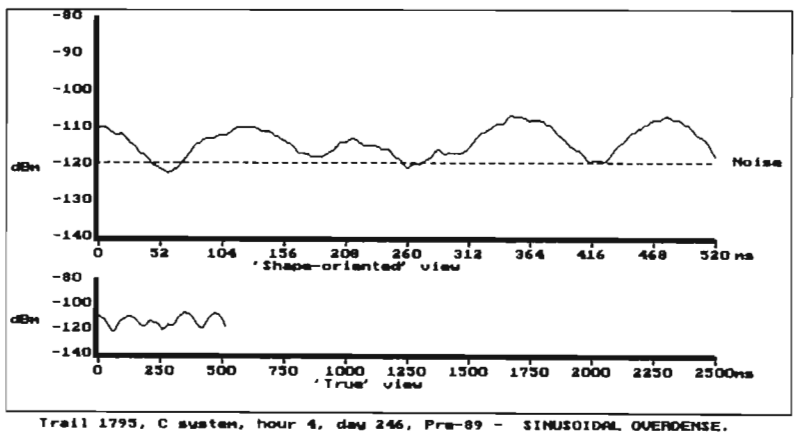

Figure 6-27 Trail type 27 - sinusoidal overdense

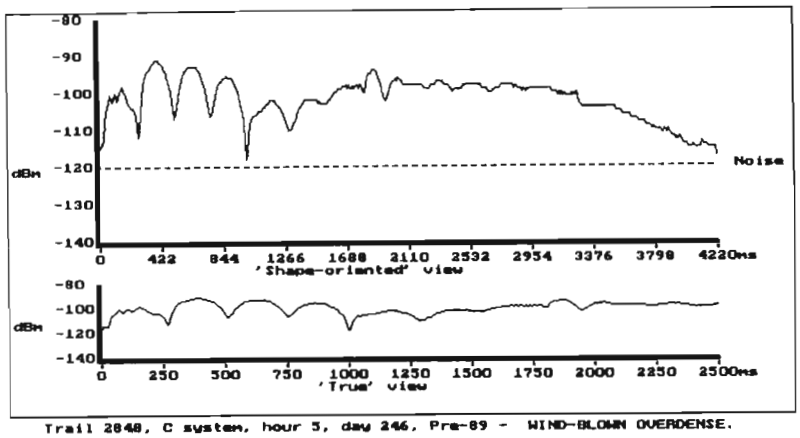

Figure 6-28 Trail type 28 - wind-blown overdense

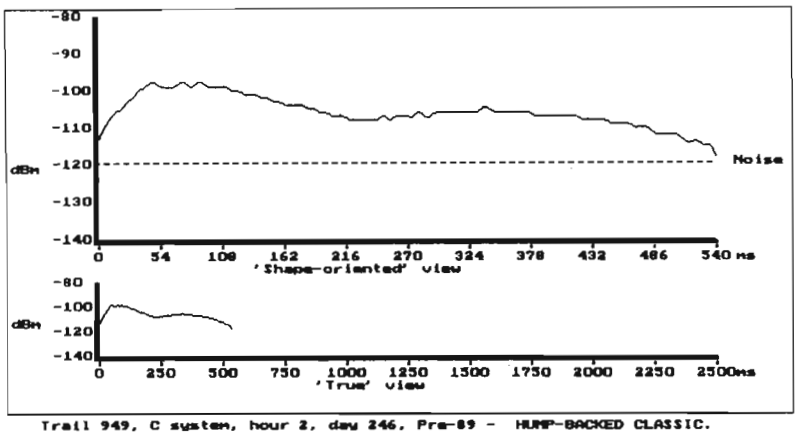

Figure 6-29 Trail type 29 - hump-backed classic

Only the first 50 or 100 ms of the trail amplitude envelope are used by the neural networks to predict parameters of the rest of the trail such as peak amplitude, duration and trail type. The target of the neural network during training, was the actual peak amplitude and the actual duration as measured. The target for predicting the trail type required the trail classification by *TrailStar*. The neural networks used for prediction may be viewed as mappings of trail feature descriptors for the first 50 or 100 ms to either peak amplitude, duration or type.

6.2.1 Data preprocessing

Different data preprocessing methods were used for each of the neural network types constructed. The preprocessing stage produced the outputs assumed to be "correct" and the data extraction stage produced the input feature vectors for the neural networks. Together they constitute the coupled input-output pairs of the training and testing data:

Trail type classification - features extracted from the entire sampled trail envelope (inputs), *TrailStar* expert system classification of entire trail (outputs).

Trail amplitude and duration prediction - features extracted from the first 50 or 100 ms of the sampled trail envelope (inputs), peak trail amplitude of entire trail (outputs). The truncated trails of 50 or 100 ms represent the entire window on which neural network prediction must be made.

Trail type prediction - features extracted from the first 50 or 100 ms of the sampled trail envelope (inputs), *TrailStar* expert system classification of entire trail (outputs). The truncated trails of 50 or 100 ms represent the entire window on which neural network prediction must be made.

6.2.2 Data extraction

A number of numeric routines were employed to determine particular features of the trails. These features formed the training and testing input vectors to the neural networks. For classification, these routines used the entire trail sample length. For prediction (truncated trails), these routines were used on the basis that feature descriptors which had been relevant in the classification of entire trails would have a high likelihood of being relevant in the classification of just one part of the trail knowing that irrelevant features would be discarded by the neural network. The feature and numeric routines involved are described below (Figure 6-30), [*Fraser*, 1992].

- Parameters B_0 and B_1 from the equation of the least squares linear regression of the entire trail ($y = B_0 x + B_1$).

- The variance σ^2 and standard deviation σ of the least squares linear regression of the entire trail.

- The maximum P_{max} and the minimum amplitude P_{min} encountered in the entire trail.

- The presence or absence of an upper plateau in the trail, together with the length of such a plateau τ_{plat}, if it exists. A plateau is defined as a region in which three or more consecutive samples are within 2 dB of one another.

- The number of local minima (fades) in the trail N_{minima}. A point is determined to be a local minimum if it is the lowest amplitude encountered as the trail follows a downward slope. The local minimum is validated when a a subsequent sample of >4 dB than the local minimum value has been encountered. This increase indicates that the trail is now on an upward slope. This approach allows for straight line trails with samples varying by one or two dB not to be confused with a trail with many fades.

- The number of local maxima (peaks) in the trail N_{maxima}. A point is determined to be a local maximum if it is the highest amplitude encountered as the trail follows a upward slope. The local maximum is validated when a subsequent sample of <4 dB than the local maximum value has been encountered. This decrease indicates that the trail is now on a downward slope. This approach allows for straight line trails with samples varying by one or two dB not to be confused with a trail with many fades.

- Parameters B_0 and B_1 from the equation of the least squares linear regression of the fall section of the trail ($y = B_0 x + B_1$). This is defined as the section from the peak amplitude position to the end of the trail.

- The variance σ^2 and standard deviation σ of the least squares linear regression of the fall slope.

- Parameters B_0 and B_1 from the equation of the least squares linear regression of the rise section of the trail ($y = B_0 x + B_1$). This is defined as the section from the beginning of the trail to the peak amplitude position.

- The variance σ^2 and standard deviation σ of the least squares linear regression of the rise slope.

- The sample n_r at which the end of the rise is determined, and that at which the start of the fall n_f is determined. This is not necessarily the peak amplitude position, as there could be an upper plateau between end of rise and start of fall.

- The variance σ^2 of the trail from the best parabolic fit to the entire trail.

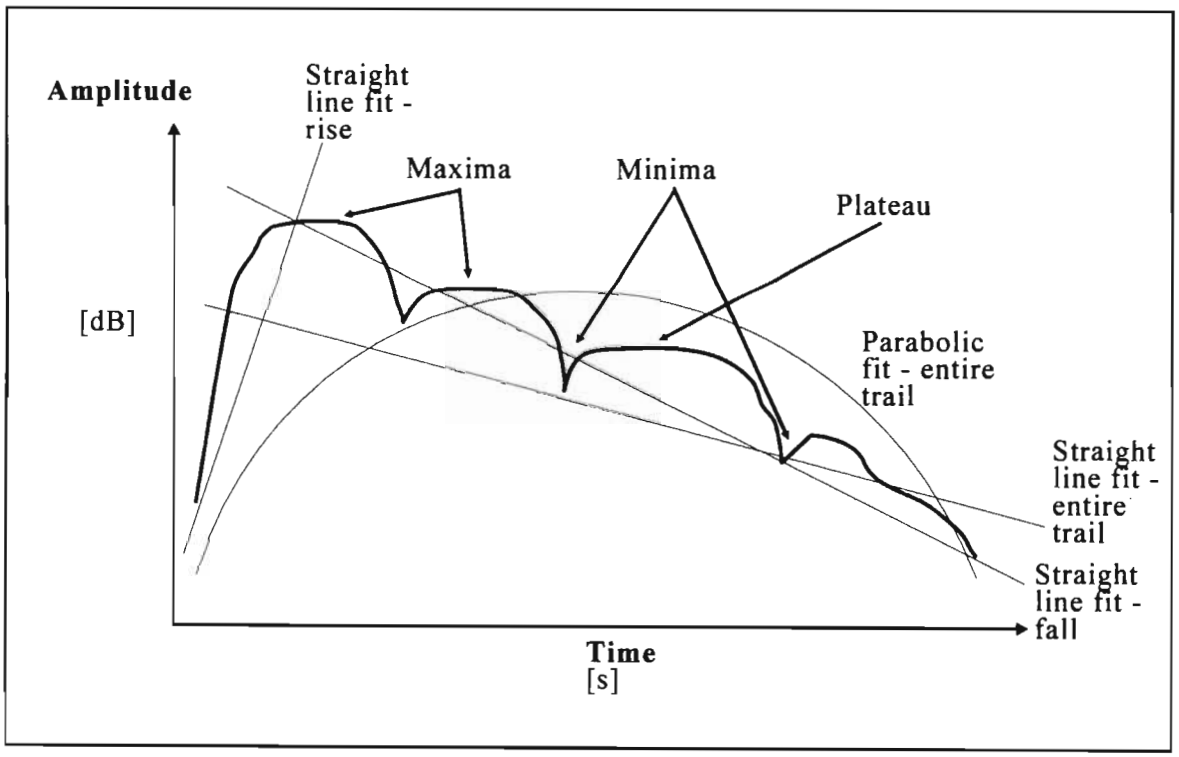

Figure 6-30 Hypothetical trail with line fits to derive trail metrics

6.2.3 Summary data processing procedure

Processing over one hundred thousand trails into a form suitable for a neural network was a difficult and time consuming task. A brief outline of the steps involved in preparing the data for neural network prediction is given below [*Fraser & Melville*, 1993a, 1993b]:

- Process over one hundred diskettes containing pre-typed trails (i.e.. trails that had been already type-classified using the *TrailStar* program).

- Extract critical data - the first 10 or 20 samples of each trail plus a concise form of header information that contains only the data that would be known regardless of trail samples (e.g.. background noise, wait time since last trail) together with the results that are to be used for training (full trail duration, full trail peak amplitude, trail type). The data from the diskettes were processed into two files, HEADERS.DTA and SAMPLES.DTA using a software routine called PREPROC.

- Determine twenty-six feature descriptors for the 100000 trails, which are now seen as consisting of just 10 or 20 samples. Combine the feature descriptors with the three 'whole-trail' results in a summary file, NETDATA. The software written to accomplish this was PREPROC2.

- Form a template file of the 26 feature descriptors (TEMPLATE.TDA) and three result files for duration prediction, peak amplitude prediction and trail type prediction respectively (NUMSAMPS.TDA, PEAKAMPS.TDA and TTYPES.TDA) using program GETEMPLT.

- Reduce the trail types in TTYPES.TDA to 3 general groups - underdense, overdense and other - using program GETGENTP to produce GENTYPES.TDA.

- For each result

  (i)Merge the result .TDA file with the TEMPLATE.TDA file to produce a NETDATA.NNA file (using program MERGE).
  (ii)Extract test data from NETDATA.NNA, placing every 25th trail in file NETTEST.NNA with the other 24 trails going to the training data file NETTRAIN.NNA, using program GETTEST.

The data for neural network classification requires a similar procedure but only the first three steps are required for the full-length trail samples.

A flow diagram of the data preparation procedure is given in Figure 6-31. This process produced a training set of 96000 trails and a test set of 4000 trails. At this stage the training and test data needed for neural network development was ready.

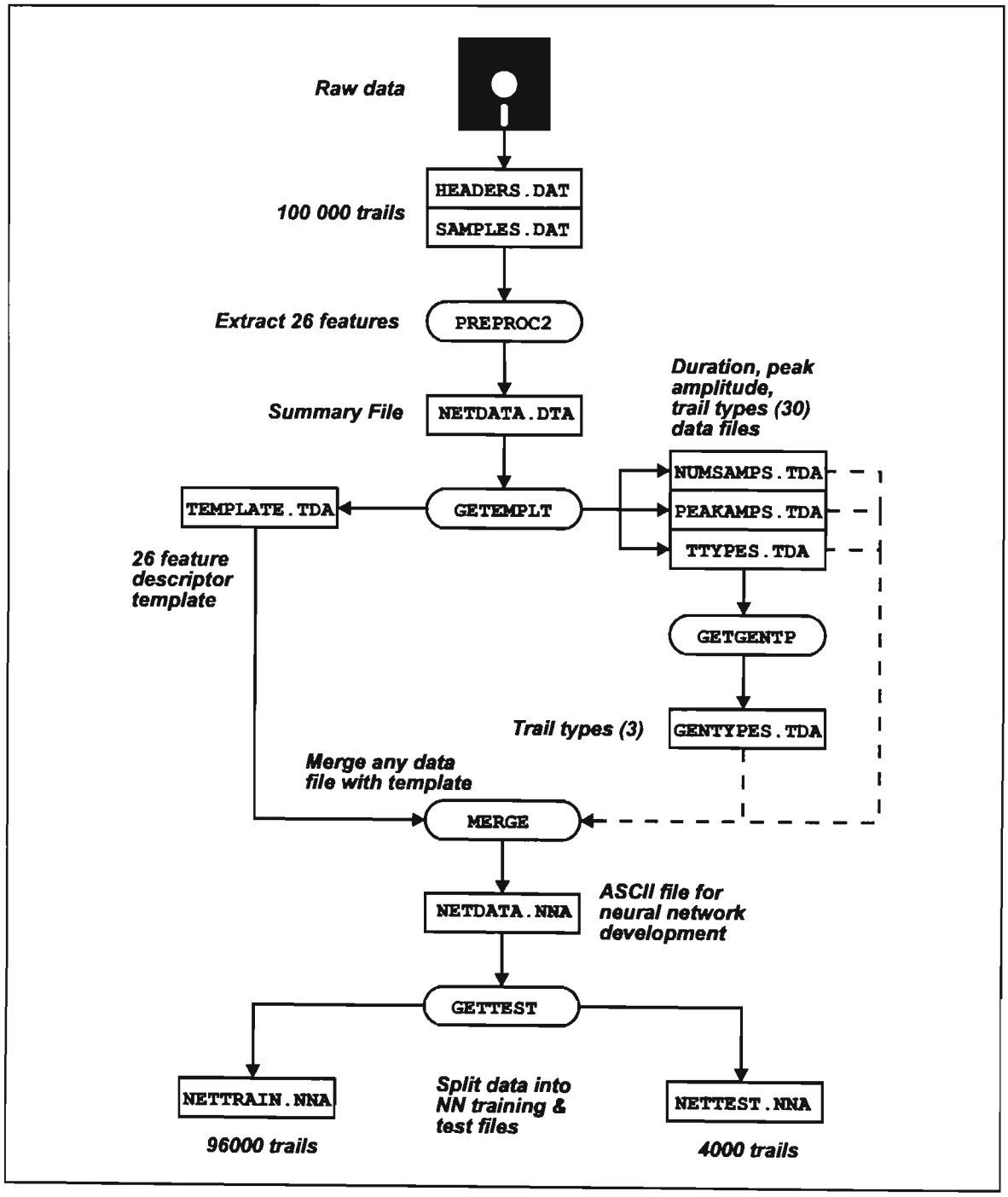

Figure 6-31 Flow diagram of data preparation procedure

For trail type prediction and classification, the decision of *TrailStar* was taken as the correct output of the data training pairs. The software preprocessor (GENTP) classified each trail, for neural network training purposes, as being of class 0, 1 or 2. Class 0 indicates the general overdense group, class 1 the general underdense group, and class 2 trails of types which cannot be conclusively determined to be in class 0 or class 1.

This latter group includes the initial 'unknown' type (type 22), the 'mush' group of trails which consist of short duration trails which appear as straight lines of various inclinations on a time-amplitude axis, and the 'bell' group. These appear as bell-like shapes on a time-amplitude display. These trails initially seemed to exhibit underdense characteristics, but a matching study of trails received by two systems indicated that many of these bells are in fact the 'tops' of overdense trails. Thus it is still debatable whether these should be classified as underdense or overdense trails, and they were included in class 2 [*Melville*, 1991c].

Class 2 trails were excluded from training and testing of the neural networks, although it is expected that the neural networks in their current form would have the same problem as humans do in deciding whether these trails were underdense or overdense.

6.3 Neural networks for classification and prediction

The work on meteor-burst communication trail classification using data from *complete* trails was the pilot application of neural networks to meteor-burst communication [*Fraser, Khan & Levy*, 1992]. The success of these neural networks motivated further research into their use as trail characteristic predictors. In the classification application, data from entire trails was processed using the methods described above and used to categorize trails according to type. For prediction, however, data from only the first 10 or 20 amplitude samples (i.e. 50 or 100 ms respectively) were processed and used to predict trail duration, peak amplitude and type. Ideally the fewest number of samples possible should be used to predict and classify trails. However, to obtain reasonable accuracy this period should be as long possible. In any system, the smallest and shortest trails will rise and fall within the 50 ms window and are therefore unpredictable. However the bulk of useful trails have a peak amplitude which occurs between 50 and 100 ms. For these trails, a 50 ms decision window is sufficiently small to predict trail characteristics which will be relevant for a high percentage of the remaining trail lifetime.

6.3.1 Neural networks for trail classification

In order to classify trails, features of the reflected signal such as shape, duration and amplitude are important. Current trail classification is performed off-line using the rule-based expert system *TrailStar* developed by *Melville* [1989]. *TrailStar* utilises characteristic trail features described in section 6.2.2 in order to classify trail reflections into 29 categories. The specific trail type is determined from the range within which the feature parameters fall. However, no two meteor trails are identical and the subtle variations between trails complicate classification via a rule-base approach. It is in this context that several neural networks were implemented to differentiate between the two major trail types (i.e. overdense and underdense).

The inputs to the classification neural networks were a subset of the 26 feature descriptors (section 6.2.2). In some neural networks the first 20 normalised ampli-

tude samples were included as inputs. The input parameters obtained and and their method of calculation is given below [*Fraser, Khan & Levy*, 1992]:

Duration of trail

This is easily obtained by multiplying the number of samples by the sampling period (5 ms).

Position and amplitude of the peak signals

The peak amplitude is obtained from a scan through the samples. The time of its occurrence is calculated from its position in the sample file.

Position and amplitude of the minimum signal

The minimum amplitude is obtained from a scan through the samples. The time of its occurrence is calculated from its position in the sample file.

Amplitude range

The difference between the maximum and minimum amplitudes.

Sample mean

This is obtained for the total trail, for the rise and for the fall zones by averaging the appropriate sample magnitudes.

Standard deviation

Once again this is obtained for the rise, fall, and total trail length. A straight line is interpolated through the appropriate points in each of these three regions, using the method of least squares. The perpendicular distance of each sample point from this line is used to compute the standard deviation.

Trail shape

The sample values were thereafter normalised to a set of twenty points. The differences between consecutive sample values was then stored in an array. These values would then provide an indication of the trend of the data, i.e.. whether the slope was increasing, decreasing or whether a plateau occurred. Each element in this difference array would therefore correspond to a particular neuron. The samples are stored in chronological order, therefore a neural network would learn not only whether the slope was increasing or decreasing but also the position in the trail where this variation occurred.

There is considerable overlap between feature descriptors because the source of the features is common, i.e. trail amplitude samples. The benefit to the neural network of using feature descriptors instead of the raw data samples alone, is that the process of deriving them reduces the amount of abstraction required by the neural network. Thus the feature descriptor inputs reduce the non-linearity of the system and hence reduce the order of the inter-relationships that the neural network must learn. This improves both learning speed and neural network accuracy, whilst reducing the number of neurons required in the hidden layers. Recall that the number of hidden neurons is proportional to the complexity (and order) of the input data. Fewer hidden neurons directly reduce neural network training time.

The input data was checked for missing and bad data as well as for data extreme values (outliers) that could skew neural network training. Missing data were detected by checking each field in every data record for missing entries and by summing the number of fields in each record. Bad or corrupted data was found by plotting histograms representing frequency of occurrence of each variable over its range of values. This method allows corrupted data and/or outliers at the extremes of the input range to be detected. However, to detect corrupt data within the normal range, a series of scatter plots of two inputs at a time were plotted. Abnormal data is identified by inspection of the regions outside the normal clustering. Traditional mean and standard deviation calculations for each input also help to identify the bad data. Owing to the large number of training data available, records with entries missing or bad were simply removed. It is important that data checking occurs before neural network construction otherwise both the training and generalisation ability of the neural network will be degraded. This filtered data then became the input to the neural networks.

Feed-forward layered neural networks with back-propagation learning were used for all whole trail classification neural networks. Back-propagation learning is a supervised learning method requiring input-output training pairs. The output data to match each input vector was provided by *TrailStar*. The same inputs used to

train the neural networks were presented to *TrailStar* for rule-based classification into underdense and overdense trail types. Thus the training pairs consisted of feature descriptors as inputs and the associated *TrailStar* decision as outputs (neural network classification target).

Neural network implementation for whole trail classification

Several neural networks were implemented using *California Scientific Software's BrainMaker* software suite (PC DOS based). *BrainMaker's* back-propagation algorithm is an adaptation of the standard layered feed-forward technique with continuously valued neurons. The standard sigmoidal neuron transfer function was used throughout the network and all initial weights randomized. The number of hidden layers was varied between 1 and 2, and the number of neurons per hidden layer between 12 and 45. The number of hidden neurons was initially kept small to reduce memorisation of the training facts and improve the generalising ability of the neural network. An increase in the number of hidden layers increased training time without a significant improvement in trained network performance.

The training tolerance, additive noise present during training and network learning rate we also varied. Training tolerance is the range of neuron output levels which are considered to be correct. For example, the normal limits of the sigmoid are 0 and 1. If an output of 0.8 is to be regarded as correct from the training data, a training tolerance of 0.1 means that any output from 0.7 to 0.9 is considered correct. A training tolerance of zero means the output must exactly match the training pattern to be considered correct. This is usually too strict a requirement resulting in non-convergence of the neural network. A 10% tolerance was found to produce a good compromise between decision accuracy and the ability of the network to converge during training.

Noise added to the connections during training led to poorer network performance under test and was thus set to zero. The main reason for using noise during training is to improve neural network generalisation, particularly where limited data is

available. However, there was sufficient data to provide an even spread of inputs without the need for added noise. With the noise set at zero, the training times were greatly shortened. With a learning rate of 1, *BrainMaker* always converges on a local minimum during training if convergence is possible. With a learning rate of 4, training times were reduced by nearly 75%, though sometimes the network failed to converge at all because the training inertia would cause the neural network to overshoot a suitable solution. To ensure convergence, a learning rate of 1 was used until near the end of training after which a rate of less than 1 aided the completion of training. Various subsets of training data were also tried, each requiring different numbers of input neurons. Training times varied from 5 minutes to over 1 hour corresponding to the number of facts used in the training file and the number of hidden neurons and layers employed.

Results

Network evaluation was performed by presenting to the network inputs with which it had not been trained, and verifying the corresponding outputs against the target output from *TrailStar*. The test data consists of data selected randomly from the total available data set. Around 4% of the data were reserved for test purposes, [*Fraser, Khan & Levy*, 1992]

The percentage of trails correctly classified as underdense or overdense ranged from 33 to 97% for various network topologies. The network configuration and test results of four typical networks implemented are shown in Table 6-1.

Table 6-1 Results of neural networks for whole trail classification

Network	Number of hidden layers	Neurons in first hidden layer	Neurons in second hidden layer	Amplitude samples present	Percentage correctly classified
A	1	12	-	NO	84%
B	1	40	-	YES	67%
C	2	40	20	YES	64%
D	1	32	-	YES	97%

It was found that the network which best discriminated between trail types (97% success rate), utilized 32 inputs, 32 hidden neurons in a single layer and two outputs representing the choice of underdense or overdense trail type. The inputs consisted of 12 trail statistics and 20 normalised sample points corresponding to the first 100 milliseconds of the received signal amplitude. These inputs were found to be the most accurate means of classifying the trails.

Discussion

The classification accuracy of 97% proved conclusively that neural networks are capable of pattern recognition in meteor-burst communications and can perform many of the tasks of rule-based systems without the need to hard-code the rules. The traditional classification methods are hampered by non-generalised rules, slow operation and intolerance to noisy or poor data. In comparison, the optimal neural network, once trained, was able to accurately classify underdense and overdense trails within milliseconds whereas the *TrailStar* expert system took several seconds. Both the speed of the neural networks and their ability to recognise signals in the presence of noise, make them ideal for signal classification applications in meteor-burst communications.

6.3.2 Neural networks for trail type prediction

For classification, the feature descriptors were derived for the entire trail and then used as the basis of trail typing. For prediction the entire trail was first processed to derive the relevant target variable (trail type, peak amplitude, trail duration). Then the feature descriptors were applied to the first 100 ms (20 samples) and the first 50 ms (10 samples) of the trail. To do this, the preprocessing package was used to truncate trails to appear as if they were only twenty or ten samples long.

By comparing the performance of the neural networks with either 50 ms or 100 ms worth of input data, measures of the relative contribution of the amount of data to the decision process could be found. Naturally for optimal prediction, the best predictor would be the one which could use the fewest number of samples while maintaining sufficient accuracy.

For neural networks to predict the trail type, it was decided, similar to the case of whole trail classification, to group the trails into overdense, underdense and a third category "other". The last category was added to provide for trails which are not obviously underdense or overdense. Members of the "other" category may be trails which are difficult to classify as either of the two dominant categories. Furthermore it allows graceful degradation of misclassifications; an important requirement for proper neural network training. Without providing a "don't know" option for the neural network output, the neural network is unnecessarily constrained to providing an answer of overdense or underdense. This condition will force the neural network to accommodate a mapping of inputs to the two main classes even though there is no basis for either choice. The neural network will perform inferiorly in both learn and recall modes due to non-optimised weights.

For trail type prediction, the procedure followed in section 6.2.3 was followed both for the 50 and the 100 ms case. The three categories were (Table 6-2):

Table 6-2 Three class categorisation of 29 trail types

Underdense - category 0		Other - category 1		Overdense - category 2	
Classification no.	Name	Classification no.	Name	Classification no.	Name
5	flat classic	1	unreasonable data	19	square root sign
9	classic	2	short, mid-peak	20	rectified sine
10	classic, with plateau	3	short mush	21	non-sine
11	round-top classic	4	medium time, mid-peak	26	extension
12	classic, late fall	6	flat bell	27	sinusoidal
13	classic, notched rise	7	strt-line mush, medium length	28	wind-blown
14	classic, bad rise	8	straight-line mush, long length		
16	multi-plateau	15	bell		
17	multi-slope	22	weird, unknown type		
18	twins	23	downward-tending straight-line mush		
24	hazy classic	25	extension mush		
29	hump-backed classic				

As is seen in section 4.7.2, the relative number of overdense trails is around 20% that of the both underdense and "other" categories. For neural networks to recognise different categories equally well, the relative contribution of each category to data should be similar. The statistical distribution of the categories must also be similar in both the training and the test data. There were two options to increase the number of occurrences of overdense trails. Firstly, classes 0 and 1 could both be reduced to 20% of their original size by random elimination of data. This was not considered as it would unnecessarily shrink the size of the training and test data. The second option chosen was to multiply the overdense data by five and insert them in the data randomly. This proved satisfactory.

The final data manipulation converted the three categories to a one-of-*n* encoding scheme. Thus category 0 became 1,0,0, category 1 became 0,1,0 and category 2 became 0,0,1. There are several benefits of this scheme. Instead of a single output neuron having to learn three classes, three output neurons are used. This increases the Hamming distance between each category and its binary structure allows for competition between output neurons. Furthermore, classification accuracy may be improved by thresholding so that an actual output of 0.2, 0.7, 0.4 could be resolved to 0,1,0 without ambiguity.

The following table (Table 6-3) shows typical outputs (from a back-propagation neural network) and their corresponding target outputs.

Table 6-3 Target back-propagation neural network outputs and actual outputs (real sample)

Target outputs			Actual outputs		
0.000	0.000	1.000	0.248	0.276	0.428
1.000	0.000	0.000	0.248	0.393	0.305
0.000	1.000	0.000	0.151	0.528	0.311
0.000	1.000	0.000	0.459	0.283	0.246
1.000	0.000	0.000	0.655	0.202	0.170
0.000	0.000	1.000	0.150	0.237	0.634

Several hundred neural networks were implemented to find optimal parametric and paradigm choices. The learning vector quantization-type neural networks performed considerably better than other types such as the back-propagation neural network. The following three neural network structures were the most successful:

Back-propagation neural network (10BPN4.NND)

- neurons: 26 input, 50 hidden layer 1, 50 hidden layer 2, 3 output
- error propagation: back-propagation
- learning rule: extended-delta-bar-delta
- transfer function: hyperbolic tangent
- training epoch size: 500
- MinMax input-output scaling (inputs are scaled from their real values to a normal value of -1 to +1, outputs are scaled back to their real values)

Learning Vector Quantization (10LVQ2.NND & 20TRY3.NND)

- neurons: 26 input, 102 Kohonen layer, 3 output
- First LVQ1 with 10000 learning iterations and 0.06 initial learning rate followed by LVQ2 with 1000 learning iterations, 0.03 initial learning rate and 0.2 width parameter (width parameter is the sphere of influence of a vector over its neighbours). LVQ1 and LVQ2 are two sub-paradigms within *NeuralWare's* implementation of the learning vector quantization algorithm
- in-class winner always learns (i.e. the vector with the closest match to the input is still kept in contention during learning), 1.0 conscience factor (conscience is the scaling factor that allows the influence of the winning vector to weaken every time it wins, thus allowing other vectors to compete and learn) and 0.0010 frequency estimation (the constant for determining the in-class win frequencies)
- MinMax input-output scaling (inputs are scaled from their real values to a normal value of -1 to +1, outputs are scaled back to their real values)

Results

The following table (Table 6-4) indicates the performance of the three best neural networks using test data set to which they had not been previously exposed.

Table 6-4 Trail type prediction results

	50 ms input data			50 ms input data			100 ms input data		
NN type	Back-propagation			LVQ			LVQ		
NN file name	10BPN4.NND			10LVQ2.NND			20TRY3.NND		
Overall classification rate	54.1%			70.7%			73.1%		
	Correct trail type (target)			Correct trail type (target)			Correct trail type (target)		
	U/D	"other"	O/D	U/D	"other"	O/D	U/D	"other"	O/D
% classified as O/D	11.38	32.30	**42.44**	7.14	17.79	**66.45**	8.77	17.47	**73.01**
% classified as "other"	8.98	**40.37**	30.23	10.99	**63.80**	17.42	12.28	**67.47**	17.79
% classified as U/D	**79.64**	27.33	27.33	**81.87**	18.40	16.13	**78.95**	15.06	9.20

The task of trail type prediction is one of classification. The most useful instrument to monitor training and testing was the classification rate matrix. The overall classification rate is the combination of the individual classification rates for each trail class. The vertical columns indicate the correct trail type (target output) and the horizontal columns, the percentage of trails classified in each.

Discussion

The results indicate that neural networks are able to discriminate between underdense and overdense trails very well on the basis of initial samples received (see Figure 6-32, 6-33).

For the 10 sample case (50 ms), the back-propagation neural network was 16.70% worse on average classification than the corresponding learning vector quantization neural network. The 70.70% classification accuracy of the 10LVQ2.NND learning vector quantization neural network was excellent considering the decisions were only based on 10 samples. The accuracy of underdense prediction (at 81.87%) underscored the relative consistency of the underdense trail type compared with 66.45% for the overdense trail type which exhibits more extreme departures from a classical trail shape. For the 10LVQ2.NND neural network, misclassifications were not evenly spread between the other two categories. If either an underdense or an overdense trail were misclassified, it would have approximately twice the probability of being classified as an "other" trail than an overdense or underdense trail respectively. This emphasises the difficulty that exists for any system (including human experts) to correctly classify borderline trails. Another possibility is that *TrailStar*, being a hard-coded rule-based system, was unable to detect the subtle differences that a neural network can detect and forced a particular classification, which was irreconcilable with the data.

It is significant that a doubling of the number of samples used from 10 to 20, resulted in an average classification increase of only 2.44% from 70.70% to 73.14%. This means that the many of the prime classification features occur early on in the trail lifetime. The difference between this level of prediction accuracy and classification accuracy for an entire trail is around 20%. Thus there are several trail features which only occur later on in the trail lifetime and cannot be used in prediction. It appears then that the practical limit for prediction is around 70-75% average classification accuracy.

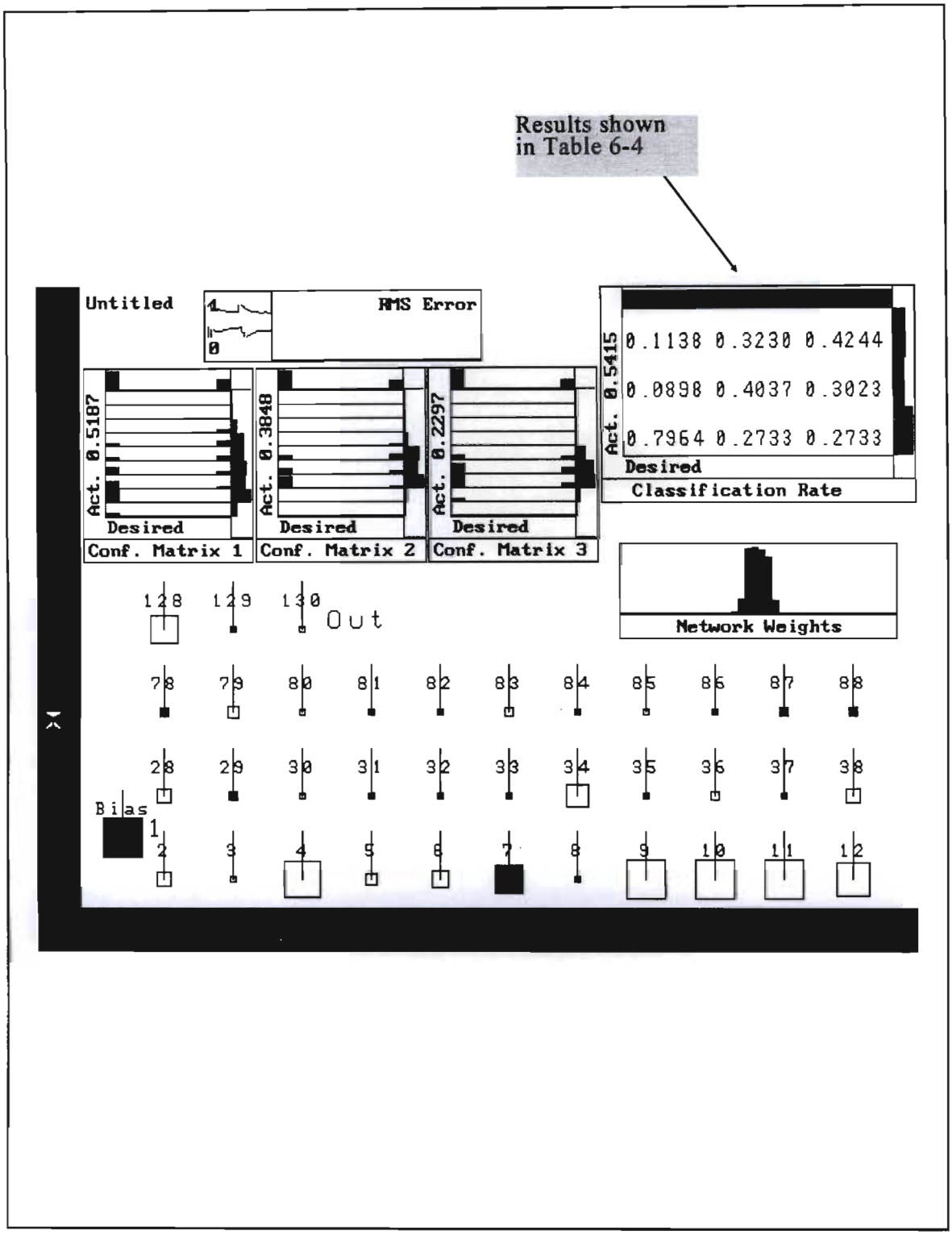

Figure 6-32 10BPN4.NND back-propagation neural network for trail type prediction

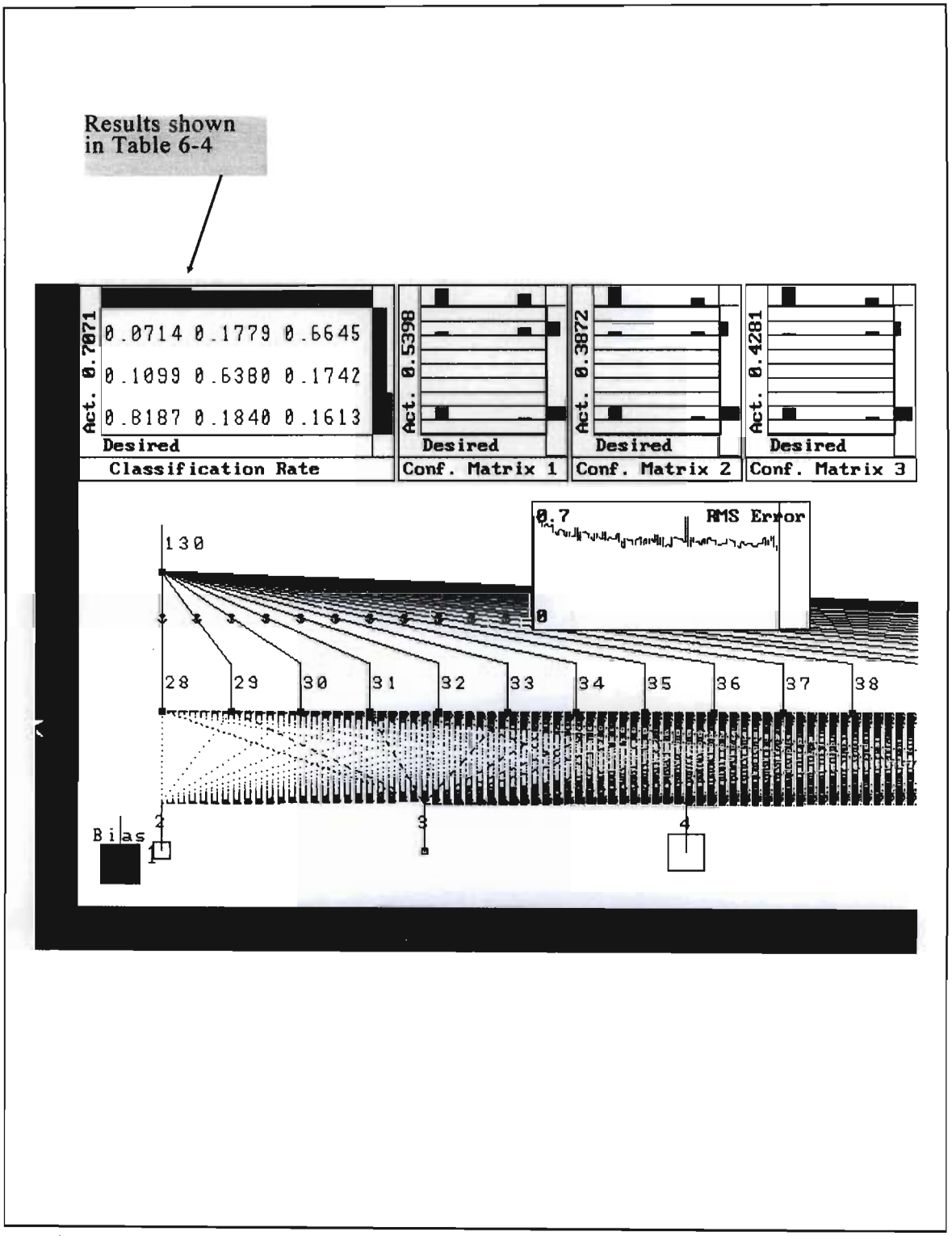

Figure 6-33 10LVQ2.NND Learning Vector Quantization neural network for trail type prediction

The overdense classification accuracy is improved most of all by using more data. The reason is likely that the distinguishing characteristics of overdense trails manifest themselves later than that of the underdense types. This can be seen in the correct classification increase for these trails from 66.45% (50 ms data) to 73.01% (100 ms data).

As a test of "transportability" of the trained neural networks across different meteor-burst communication links, the neural network 10LVQ2.NND was tested on data from the 1100 km Pretoria to Cape Town link. The two systems have markedly different characteristics in a number of respects, including path length and antenna configurations. If a neural network trained on the one system could be a reasonable predictor for another then neural network implementation for purposes of adaptive data rates etc. would be a great deal simpler - the alternative being to train a neural network every time a new link is established. Earlier work on trail classification [*Melville* et al., 1989] had shown that the same trail types could be expected across a wide variety of systems, but was unable to determine whether or not the proportions of the various types would be the same across systems, so the question was still open as to whether a neural network trained on one system would be effective on another.

On testing this hypothesis, the results were very good. The accuracy of classification on the 1100 km link varied by a maximum of 5% over the 550 km link on which the neural network had been trained. The greatest change was in the overdense trail category (which appeared more on the longer than on the shorter link) and the least change in the underdense category. Thus the neural network had generalised sufficiently well, recognising fundamental trail features while being tolerant of system variations. For this application at least, the neural network will be transportable across systems with minimum performance loss. For optimal classification, however, a neural network could be retrained further in the new link. In addition the benefits of thresholding as discussed in 6.3.2 would reduce the uncertainty in trail classification to near zero.

6.3.3 Neural networks for peak trail amplitude prediction

Prediction of the peak trail amplitude is a regression problem unlike the prediction of trail type which is a classification task. Despite this fundamental difference in approach, neural networks in general, are pattern recognisers. This allows neural networks to recognise general trends and interpolate from them. It must be noted however that neural networks cannot extrapolate beyond the *n*-dimensional bounds of the data with which it has been trained. This emphasises the importance of representative and plentiful data for meaningful interpolated results.

Again, the feature descriptors were derived for the entire trail and then used as the basis of peak amplitude prediction. For prediction the entire trail was first processed to find the peak amplitude. Then the feature descriptors were applied only to the first 100 ms (20 samples) and the first 50 ms (10 samples) of the trail. To do this, the preprocessing package was used to truncate trails to appear as if they were only twenty or ten samples long.

For optimal prediction, the best predictor would be the one which could use the fewest number of samples while maintaining sufficient accuracy. In the peak amplitude case, the number of samples used must be kept purposefully small to prevent the peak from occurring within the data presented to the neural network. This was remedied in two stages. Firstly the statistics of position of peak occurrence for the entire trail were calculated. The results are found in the table below (Table 6-5):

Table 6-5 Amplitude peak statistics for whole trails

Mean position of trail peak from trail commencement	$\mu = 59.85$ ms
Standard deviation of position of trail peak	$\sigma = 27.8$
Maximum peak amplitude (all trails)	-80 dBm
Minimum peak amplitude (all trails)	-127 dBm
Mean peak amplitude (all trails)	$\mu = -109$ dBm
Standard deviation of peak amplitude (all trails)	$\sigma = 6$

It can be seen that the majority of peaks occur between 50 and 100 ms from trail commencement. Thus for prediction only the 50 ms data should be considered. There are still many trails which have a peak before 50 ms as the standard deviation shows. To ensure that the neural networks correctly learn to predict and not merely to measure the peak amplitude within the 10 samples, the input relating to the maximum amplitude within the 50 ms data window and the position of this amplitude peak are removed from the input feature vectors by disabling the relevant input neurons. This forced other trail feature descriptors to be used rather than those directly correlated to the position and magnitude of the peak.

Several hundred neural network architectures and paradigms were implemented including back-propagation neural networks, probabilistic neural networks and general regression neural networks. The following three neural network structures were the most successful:

Back-propagation NN (10BPN1.NND)

- neurons: 26 input, 50 hidden layer 1, 50 hidden layer 2, 1 output
- error propagation: back-propagation
- learning rule: extended-delta-bar-delta
- transfer function: hyperbolic tangent
- training epoch size: 500
- MinMax input-output scaling
- inputs eliminated: peak amplitude within 50 ms data and position of peak within 50 ms (X's on relevant input neurons Figure 6-35)

Back-propagation NN (10BPN2.NND)

- neurons: 26 input, 50 hidden layer 1, 50 hidden layer 2, 1 output (linear neuron transfer function)
- error propagation: back-propagation
- learning rule: extended-delta-bar-delta
- transfer function: hyperbolic tangent
- training epoch size: 500
- MinMax input-output scaling

Back-propagation NN (10BPN5.NND)

- neurons: 26 input, 100 hidden layer 1, 1 output (linear neuron transfer function)
- error propagation: back-propagation
- learning rule: extended-delta-bar-delta
- transfer function: hyperbolic tangent
- training epoch size: 500
- MinMax input-output scaling
- inputs eliminated: peak amplitude within 50 ms data and position of peak within 50 ms (X's on relevant input neurons - Figure 6-37)

Results

The following table (Table 6-6) indicates the performance of the three best neural networks using test data set to which they had not been previously exposed.

Table 6-6 Trail peak amplitude prediction results

	50 ms input data	50 ms input data	50 ms input data
NN type	Back-propagation	Back-propagation	Back-propagation
NN file name	10BPN1.NND	10BPN2.NND	10BPN5.NND
Confusion matrix r^2	0.7342	0.7671	0.8356
RMS error	10%	7%	8%
Overall classification rate	73.42%	78.3%	83.8%
Amplitude related inputs eliminated	Yes	No	Yes

Peak amplitude prediction is a regression problem. The most useful instruments to monitor training and testing were the confusion rate matrix and the RMS error.

Figure 6-34 shows a scatter plot of target output (x-axis) and actual output (y-axis) of the best performing back-propagation neural network (10BPN5.NND). The solid line y = x corresponds to perfect correlation.

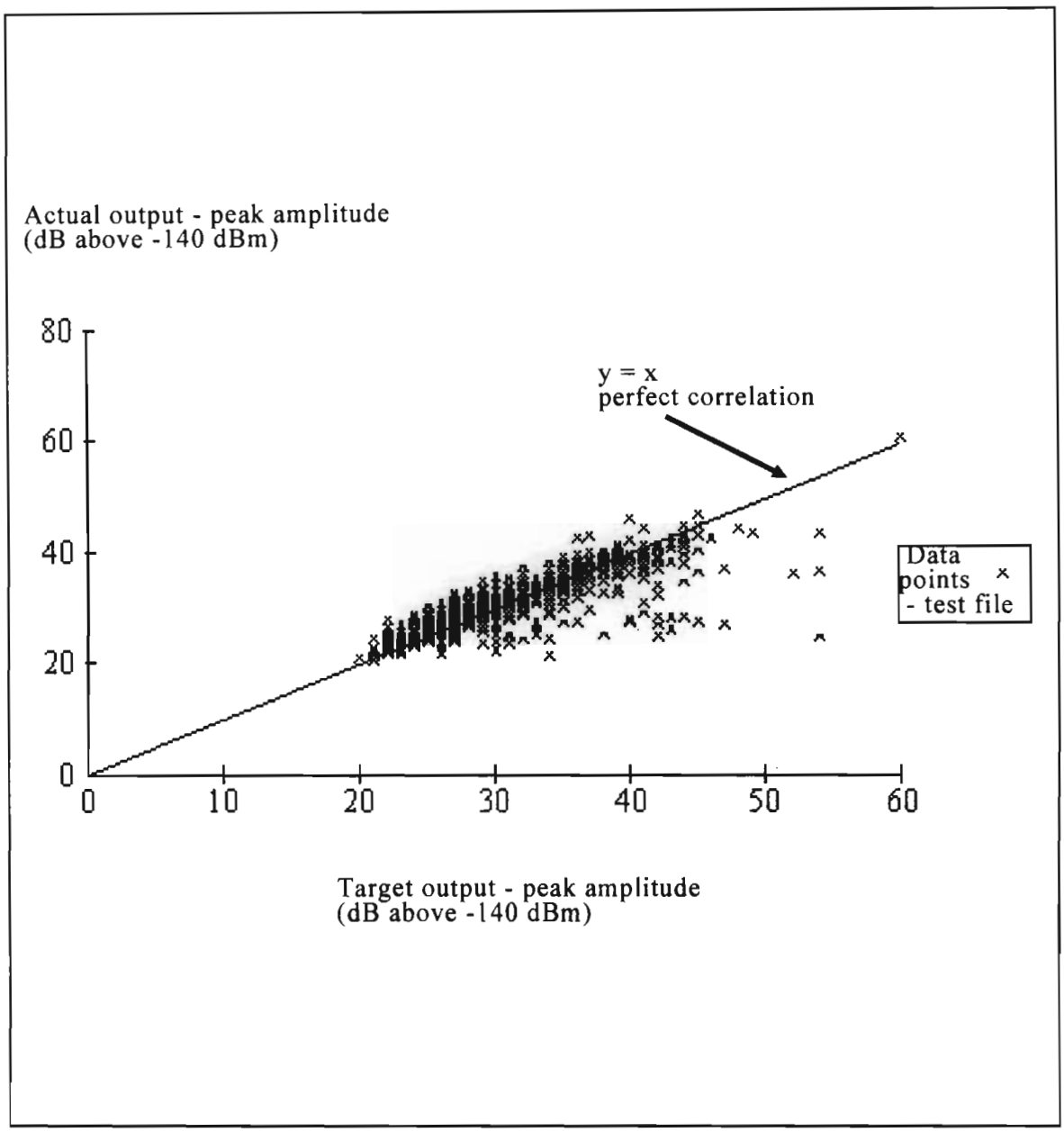

Figure 6-34 Scatter plot of target output (x-axis) and actual output (y-axis) for peak amplitude prediction. Solid line y = x is perfect correlation. (50 ms data)

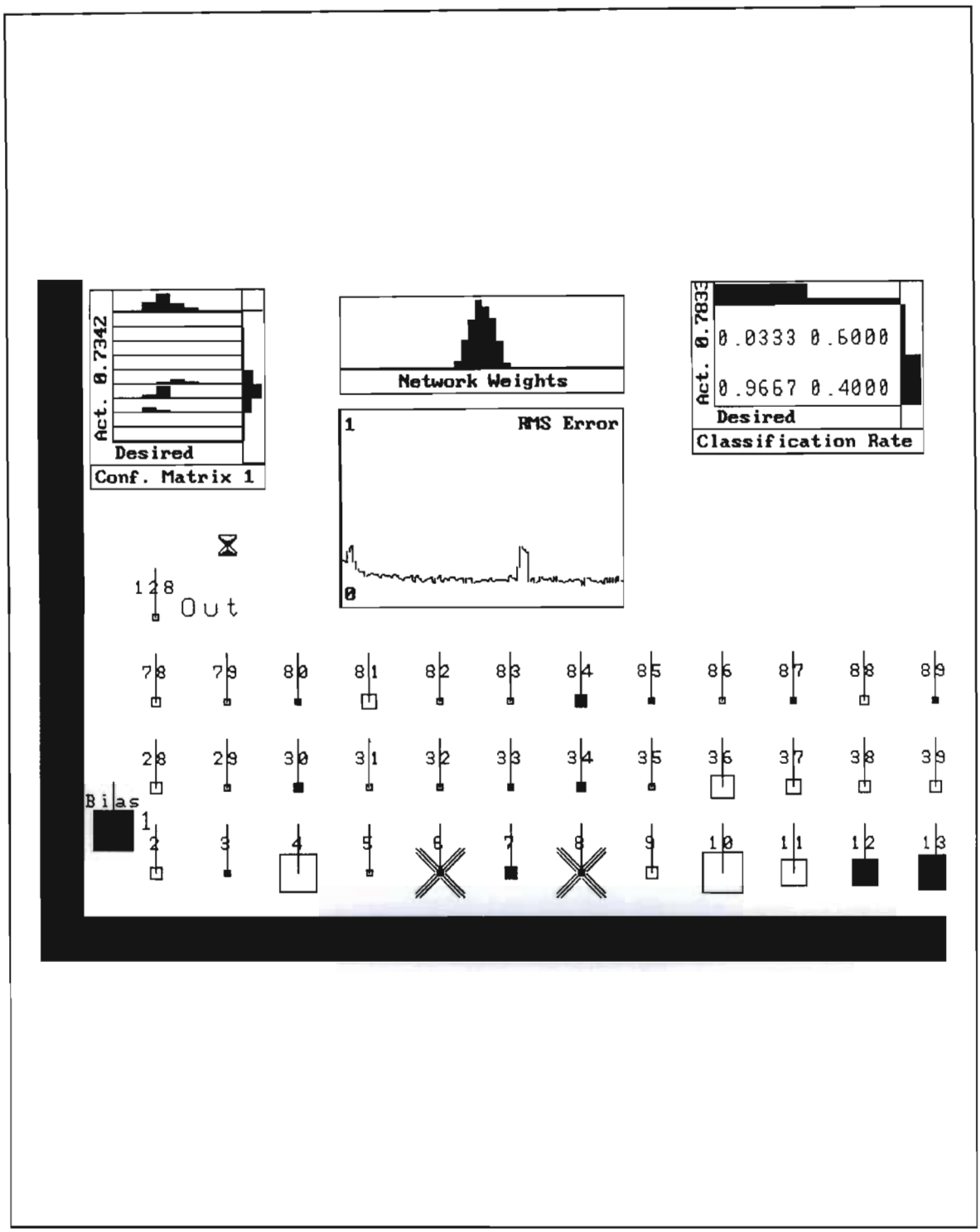

Figure 6-35 10BPN1.NND back-propagation neural network for peak amplitude prediction

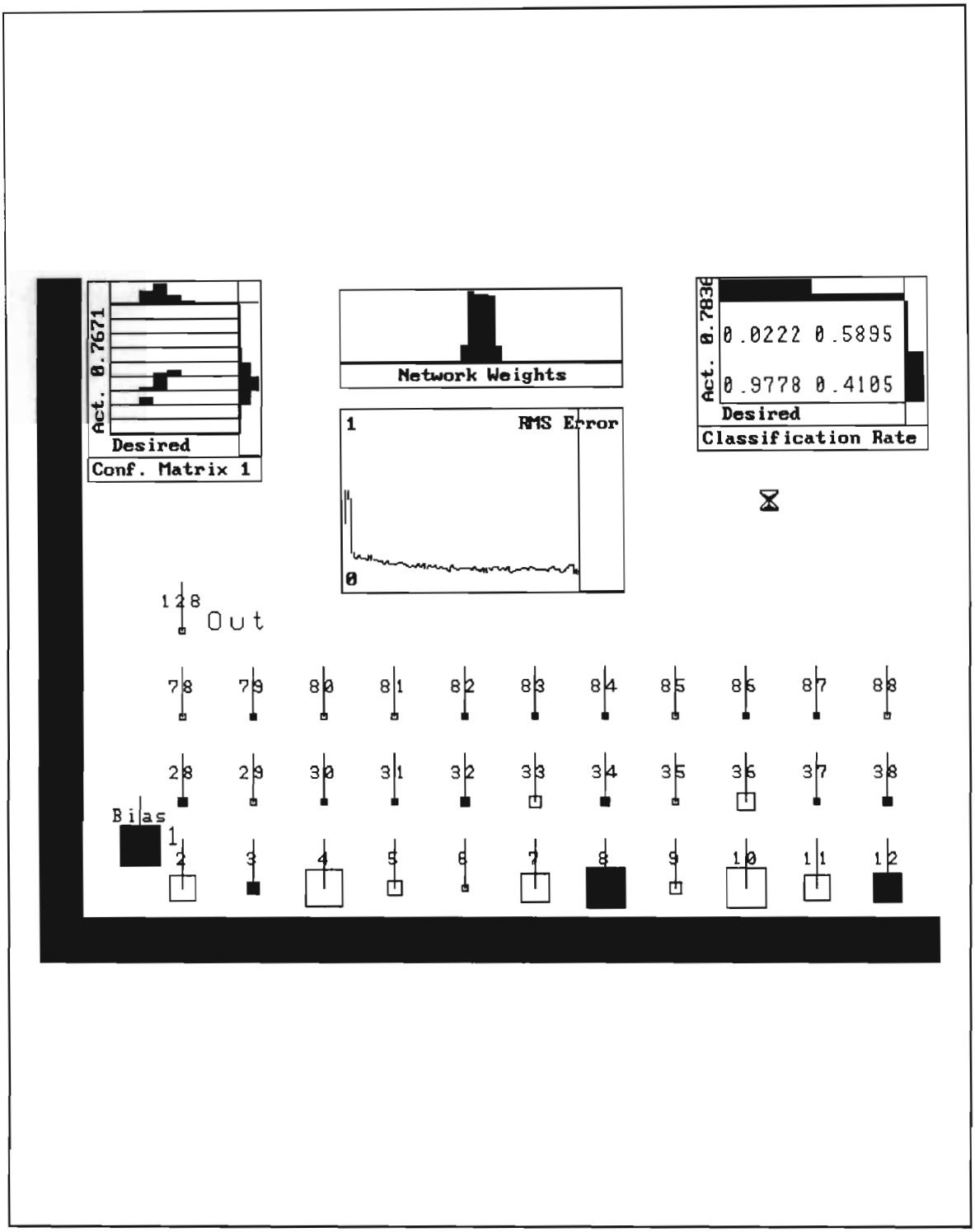

Figure 6-36 10BPN2.NND back-propagation neural network for peak amplitude prediction

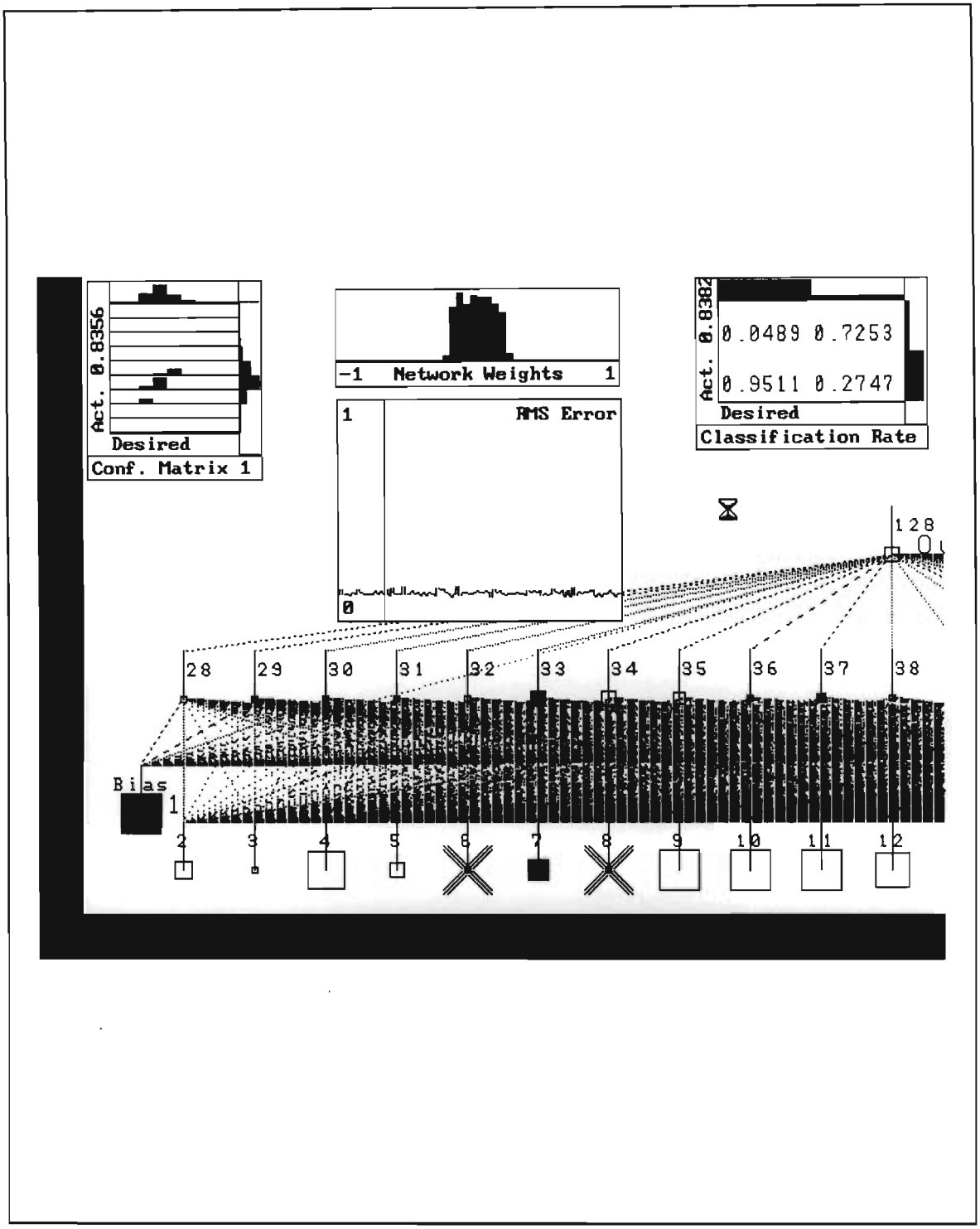

Figure 6-37 10BPN5.NND back-propagation neural network for peak amplitude prediction

Discussion

The back-propagation neural network (10BPN5.NND) performed amplitude prediction a correlation coefficient of 0.8356 which is excellent, especially since it is only based on 50 ms of data and all amplitude related inputs were eliminated. The scatter plot conceals the extent of the strong correlation around $y = x$ due to the number of overlapping data points. However it can be seen that the correlation was good across the entire range of peak amplitude levels (on the scatter plot, the data points are aligned in vertical bars due to the 1 dB measurement granularity).

The results indicate that the performance of the single layered neural network was superior to the of the two-layered neural network in this application. It was noted that for this, and many regression-type problems, the use of a linear transfer function in the output neuron is advantageous.

Inputs which had the greatest positive contribution to amplitude estimation were: the number of samples at peak amplitude and the line fit from the beginning of the trail to the peak. Several inputs had little effect, viz. the line fit to the entire trail (considered to be 50 ms long), the position where the rise to peak ends, the position where the fall begins, the position of the maximum difference to the straight line, and the parameters of the best parabolic fit to the concatenated trail. In practice, these small contributors can be eliminated from training, thus speeding up learning and enhancing accuracy.

6.3.4 Neural networks for trail duration prediction

Prediction of the trail duration is a regression problem similar to the prediction of peak trail amplitude trail. Once again, the feature descriptors were derived for the entire trail and then used as the basis of prediction. For prediction the entire trail was first processed to derive the duration. The feature descriptors were then applied to the first 100 ms (20 samples) and the first 50 ms (10 samples) of the trail. The preprocessing package was used to truncate trails to appear as if they were only twenty or ten samples long.

As in the previous two prediction cases, the best predictor would be the one which could use the fewest number of samples while maintaining sufficient accuracy. However, it has been shown in chapter 4 that predicting duration based on the few initial samples would be difficult. Unfortunately, many trails, particularly the large ones such as rectified-sine overdense trails, repeat patterns many times before diffusion takes place. As such, there appears to be no way to predict how long the trails will be on the basis of 50 or 100 ms data alone.

Several neural network architectures and paradigms were implemented including back-propagation neural networks, probabilistic neural networks and general regression neural networks. The performance of the 100 ms data neural networks was so poor that no development of 50 ms data neural networks took place on the basis that they would not perform any better.

An attempt to correlate the inputs with the target output yielded few feature descriptors with a significant coefficient of correlation. A reduced training and test data set were produced by stripping the four most significant inputs from the 26 field superset viz. the B_1 parameter of the straight line fit to the trail, the position where the peak begins, the B_0 parameter of the line fit from the trail beginning to the peak, and the position where the rise to the peak ends.

The following two neural network structures were representative of the more successful neural networks. Many neural networks failed to converge on any solution at all.

Back-propagation NN (20BPN1.NND)

- neurons: 4 input, 10 hidden layer 1, 1 output
- reduced training and test data set (4 inputs only)
- error propagation: back-propagation
- learning rule: extended-delta-bar-delta
- transfer function: hyperbolic tangent
- training epoch size: 500
- MinMax input-output scaling

Back-propagation NN (20BPN2.NND)

- neurons: 26 input, 58 hidden layer 1, 1 output
- full training and test data set (26 inputs)
- error propagation: back-propagation
- learning rule: extended-delta-bar-delta
- transfer function: hyperbolic tangent
- training epoch size: 500
- MinMax input-output scaling

Results

None of the neural networks performed well, despite 100 ms worth of input data. The best performing neural network achieved a correlation of 0.38. Table 6-7 below shows the results of the test data, to which they had not previously been exposed, on the two best neural networks.

Table 6-7 Trail duration prediction results

	100 ms input data	100 ms input data
NN type	Back-propagation	Back-propagation
NN file name	20BPN1.NND	20BPN2.NND
Confusion matrix correlation coefficient	0.208	0.380
RMS error	8%	10%
Overall classification rate	0.50 (meaningless)	0.50 (meaningless)

Figure 6-38 shows a scatter plot of target output (x-axis) and actual output (y-axis) of the best performing back-propagation neural network (20BPN2.NND).

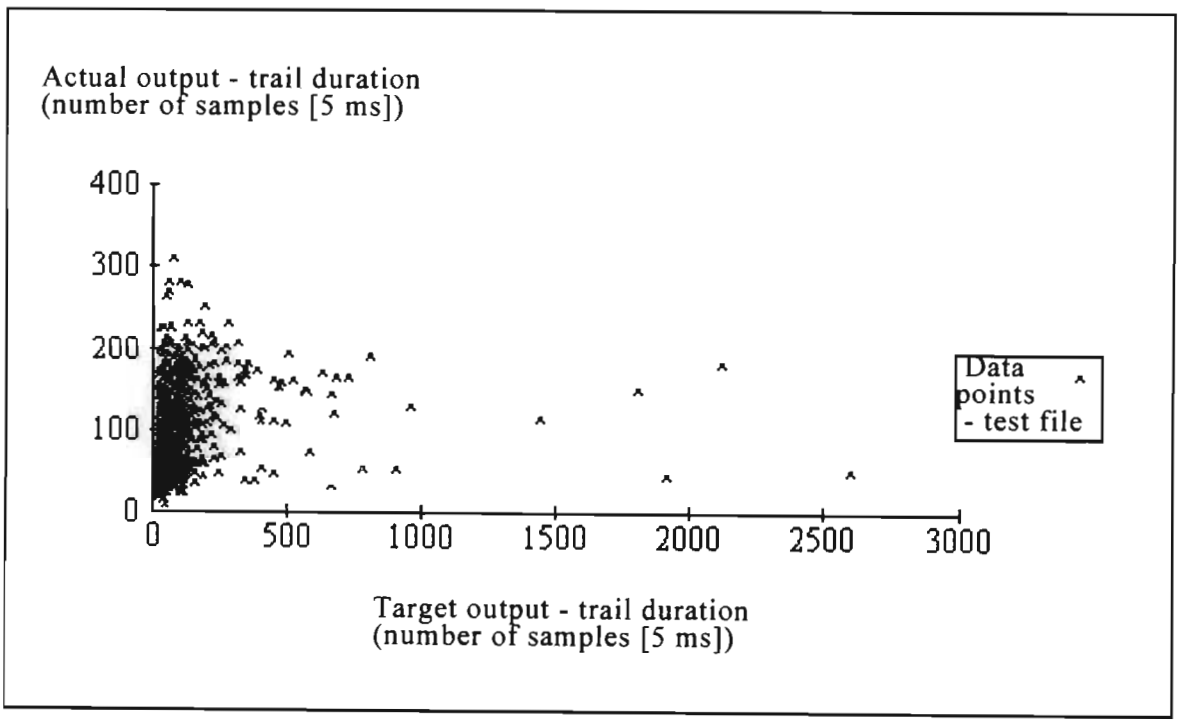

Figure 6-38 Scatter plot of target output (x-axis) and actual output (y-axis) for duration prediction. Solid line y = x is perfect correlation. (100 ms data)

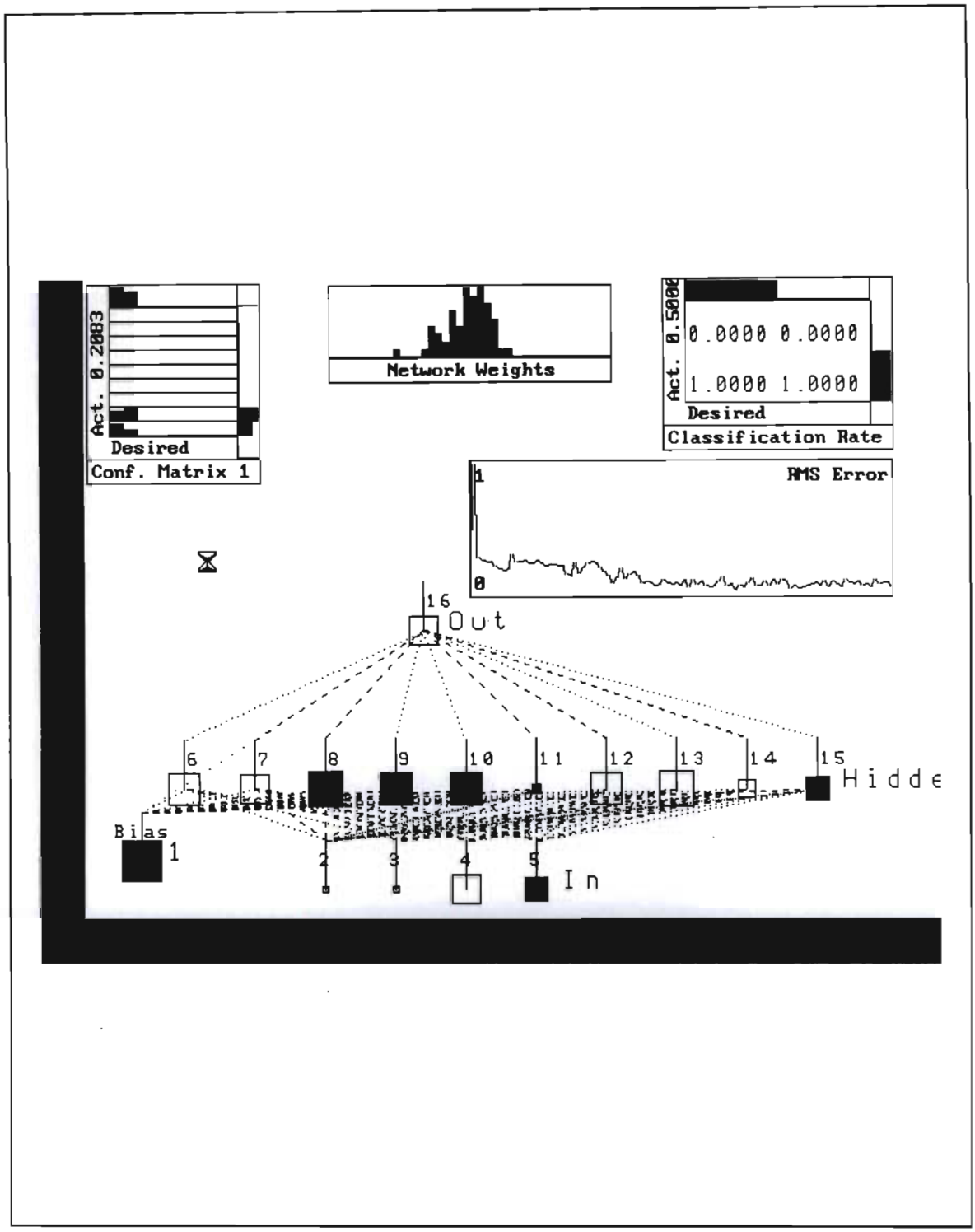

Figure 6-39 20BPN1.NND back-propagation neural network for duration prediction

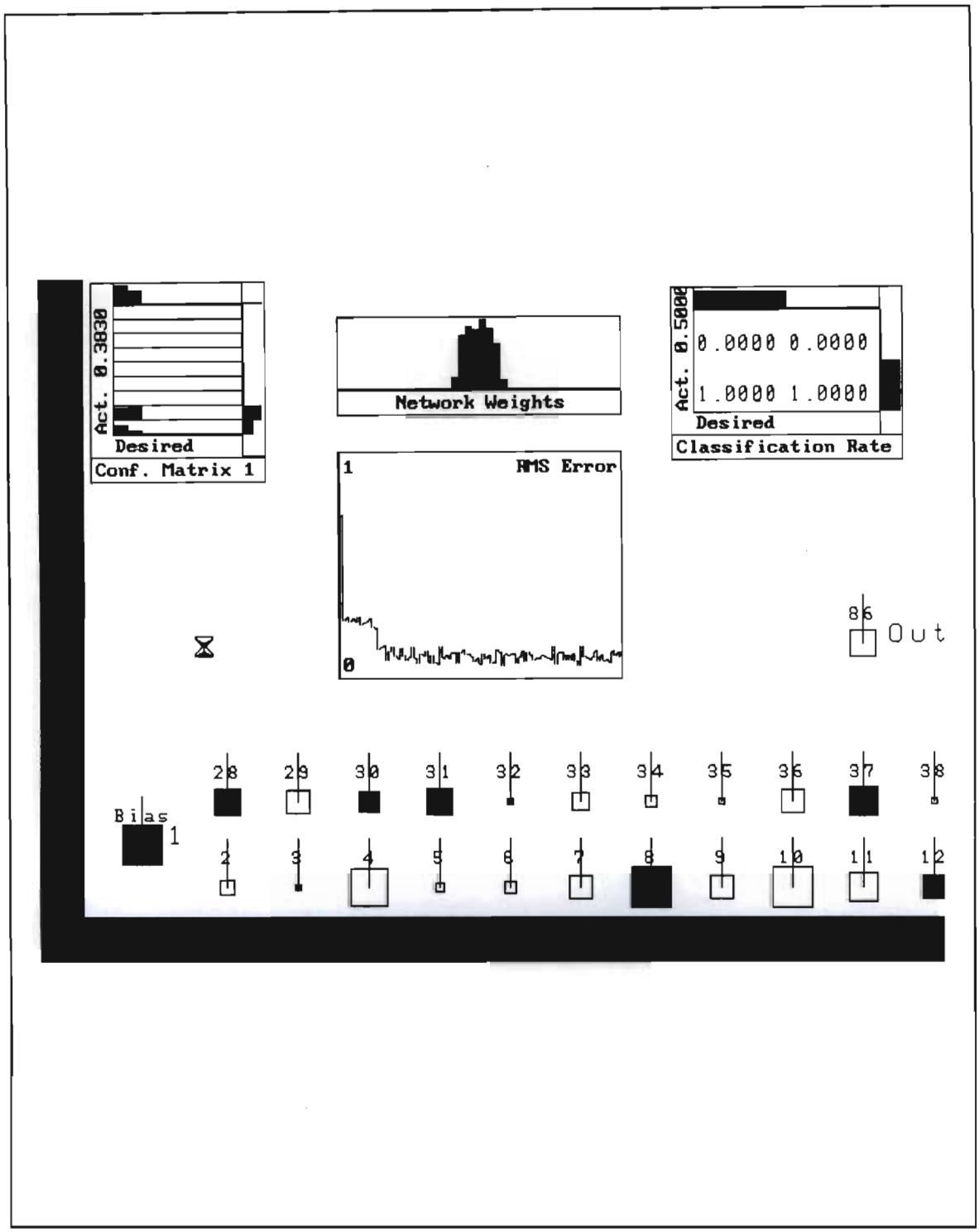

Figure 6-40 20BPN2.NND back-propagation neural network for duration prediction

Discussion

Neither of the better neural networks produced results of statistical significance. The best correlation coefficient of 0.38 fails to indicate any useful duration prediction ability. The result is, however, not totally unexpected.

It appears that duration prediction cannot be linked to parameters derived from amplitude features, e.g. peak amplitude, slopes, plateaus, maxima/minima etc. By comparing various trail types there are instances of both low and high signal-to-noise ratio trails exhibiting short and long durations. For example, a small, but high velocity meteor provides an initial high peak signal-to-noise-ratio but does not last. A second meteor, much larger but of similar velocity also produces a large peak signal-to-noise ratio but lasts much longer owing to its greater mass. This cannot be simply determined from ground based measurements. Furthermore, the apparent signal-to-noise ratio is not representative of the true ionisation line density because of the relative geometry of the incident meteor with respect to the forward scatter link. A possible way around this difficulty is the use of a modular neural network structure in which a trail type prediction neural network prefilters the data for presentation to a duration neural network. This would allow groups of similar characteristic trails to learn duration data specific to them. Such a modular neural network would require considerable processing power. The amplitude data received would have to be processed to produce the trail features. After either 50 or 100 ms, the features would be passed to a parallel array of 4 neural networks. The first would be a trail type predictor, and the other three an underdense-specific duration estimator, an overdense-specific duration estimator and an "other"-specific duration estimator. The first neural network would gate the three parallel neural networks depending on the trail type predicted. It is believed that such an arrangement may show more promise for duration prediction than the single mixed-type neural network considered here.

6.4 General conclusions

The steps required to preprocess the raw meteor-burst communication data have been presented as well as relevant feature extraction procedures. It was observed that careful input conditioning and parameter selection greatly enhanced the ability of the neural networks to converge on useful solutions. Furthermore the quantity of data is as important as the quality of data so that the statistical distribution of the input data matches the neural network application. For example, a neural network with a small training data set with too few occurrences of rare events, will fail to recognise them in the learning procedure, owing to the cumulative update of weights. It was found that at least half of the neural network development time was spent on data preparation.

Several neural networks were demonstrated which could perform classification and parametric prediction tasks. A neural network for trail type classification performed underdense/overdense classification with a high degree of accuracy (97%). This was based on data from the whole trail. The result is important since it indicates that a neural network can perform the task of a rule-based expert system without explicit formalization of the rules.

The neural network designed for trail type prediction used truncated trail data (50 and 100 ms). It was able to correctly predict overdense trails 73% of the time, underdense trails 79% of the time and "other" types 68% of the time. The significance of these predictions is that for many trails they broadly predict the shape and amplitude of the coming trail, *before* the trail is completely formed. Furthermore, the positive results of testing the trail type prediction neural networks on data from another meteor-burst communication system showed that the neural networks had trained on largely invariant features of the trails rather than on data specific to a single link.

The application of neural networks to peak trail amplitude prediction was also shown to be highly successful (83.56% correlation between predicted and actual

peak amplitudes). The success of these neural networks shows that sufficient features for peak amplitude prediction are present in the early trail samples. In development of these neural networks, steps were taken to ensure that the neural networks actually estimated the amplitude and didn't merely measure it. This included using only 50 ms worth of data and the elimination of inputs related to peak amplitude and position within the 50 ms data.

Finally, neural networks designed to predict trail duration were trained on 100 ms data sets. Despite numerous efforts to get the neural networks to converge on a good solution, the best that was achieved was a correlation of 0.38 between the predicted and actual trail duration. A single neural network is unable to resolve dichotomies such as both large and small signal-to-noise ratio trails exhibiting similar durations and it is proposed that a modular neural network approach be taken to solve this problem.

In conclusion, novel methods of classifying whole trails and predicting trail type and peak trail amplitude have been presented. They represent a successful advance on previous techniques such as rule-based expert systems. They have the potential to be used as predictors in open-loop adaptive data rate schemes and for trail pre-classification in military and trucking applications.

Chapter 7

Conclusion

7.1 Discussion and conclusions

The standard technology for adaptive data rate meteor-burst communications is a full-duplex closed-loop decision-feedback system. The only alternative to closed-loop decision feedback is open-loop predictive control of data rates. This is achieved by measuring the channel for a few milliseconds, predicting its characteristics over its lifetime, and then transferring data at a rate commensurate with the predictions. This method has previously been unused because of a lack of adequate predictors of trail characteristics. This thesis examined several possibilities for such predictors.

In Chapter 2, current half-duplex and full-duplex meteor-burst protocols were reviewed. An adapted form of the go-back N ARQ protocol was proposed for use in an half-duplex open-loop predictive manner. This open-loop protocol has no explicit decision-feedback path for data rate adaptation between sender and receiver. Instead, channel predictors are used to estimate optimal data rates on a trail-by-trail basis. This scheme, while by no means optimal, provides a considerable improvement over fixed-rate systems. It is ideally suited to telemetry applications with short messages in which the signal-to-noise ratio fluctuates little and to low-cost half-duplex equipment.

The main thrust of the research was directed towards the investigation of suitable predictors which would give an indication of future trail characteristics based on

data measured during the first few milliseconds of a trail's lifetime. Two different prediction techniques were developed: early fast Doppler to predict large overdense trails, and artificial neural networks to predict trail types, peak trail amplitude and trail duration. The data for both techniques was provided by the measurement system described in Chapter 3.

The early fast Doppler phenomenon was investigated in Chapter 4 for use as a predictor from two angles, viz. an heuristic and a statistical approach. The statistical correlation of early fast Doppler and trail parameters such as peak amplitude and duration yielded a poor result, i.e. there appeared to be no direct relationship between early fast Doppler and trail parameters. However, the heuristic approach of detecting the presence of early fast Doppler as an indication of trail type proved successful. It was found that early fast Doppler occurs at the commencement of roughly 30% of the large signal-to-noise ratio, long duration overdense trails. Despite the relatively low count of such trails each hour, they comprise a large fraction of the hourly channel duty cycle. A novel technique using the presence or non-presence of early fast Doppler to toggle the data rate between a standard rate and a higher rate (for the long duration and/or large amplitude trails with early fast Doppler) was proposed. This would allow roughly 20% of the hourly duty cycle to benefit from a higher data rate. Such a system would be both cheap and simple to implement. This method would find application in cheaper bi-rate half-duplex remote stations such as are used for telemetry.

For a multi-rate adaptive data-rate scheme without decision feedback, a more sophisticated approach was presented. Chapters 5 and 6 detailed a novel neural network solution to the problem of trail prediction and classification. Using features extracted from the first 50 or 100 ms of the trail amplitude, neural networks were developed to predict trail characteristics (trail type, peak trail amplitude and trail duration). Several hundred neural networks were developed and the results of the best networks presented.

Trail type prediction based on 50 ms worth of data from the commencement of the trail was very successful. The correct prediction of underdense trails was 78.95%, overdense trails 66.45% and "other" trail types 63.80%. It was noted that the classification rate would be considerably improved through the use of thresholding. There was sufficient tolerance between each trail category to enable this technique to bring the classification rate closer to 100%.

The success of neural networks for trail type prediction may open up many potential avenues of application. For example, if the first 50 ms can determine the trail type based on measurement of probe amplitude, then a remote unit operating under covert conditions could decide to use underdense trails rather than overdense trails which have a higher probability of interception owing to their large-footprint. This philosophy could be extended to cover other propagation modes such as sporadic E. A similar condition may apply in meteor-burst truck telemetry where underdense trails alone may be used to improve spatial diversity in a dense network environment. Here again, fore-knowledge of large overdense trails by either early fast Doppler or neural network technique would be extremely valuable.

Peak amplitude prediction yielded a best correlation between predicted and actual peak amplitude of 0.836 which was highly significant. This singular feature is of great value as an estimator of trail signal-to-noise ratio and hence optimum data rate. Instead of just using a binary toggle of data rate, the neural peak amplitude predictor would provide a far finer estimate of the trail magnitude. Even if this were divided into five bands say, very small, small, medium, large and very large amplitude, would provide a closer "fit" to the actual trail signal-to-noise ratio than the sub-optimal bi-rate method.

Prediction of trail duration was poor with a correlation of 0.380 for 100 ms worth of data. It was suggested that a modular neural network approach be taken in future for duration prediction instead of the single neural network approach. Four neural networks would be created, three of which would be optimised for duration

prediction on underdense, overdense and other trail types respectively, and the fourth, a trail type prediction neural network, used to gate their outputs.

The positive results from the trail type and peak trail amplitude neural networks show that they would make excellent predictors in an open-loop half-duplex system. As a solution, it would be more costly to implement than the early fast Doppler method, but would provide information for multiple data rates to suit individual trail signal-to-noise ratios better. The neural network based predictors also generalised extremely well. They were trained on a particular test link, but when tested on another twice as long, their performance was degraded by a mere 5%. This showed that the neural networks had learnt features of the trails themselves rather than features of a specific link. Provided the deployed systems are not vastly different, a neural network trained on one system should operate on a second with minimal error.

It is the author's belief that this is the first successful development of practical meteor-burst communication predictors and that the aims of the thesis have been met using two novel predictive techniques.

7.2 Future possibilities

Many artificial intelligence solutions are frequently a fusion of methods. For example, it may prove advantageous to combine both early fast Doppler and neural network methods for prediction by means of a hybrid neural network and rule-based system. This combination would enhance decision making by including both conditional logic rules and neural network regression analysis. Other inputs such as link parameters and conditional probabilities such as diurnal variations could also then be applied.

Similarly, the panel-of-experts approach of a modular neural network, may yield even further performance benefits. Each neural network could be trained on a

smaller subset of the total data to enhance individual neural network accuracy. Their outputs would then be combined either by another neural network or by means of a rule-based system.

Another useful development may be an unsupervised learning neural network to classify trails based on their measured characteristics rather than using the decision of the *TrailStar* rule-based expert system. The benefit would be that similar trails, from the point of view of their descriptive feature vectors, would be clustered together, rather than forcing groupings according to strict underdense/overdense rule-based classifications. This would extend the classification of trails to "useful" and "non useful" trails on the basis of signal-to-noise ratio and duration and not on their shape features.

References

Abel, M.W., 1986, "Meteor Burst Communications: Bits Per Burst Performance Bounds", *IEEE Trans. Comm.*, Vol. COM-34, pp 927-936.

Alspector, J., Goodman, R. and Brown, T.X., 1993, Applications of Neural Networks to Telecommunications, INNS Press and Lawrence Erlbaum and Assoc., Hillsdale, NJ.

Black, U.D., 1983, Data Communications Networks and Distributed Processing, Prentice-Hall, Reston, Englewood Cliffs, NJ, pp 235-240.

Carpenter, G.A., and Grossberg, S., 1987a, "A Massively Parallel Architecture for a Self-Organizing Neural Pattern Recognition Machine", *Computer Vision, Graphics and Image Processing 37*, pp 54-115.

Carpenter, G.A., and Grossberg, S., 1987b, "ART2: Self-Organization of Stable Category Recognition Codes for Analog Input Patterns", *Applied Optics*, pp 4919-1930.

Carpenter, G.A., and Grossberg, S., 1988, "The ART of Adaptive Pattern Recognition by a Self-Organizing Neural Network", *Computer*, pp 77-88, March 1988.

Cavers, J.K., 1972, "Variable-Rate Transmission for Rayleigh Fading Channels", *IEEE Trans. Comm.*, Vol 20, pp 15-22.

Cichocki, A. and Unbehauen, R., 1993, Neural Networks for Optimization and Signal Processing, John Wiley & Sons, Chichester, UK.

Fahlman, S.E., 1988, "An Empirical Study of Learning Speed in Back-Propagation Networks", *Tecnical Report CMU-CS-88-162*, Carnegie-Mellon University, June 1988.

Fraser, D.D., 1989a, "Phase Effects in Meteor Scatter Communication Systems", *Research Repor*t, Salbu (Pty) Ltd, Private Bag 2352, Wingate Park, 0153, South Africa, July 1989.

Fraser, D.D., 1989b, "Investigation into the Effects and Mechanisms of Phase Distortion and their Influence on Modem Performance", *Research Report*, Salbu (Pty) Ltd, Private Bag 2352, Wingate Park, 0153, South Africa, September 1989.

Fraser, D.D., 1990, "Design, Construction and Testing of a New Meteor Monitoring Unit to Include Phase Measurement", *Research Report,* Salbu (Pty) Ltd, Private Bag 2352, Wingate Park, 0153, South Africa, February 1990.

Fraser, D. D., 1991a, "Phase Effects in Meteor-Burst Communication Systems", *MSc Thesis*, Department of Electronic Engineering, University of Natal, Durban, South Africa.

Fraser, D.D., 1991b "Phase Characteristics of the Meteor Burst Channel", *IEEE Comsig '91 Proceedings*, Pretoria, pp 93-98.

Fraser, D.D., 1991c, "Channel Phase Characteristics", *Research Report*, Salbu (Pty) Ltd, Private Bag 2352, Wingate Park, 0153, South Africa, February 1991.

Fraser, D.D., 1991d, "Early Fast Doppler as an MBC Amplitude Predictor", *Research Report*, Salbu (Pty) Ltd, Private Bag 2352, Wingate Park, 0153, South Africa, July 1991.

Fraser, D.D., 1992, "Neural Networks and EFD in MBC Amplitude Prediction", *Research Report*, Salbu (Pty) Ltd, Private Bag 2352, Wingate Park, 0153, South Africa, February 1992.

Fraser, D.D., 1993, "Neural Networks and Meteor-Burst Communications", *IEEE Milcom '93*, Boston USA, 11-14 October 1993, pp 418-422.

Fraser, D.D., & Broadhurst, A. D., 1992a, "Early Fast Doppler as a Meteor-Burst Communications Amplitude Predictor", *IEEE Comsig '92 Proceedings*, Cape Town, 11 September, 1992.

Fraser, D.D., & Broadhurst, A. D., 1992b, " Factors influencing Early Fast Doppler in Meteor-Scatter Propagation", *IEEE AP&MTTS*, Durban, 14 September, 1992.

Fraser, D.D., & Broadhurst, A. D., 1993a, "Open-Loop Amplitude Prediction in Meteor-Burst Communications" *Trans. SAIEE*, Vol. 84, No. 2, pp 74-80.

Fraser, D.D. & Broadhurst, A. D., 1993b, "Phase Effects in Meteor-Burst Communications", *Trans. SAIEE*, Vol. 84, No. 2, pp 81-89.

Fraser, D.D., Khan, Z., & Levy, D.C., 1992, "A Neural Network for Meteor Trail Classification", *ICANN '92 Proceedings*, Brighton, U.K., 4-7 September, 1992.

Fraser, D.D., & Melville, S.W., 1992, "Artificial Neural Networks for MBC Amplitude Prediction", *Research Report*, Salbu (Pty) Ltd, Private Bag 2352, Wingate Park, 0153, South Africa, September 1992.

Fraser, D.D., & Melville, S.W., 1993a, "Artificial Neural Networks for MBC Trail Type Prediction", *Research Report*, Salbu (Pty) Ltd, Private Bag 2352, Wingate Park, 0153, South Africa, February 1993.

Fraser, D.D., & Melville, S.W., 1993b, "Artificial Neural Networks for MBC Trail Classification", *Research Report*, Salbu (Pty) Ltd, Private Bag 2352, Wingate Park, 0153, South Africa, September 1993.

Goldstein, H., Melville, S.W., & Fraser, D.D., 1992, "A Neural Net for Meteor Trail Prediction", *Proceedings of the 3rd South African Workshop on Pattern Recognition*, Pretoria, South Africa, 26 November 1992.

Greenhow, J.S., and Neufeld, E.L., 1956, "Phase Changes and Resonance Effects, Radio Echoes from Meteor Trails", *Proc. Phys. Soc.*, Vol. B69.

Grossi, M.D., and Javed, A., 1978, "Time and Frequency Spread, Meteor-Burst Propagation Paths", *AGARD Conference - Electromagnetic Wave Propagation Panel, 23rd Symp, Aspects of EM Wave Scattering, Radio Commun.*, No.244.

Handley, P.A., & Fraser, D.D., 1992, "Meteor-Burst Communications for Rural Environments", *AFRICON '92 Conference Proceedings*, Swaziland, September, 1992.

Handley, P.A., & Fraser, D.D., 1993, "Application of Meteor-Burst Technology in Africa", *Trans. SAIEE*, Vol. 84, No. 2, pp 69-73.

Hines, C.O. and Forsyth, P.A., 1957, "The Forward-Scattering of Radio Waves from Overdense Meteor Trails", *Canad. J. of Phys.*, Vol. 35, pp 1033-1041.

Jacobs, R.A., 1988, "Increased Rates of Learning through Learning Rate Adaptation", *Neural Networks*, Vol. 1, pp 295-307.

James, J.C., and Meeks, M.L., 1956, "On the Relative Contributions of Various Sky Regions to Meteor-Communications", *Georgie Institute of Technology*, Atlanta, Georgia, Engineering Experiment Station, Naval Research Contract No. NOnr-991(02), Technical Report No. 1.

Kaiser, T.R., 1953a, "Radio Echo Studies of Meteor Ionization", *Trans. IRE - Antennas and Propagation*, Vol. AP-1.

Kaiser, T.R., 1953b, "Radio Echo Studies of Meteor Ionization", *Phil. Mag. Supp.*, Vol. 2, pp 495-544.

Kaiser, T.R., 1955, "The Interpretation of Radio Echoes from Meteor Trails", *Spec. Supp J. Atmos. Terr. Phys.*, Vol. 2, pp 55-64.

Kohonen, T., 1988, "Statistical Pattern Recognition with Neural Networks: Benchmark Studies", *Proc. of the 2nd Annual IEEE International Conference on Neural Networks*, Vol. 1, 1988.

Kosko, B., 1987, "Bidirectional Associative Memories", *IEEE Trans. on Systems, Man, and Cybernetics*, 1987.

Larsen, J.D., Melville, S.W., Mawrey, R.S., Letschert, R.Y., and Goddard, W.D. 1990a, "Throughput Capacity of Meteor Burst Communications", *Trans. SAIEE*, Vol. 81, pp 20 - 30.

Larsen, J.D., Melville, S.W., and Mawrey, R.S.M., 1990b, "Adaptive Data Rate Capacity of Meteor-Burst Communications", *Conference Record of the 1990 IEEE Conference on Military Communications*, Vol. 2, pp 40.1.1 - 40.1.5.

Lovell, A.C.B, and Clegg, J.A., 1948, "Characteristics of Radio Echoes from Meteor Trails: I The Intensity of the Radio Reflections and Electron Density Trails", *Proc. Physical Society of London* , Vol. 60.

Manning, L.A., Villard, O.G., and Peterson, A.M., 1952, "Double Doppler Study of Meteoric Echoes", *Journal of Geophysics Research*, Vol. 57, No. 3.
March, D.N., 1966, "The Phase Stability of a VHF Meteor Trail Forward-Scatter Channel and an Application: A Time Synchronization System", *PhD Thesis*, Montana State University.

March, D.N., 1966, "The Phase Stability of a VHF Meteor Trail Forward-Scatter Channel and an Application: A Time Synchronization System", *Doctoral Thesis*, Montana State University.

Maren, A., Harston, C. and Pap, R., 1990, Handbook of Neural Computing Applications, Academic Press, San Diego, CA.

Mawrey, R.S., 1988, "A Meteor-Scatter Measurement System", *MSc Thesis*, University of Natal, Durban, South Africa.

Mawrey, R.S., 1990, "A Comparison between Predicted and Measured Annual Cycles of Meteors", *IEEE Comsig '90 Proceedings*, Johannesburg, pp 32-37.

McKinley, D.W.R., 1961, "Meteor Science and Engineering", McGraw-Hill, New York, NY.

Melville, S.W., 1991a, "PHASER - Phase Extraction Software", *Research Report*, Salbu (Pty) Ltd, Private Bag 2352, Wingate Park, 0153, South Africa.

Melville, S.W. 1991b, "Channel Phase Evaluation", *Research Report*, Salbu (Pty) Ltd, Private Bag 2352, Wingate Park, 0153, South Africa.

Melville, S.W., 1991c, "A Practical Investigation of Meteor-Burst Communications", *Doctoral Thesis*, Department of Computer Science, University of Natal, Durban, South Africa.

Melville, S.W., & Fraser, D.D., 1992, "Meteor-Burst Communications: The State of the Science", *IEEE Comsig '92 Proceedings*, Cape Town, 11 September, 1992.

Melville, S.W., & Fraser, D.D., 1993, "Meteor-Burst Communication: A Review", *Trans. SAIEE*, Vol. 84, No. 2, pp 60-68.

Melville, S.W. and Larsen, J.D., 1992, "Wait Time, Meteor-Burst Communications", *Trans. SAIEE*, Vol. 83, No 1, pp 32 - 37.

Melville, S.W., Larsen, J.D., Letschert, R.Y. and Goddard, W.D., 1989, "The Classification of Meteor Trail Reflections by a Rule-Based System", *Trans. SAIEE*, Vol. 80, No. 1, pp 104-116.

Minai, A.A., and Williams, R.D., 1990, "Acceleration of Backpropagation Learning through Learning Rate and Momentum Adaptation", *International Joint Conference on Neural Networks*, Vol. I, pp 676-679, January 1990.

Nagaoka, H., 1929, "Possibility of Disturbance of Radio Transmission by Meteor Showers", *Proc. Imperial Academy of Tokyo*, Vol. 5, pp 632.

National Communications System Office of Technology and Standards (NCSOTS), 1989, *Proposed Federal Standard 1055, Telecommunications Interoperability Requirements for Meteor Burst Communications*, Section 4.6, Washington, DC June 1989.

Neural Computing, 1993, NeuralWare Inc., Pittsburgh, PA (no listed author).

Parker, D.B., 1985, "Learning Logic", *Technical Report TR-47*, Center for Computational Research in Economics and Management Science, MIT, Cambridge, MA.

Pickard, G.W., 1931, "A Note on the Relation of Meteor Showers and Radio Reception", *Proc. IRE*, Vol. 19, pp 1166-1170.

Ralston, W.T., Weitzen, J.A., and Ostergaard, J.C., 1993, "Distribution of Underdense Meteor Trail Durations and Duty Cycles, and Applications to Meteor Scatter Communication System Design", *Radio Science*, Vol. 28, pp 747-759.

Rodman, P.J., 1991, "A Microcomputer-based Meteor-Burst Data Capture System", *Research Report*, Salbu (Pty) Ltd, Private Bag 2352, Wingate Park, 0153, South Africa.

Rumelhart, D.E., McClelland, J.L., and the PDP Research Group, 1986, Parallel Distributed Processing: Explorations in the Mircrostructure of Cognition, MIT Press, Cambridge, MA.

Sander, W.R., Tashiro, S., Albright, D.L. and March, D.N., 1966, "An Automatic Meteor Burst Time Synchronization System for Aerospace Applications", *Supp Trans. IEEE Aerospace and Electronic Systems*, Vol. AES-2, No. 4, pp 624-629.

Schanker, J.Z., 1990, Meteor Burst Communications, Artech House, Norwood, MA.

Schilling, D.L., 1993, Meteor Burst Communications: Theory and Practice, John Wiley and Sons, New York, NY.

Skellet, A.M., 1932, "The Ionizing Effect of Meteors, Relation to Radio Propagation", *Proc. IRE*, Vol. 20, pp 1933-1940.

Smith, D.K., and Donich, T.G., 1989, "Maximising Throughput Under Changing Channel Conditions", *Signal*, pp 173 - 178.

Specht, D.F, 1988, "Probabilistic Neural Networks for Classification, Mapping and Associative Memory", *Proc. International Conference on Neural Networks 1988.*

Specht, D.F, 1990, "Probabilistic Neural Networks", *Neural Networks*, November 1990.

Stone, R.R. and March, D.N., 1975, "Final Report MBCS Evaluation and Improvement", *ERL Report #3775.*

Sugar, G.R., 1964, "Radio Propagation by Reflection from Meteor Trails", *Proc. IEEE*, Vol. 52, pp.116-136.

Weitzen, J.A., 1983, "Feasability of High Speed Digital Communications on the Meteor Scatter Channel", *Doctoral Thesis*, University of Wisconsin-Madison.

Weitzen, J.A., Grossi, M.D., and Birkemeier, W.P., 1983 "High Resolution Multipath Measurements of the Meteor Scatter Channel", *Radio Science*, Vol. 19, No. 1.

Weitzen, J.A., Birkemeier, W.P., and Grossi, M.D., 1984, "An Estimate of the Capacity of the Meteor-Burst Channel", *IEEE Trans. Comm.*, Vol. COM-32, pp 972-974.

Weitzen, J.A., 1986, "The Multipath and Fading Profile of the High Latitude Meteor Burst Communication Channel", *RADC Interim Report RADC-TR-86-166*, Rome Air Development Center.

Weitzen, J.A., Bourque, S., Horton, M., Bench, P.M., Baily, A.D., and Ostergaard, J.C., 1990, "Predicting the Amplitude Distribution of Meteor Trails with Applications to System Engineering", *Proc. International Phoenix Conference on Computers and Communication*, Scotsdale AZ, March 21-23, 1990

Werbos, P.J., 1974, "Beyond Regression: New Tools for Prediction and Analysis in the Bahavioral Sciences", *Doctoral Thesis*, Applied Math., Harvard University.

Werbos, P.J., 1988, "Backpropagation: Past and Future", *IEEE Proc. of the Intl. Conf. on Neural Networks*, Vol I, pp 343-353, New York, July 1988.

Widrow, B., and Stearns, S.D., 1985, Adaptive Signal Processing, Prentice-Hall, Englewood Cliffs, NJ.

Yuhas, B. and Ansari, N, 1994, Neural Networks in Telecommunications, Kluwer Academic Publishers, Netherlands.

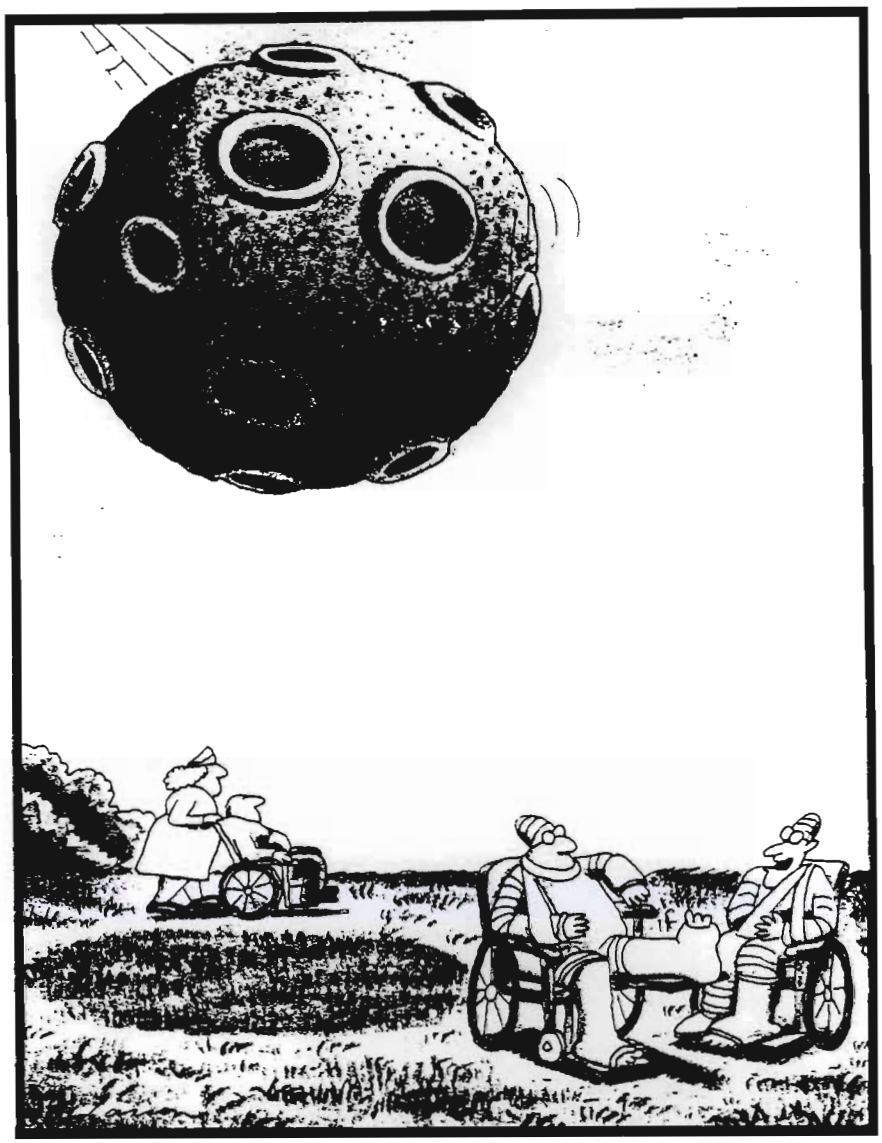

"You're kidding! . . . I was struck twice by lightning too!"

Alien(ated) rock on mayor's roof

PORT ELIZABETH: Two rocks believed to be meteorites have been found in George — one of them on the mayor's roof.

Workmen cleaning the roof of a business belonging to mayor Mr Louis van Rensburg, found one rock, which struck the roof with such force it left a cut in the zinc roof. The lump looks like a conglomerate of rock and is about the size of an egg.

The other stone - which looks like solid metal - was found in the garden of a local resident.

Both stones will be sent to the Council for Scientific and Industrial Research (CSIR), for analysis.

However the curator at the George Museum, Johan van Wyk believes its possibly a chip of fire block that fell from a jet and landed on the mayor's roof.—ECNA

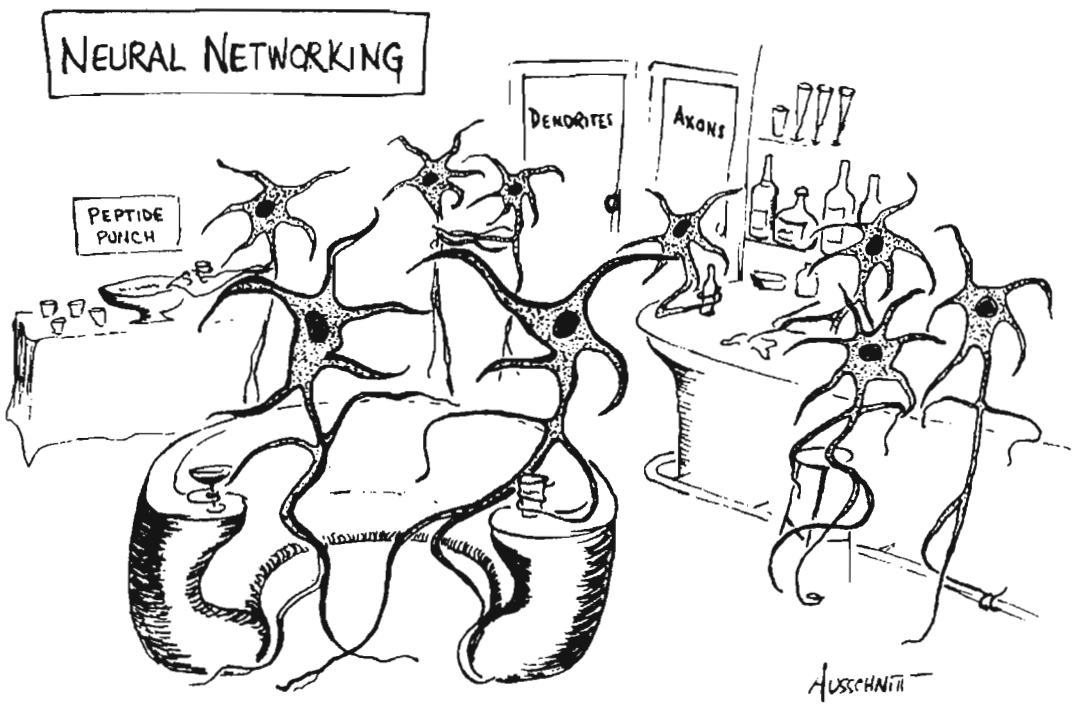
NEURAL NETWORKING
DENDRITES
AXONS
PEPTIDE PUNCH
HUSSCHNITT